CHALMERS

Line-of-Sight MIMO for Microwave Links

Adaptive Dual Polarized and Spatially Separated Systems

Master of Science Thesis in Communication Engineering

Tryggvi Ingason
Liu Haonan

Department of Signals and Systems
CHALMERS UNIVERSITY OF TECHNOLOGY
Göteborg, Sweden, July 2009

EX064/2009

Line-of-Sight MIMO for Microwave Links
Adaptive Dual Polarized and Spatially Separated Systems

Tryggvi Ingason
Liu Haonan

Examiner: Mats Viberg

Department of Signals and Systems
Chalmers University of Technology
SE-412 96 Göteborg
Sweden
Telephone + 46 (0)31-772 1000

Department of Signals and Systems
Göteborg, Sweden, July 2009

Abstract

With mass uptake of mobile broadband such as HSPA, LTE and advanced LTE there will be a rapid increase of demand for capacity in the mobile backhaul. The traditional frequency bands used for mobile backhaul microwave links are narrow and may become a future capacity bottleneck. Line-of-sight MIMO is one possible technology for increasing the spectral efficiency of these links. By using multiple antennas at both the transmitter and receiver the capacity of such systems could be multiplied using the same spectrum.

Line-of-sight MIMO works by making the signal streams orthogonal to each other either by spatially separating the antennas at the transmitter and receiver or by using orthogonally polarized antennas.

In this thesis both 2x2 spatially-separated and 4x4 spatially-separated and dual-polarized line-of-sight MIMO are numerically investigated. Adaptive algorithms for a space-time-equalizer are proposed and evaluated against detrimental affects such as frequency selective channels, mast swing (antenna movement), polarization leakage and phase noise (correlated and differential). The algorithms are either decision-directed or blind, those are LMS and WRLS and CMA, SCMA and MCMA respectively.

The simulations show that line-of-sight MIMO needs higher system margins and a more complex receiver structure. Convergence of blind algorithms can be difficult to achieve for some channel conditions as well as for differential phase noise. Mast swing will further more put higher requirements on spatially-separated MIMO systems than on its SISO counterpart.

Preface

This report is the result of our master thesis project carried out at the product development unit (PDU) for Microwave Networks, Ericsson AB in Mölndal. The thesis is also the final examination for the Master Degree "Communication Engineering" at Chalmers University of Technology, Göteborg, Sweden and is done in cooperation with Chalmers Antenna Systems Excellence center (Chase).

PDU Microwave Networks is a product development unit for the MINI-LINK product family which is a microwave link mainly used in backhaul networks. Ericsson holds about one-third of the total microwave market and has sold more than 1.5 million MINI-LINK solutions.

We would like to thank the following people: Dr. Jonas Hansryd from Ericsson, Dr. Mikael Coldrey from Ericsson and Dr. Andreas Wolfgang from Chalmers for being our supervisors and giving good advice and comments. We would also like to thank Professor Mats Viberg from Chalmers for being our examiner, Assistant Professor Tommy Svensson from Chalmers for initiating the project and finally Dr. Mats Rydström from Ericsson, M.Sc. Dan Weinholt from Ericsson and M.Sc. Björn Gävert from Ericsson for their helpful inputs.

Contents

List of Figures

List of Tables

Chapter 1

Introduction

1.1 Background

Todays mobile traffic is dominated by voice from GSM and WCDMA. In the not-so distant future the traffic will be dominated by broadband data. The evolution of HSPA and the arrival of LTE will increase data rates of future wireless networks manyfold creating tougher requirements on the capacity of the backhaul networks. A backhaul link is a link that connects base stations to network controllers, these base stations are located on the field often making them inaccessible to fiber- and DSL solutions. A microwave radio link is thus a commonly used solution since it does away with a direct cable connection. It is very important that the throughput of these radio links keep up with demand, preferably without requiring a purchase of more spectrum which can be scarce and expensive.
Wireless MIMO technology allows for higher throughput for the same spectrum because of it's ability to transmit and receive multiple streams simultaneously. For most applications MIMO requires a non-line-of-sight- and a rich scattering environment to work properly but microwave links usually have non of this. These links use highly directional antennas that have a direct line-of-sight (LoS) component dominating the transmission. However, it may be shown that at microwave frequencies it is possible to transmit multiple streams over a single frequency band if the antennas at the transmitter and receiver are separated sufficiently. Combining this with dual-polarized antennas it is possible to quadruple the throughput without making the required antenna separation infeasible. Unlike the mobile MIMO channel which is inherently random the LoS MIMO channel is determined by geometry which essentially remains static over the operational lifetime. A properly installed link is thus more predictable than its mobile counterpart.

1.2 Problem Description

This thesis was started to be able to better understand what requirements the LoS MIMO channel would put on the system, both spatially separated and dual polarized systems. Adaptive algorithms for these systems were investigated, *e.g.* equalizers able to cancel inter-stream interference and cross polarization distortion as well as conventional intersymbol interference. The performance of these algorithms were investigated for different channel conditions having time-variant frequency selectivity due to mast swing. Phase noise tolerances were also inves-

tigated as well as the effects of suboptimal antenna installation and high cross polarization couplings. The algorithms considered were training-based, semi-blind and blind. The thesis outcome should give a guideline of tolerances of such systems to channel effects as well as on installation requirements.

1.3 Thesis Outline

The report consists of seven chapters and two appendices. The first chapter along with the abstract give an overview of the work carried out. The second chapter is a high level overview of wireless communication using microwaves. Chapter three discusses MIMO technology with an emphases on LoS MIMO both spatially-separated and dual-polarized. Chapter four is a theoretical overview of equalizers and adaptive algorithms for MIMO. Chapter five describes how the simulations were carried out. Chapter six lists all the results obtained by simulations and finally chapter nine summarizes the results and gives some conclusions.

1.4 Notation

1.4.1 Abbreviations

ADC	Analog to Digital Converter
ADSL	Asymmetric Digital Subscriber Line
AWGN	Additive White Gaussian Noise
BER	Bit Error Rate
CIR	Channel Impulse Response
CMA	Constant Modulus Algorithm
CSIR	Channel State Information at the Receiver
CSIT	Channel State Information at the Transmitter
DAC	Digital to Analog Converter
DD	Decision Directed
DFE	Decision Feedback Equalizer
DP	Dual Polarized
DTFT	Discrete-time Fourier transform
FIR	Finite Impulse Response
GUI	Graphical User Interface
IEEE	The Institute of Electrical and Electronics Engineers
ISI	Intersymbol Interference
LMS	Least Mean Square
LoS	Line of Sight
LS	Least Square
LTE	Long Term Evolution
MCMA	Modified Constant Modulus Algorithm
MIMO	Multiple Input Multiple Output
MISO	Multiple Input Single Output
MLSE	Maximum Likelihood Sequence Estimation
MMA	Modified Modulus Algorithm
MRLA	Modified Recursive Least Square

MSE	Mean Square Error
MTI	Multiple-Transmitting-Interference
NLoS	None-Line of Sight
PRBS	Pseudorandom Binary Sequence
PSK	Phase Shift Keying
QAM	Quadrature Amplitude Modulation
RLS	Recursive Least Square
Rx	Receiver
SCMA	Simplified Constant Modulus Algorithm
SIMO	Single Input Multiple Output
SIP	Superimposed Pilots
SISO	Single Input Single Output
SNR	Signal To Noise Ration
SP	Single Polarized
STE	Space Time Equalizer
SVD	Singular Value Decomposition
Tx	Transmitter
WiMAX	Worldwide Interoperability for Microwave Access
WRLS	Weighted Recursive Least Squares
XPD	Cross-Polarization Discrimination
XPIC	Cross-Polarization Interference Canceler

1.4.2 Symbols

α	The mixing parameter for SCMA
β	Roll-off-factor for the root-raised Cosine filters
$\beta_{\mathbf{max}}$	Maximum tilt of antenna masts
δ	System delay in symbol periods
$\hat{s}$	Estimated Signal (Hard Decision)
κ	Condition Number
σ	Singular Value
b	The ground reflection factor
μ_{cma}	The stepsize of the CMA.
μ_{lms}	The stepsize of the LMS in the Decision-Directed Mode
μ_{mcma}	The step-size of the MCMA
ω	Angular frequency
ω_c	Carrier Angular Frequency
$\mathbf{H}$	MIMO Channel Matrix
B_c	Coherence bandwidth
B_s	Signal bandwidth
C	Capacity
c	Eigenvalues
d_R	Rx antenna separation
d_T	Tx antenna separation
F_{MS}	Frequency of mast swing

F_c	Carrier frequency
F_s	The sampling frequency
k	Wavenumber
λ	Weighting Factor for WRLS
L	Number of filter taps for each filter in the STE
L_{tr}	Number of training symbols
L_H	Tx and Rx antenna mast horizontal distance
L_L	Rx landscape height
L_R	Rx antenna mast height
L_t	The placement of the central tap in each filter in the STE
L_T	Tx antenna mast height
M	Number of Rx antennas
N	Number of Tx antennas
$p(t)$	Matched Filter
P_b	Bit Error Rate
Q	Oversampling rate at the Tx filter
R	The average constant magnitude of Blind algorithm
R_H	Rank of matrix $\mathbf{H}$
r_n	Received Symbol n
s_n	Transmitted Symbol n
T_{Qs}	Symbol period of the oversampled signal
T_c	Coherence time
T_s	Symbol period
V_{MS}	Velocity of the antennas
y_n	Equalized Signal (Soft Decision)
M	Modulation order for M-QAM

1.4.3 Operators

$(\cdot)^{\text{T}}$	Transpose
$(\cdot)^{\text{H}}$	Complex conjugate transpose (Hermitian transpose)
$\Re\{\cdot\}$	Real-part operator
$\Im\{\cdot\}$	Imaginary-part operator
E[·]	Expectation value operator
trace{·}	The trace of a matrix
$< \cdot, \cdot >$	Inner product
$\mathcal{L}\{\cdot\}$	Laplace transform operator
$\delta(\cdot)$	Dirac's delta function

Chapter 2

Wireless Microwave Systems

This chapter will give a high level overview of wireless digital communication. Basic system designs are discussed as well as challenges that need to be overcome by these systems.

2.1 Overview

Communication devices have become so customary and their use so habitual that we hardly ever take time to wonder how all of this can even be possible. The complexity of todays systems are immense but their basic design and operational principles have remained the same for quite some time. This design and these principles can easily be understood at a high level.

Be it wireless cell phones or wired ADSL computer modems the purpose is the same, to communicate through an exacerbating channel. In order to do that the transmitter sends special signals that are tailored in a way so that they are retrievable at the receiver. The receiver may improve the quality of the received signal by applying signal processing in order to filter out noise, remove interfering signals and combat other depriving effects of the channel to get an estimate of the symbols being sent.

Analog and digital communication differ in the fact that digital signals have a finite signal set while analog transmission has an infinite amount (is continuous). Wherever one desires digital information at the endpoints of the system it is in fact necessary to use digital communication. Seeing that the vast majority of information is stored and processed digitally and the fact that digital communication can be designed to be functionally superior in almost all cases compared to analog communication, it is no wonder that the vast majority of today's communication systems are digital. From now on only digital systems will be considered.

For all communication systems there are two universal design parameters that need to be optimized. These are spectral efficiency and power efficiency, both have a profound impact on wireless links. Spectral efficiency quantifies the information content transmitted over a given bandwidth and has the unit bits/Hz/s. Power efficiency quantifies the signal-to-noise (SNR) requirement at the receiver to obtain a specific bit error rate (BER). Design and optimization needs then be done without adding excessive complexity to the system. One can state that the brunt of the research effort done in recent times on digital wireless transmission

is concerned with optimizing for these three requirements.

A high level view of a communication system can be stated as follows. The transmitter takes data and maps it into a sequence of suitable modulated and filtered symbols that are sent over a channel. The channel, which is comprised of a certain environment, then distorts the signal by adding noise and interfering signals, spreading out the signal in time causing inter symbol interference (ISI) and attenuating the signal power. The receiver then needs to undo as much of the effects of the channel as possible before interpreting the transmitted data and outputting (hopefully) the original data.

2.2 Basic System Design

A schematic representation of a communication system can be seen in Figure 2.1. Each block represents a conceptual or logical part of the system and is useful in obtaining a high level understanding.

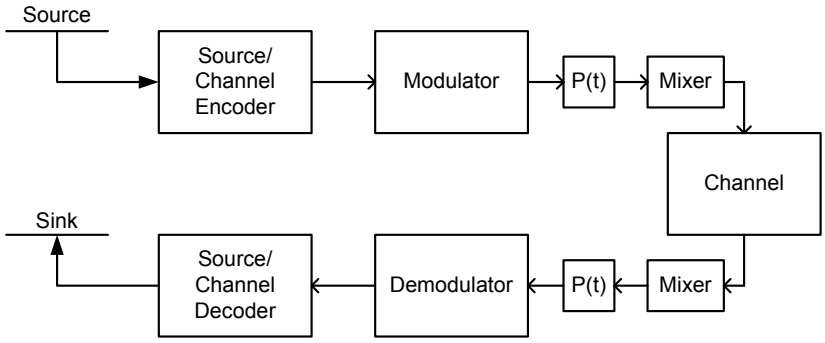

Figure 2.1: A schematic view of a basic communication system.

The transmitter is fed by some signal source (*e.g.* a voice signal) and the source encoder converts that signal into a suitable digital format. The channel encoder then adds redundancy (i.e. extra bits) to the bit sequence to enable error detection and/or error correction at the receiver. The modulator then maps the bit sequence into discrete symbols. There are a number of possible symbol sets but two of the more popular can be seen in Figure 2.2(a) and Figure 2.2(b). The symbols (S_i) are mapped onto a 2-D symbol space with an orthogonal basis expressed using real- and imaginary numbers. Having the symbols in complex format is a convenient expression, in a real transmitter the imaginary- and real parts are separated before being signal processed and finally mixed up to carrier frequency using the same carrier but with a 90° offset (in phase and quadrature phase). This phase offset in the carrier realizes the orthogonal basis expressed by the complex numbers. Transmission scheme like this are called quadrature multiplexed and part of such transmitter can be seen in Figure 2.2(c). The symbol S_i is split into its real and imaginary parts before being processed and mixed up in frequency using carriers with a 90° offset.

The pulse shaping filter is denoted as $p(t)$, it maps the symbols onto a sequence of Nyquist

pulses. If the time between symbols is denoted as T_s (symbol time) then a Nyquist pulse must satisfy for some integer N the relation

$$p(NT_s) = \begin{cases} 1 & \text{if } N = 0 \\ 0 & \text{if } N \neq 0 \end{cases}$$

This means that the pulse only has a value at the current sampling time but is zero for all other sampling times. This can be seen in Figure 2.2(d) where three symbols have been sent through a Nyquist pulse shaping filter. At exactly the symbol time (multiples of the symbol period) the surrounding symbols are zero so no interference between symbols is observed. After the signal has gone through the pulse shaping filter at the transmitter, and turned analog using a DAC (Digital to Analog Converter), it is up converted using a mixer.

A mixer is an essential part for most wireless systems. A typical digital radio performs its signal processing at the baseband, that is between 0 and B [rad/s]. In order to utilize the available spectra in an efficient way, the signal is upconverted to a frequency band pre-allocated for the given application. It is also impractical to transmit a baseband signal so it is necessary to upconverted to the carrier frequency ω_c. Since all signals can be expressed via Fourier analysis by a sum of sinusoids it is enough to consider only a signal $x_b(t) = A_b \sin(\omega_b t)$ where $0 \leq \omega_b \leq B$ and A_b is the amplitude. Mathematically a mixer performs the upconversion in the following way

$$x_c(t) = x_b(t) \sin(\omega_c t) = \frac{A_b}{2} \left[\cos((\omega_c - \omega_b)t) - \cos((\omega_c + \omega_b)t)\right] \tag{2.1}$$

where $\sin(\omega_c t)$ is generated by an oscillator. From the expression in equation (2.1) it can be seen that the signal frequency is now spaced between $\omega_c - B$ and $\omega_c + B$.

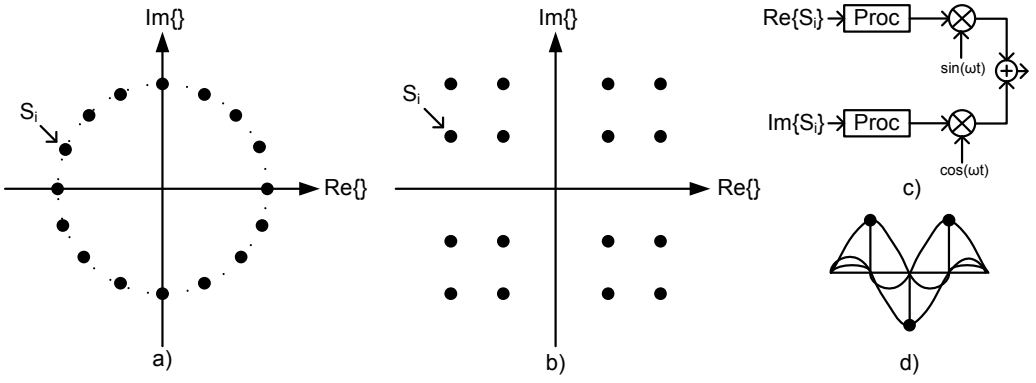

Figure 2.2: a) 16-PSK modulation format (signal constellation) where S_i represents one symbol b) 16-QAM modulation format c) A quadrature multiplexed transmitter. d) 3 symbols that have gone through a pulse shaping filter.

At the receiver the signal is down converted with a mixer, filtered with a matched filter (same kind of filter as at the transmitter) to minimize the effect of noise and then sampled with an analog to digital converter (ADC). Then it is sent through the demodulator followed by

source/channel decoders which undoes the encoding operations at the transmitter. Finally the data sink operates on the data in some way, *e.g.* reproduces a voice signal. A much more detailed discussion can be found in many textbooks such as [1, 53].

2.3 The Wireless Channel

A channel is here defined as the paths over which an electrical signal traverses between a transmitter (Tx) and receiver (Rx). That can include parts of the Tx and Rx, such as amplifiers and oscillators, depending on preference. Wireless channels are specially challenging compared to wired channels. The ether (or transmission media) is firstly shared by all users making it very prone to interference, secondly it is composed of the ever changing environment we all live in making it highly time varying. From a signal processing stand point the channel can introduce noise and other interfering signals as well as inter symbol interference (ISI) and fading. These effects will be discussed in the following sections.

2.3.1 Noise

Additive White Gaussian Noise (AWGN) is a common noise model for numerical and analytical analysis since it approximates many noise sources (*e.g.* thermal noise, shot noise and black body radiation) that are fundamentally different into a single expression. It is additive so that it is added to the signal, it is white meaning that it has the same power for all frequencies within the bandwidth of the system and it is Gaussian meaning that its real- and imaginary values follow a Gaussian distribution. The ratio between signal- and noise power is the signal-to-noise ratio (SNR) defined as

$$\mathrm{SNR} = \frac{\mathrm{E}\left[|r(t)|^2\right]}{\mathrm{E}\left[|n(t)|^2\right]} = \frac{E_s}{N_0 B T_s} = \frac{E_b}{N_0 B T_b} \tag{2.2}$$

where T_s is the symbol time, T_b is the bit time, $N_0 B$ is the noise power, E_s and E_b are bit- and symbol energies respectively, $r(t)$ is the received signal and $n(t)$ is the AWGN noise.
A second noise source (called phase noise) originates from the oscillators downconverting the signal from the carrier frequency to the baseband. Instead of producing a perfect sinusoid as is assumed in (2.1) the sinusoidal output has a small random phase and amplitude fluctuation

$$r(t) = A\left[1 + a(t)\right]\cos\left(\omega_c t + \phi\left(t\right)\right) \tag{2.3}$$

Here A is the amplitude of the wave, $a\left(t\right)$ is the amplitude noise, $\phi\left(t\right)$ is the phase noise and ω_c is the carrier oscillator central angular frequency. The amplitude noise can usually be neglected (because of amplitude limiting mechanisms) while the phase component is more difficult to handle. The origins and distribution of oscillator phase noise will not be discussed here but the most important thing to note is that phase noise will rotate the signal constellation (*e.g.* Figure 2.2) in a random manner and if left untreated will completely ruin the reception. A detailed discussion on phase noise can be found for example in reference [22].

2.3.2 Fading

A radio frequency (RF) signal that is transmitted from one location to another can reach the endpoint along multiple paths. This is because the signal can be reflected off surfaces and thus in a rich environment there is a multitude of copies of the same signal reaching the receiver, each with its own delay, phase and signal strength. These different copies of the signal can combine constructively or destructively so that the signal power is attenuated and we say that we are in a deep fade. Taking the Fourier transform of the channel impulse response the response of the channel to different frequencies can be visualized. If there is a notable discrimination between different frequencies within the signal bandwidth B_s the channel is said to be frequency selective. If the channel is similar within the signal bandwidth the channel is flat. The coherence bandwidth B_c quantifies the bandwidth for which the channel can be considered to be flat. So if the signal bandwidth is smaller than the coherence bandwidth we have a flat channel but if the signal bandwidth is lower we have a frequency selective channel. If the channel is known, that is if the power delay profile is known the coherence bandwidth can be calculated, this is done in [20, ch.3].

Since the properties of a wireless channel depend on the surroundings which can be highly erratic the channel also changes with time. These changes are either due to the movement of the transmitter or receiver or because a change in the environment (*e.g.* a car moves). Coherence time T_c quantifies the speed of these changes and is a statistical measure of the time period over which the channel impulse response is time invariant. If the symbol time T_s is smaller than the coherence time, the channel is said to be slow fading meaning that each symbol sees the same fading for the whole symbol period. If the symbol time is larger than the coherence time the channel exhibits fast fading. [20, ch.3] treats the calculation of the coherence time by using the Doppler spectrum.

A frequency selective channel will distort the signal making the entire system response (matched filters at the Tx and Rx as well as the channel) non-Nyquist. This will in turn cause Intersymbol Interference (ISI) discussed in the next section.
These effects are summarized in Figure 2.3. The channel studied in this thesis is characterized as exhibiting slow and frequency selective fading.

2.3.3 Intersymbol Interference

Intersymbol Interference (ISI) is observed when the current received symbol is affected and distorted by the surrounding symbols. Looking at Figure 2.2(d) it can be seen that if one symbol is shifted in time it will start affecting the surrounding symbols. Since in a multipath environment each symbol can arrive at multiple time slots and/or shifted within its own it is apparent that ISI can ruin the reception if not properly counteracted. Two other mechanisms that can introduce ISI are symbol timing errors and non-Nyquist filter pairs at the Tx and Rx.

The above effects can be seen by looking at the channel impulse response which can be made to include Tx and Rx circuitry, that is filters ($p(t)$) and analog/digital converters for example. An example of a channel impulse response that causes ISI can be seen in Figure 2.4. To see how this channel impulse response causes ISI it can be convolved with a symbol sequence s_n.

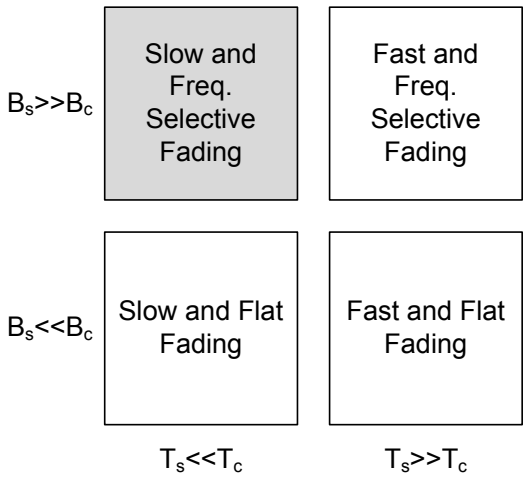

Figure 2.3: Channel characterization. There are four different kinds of channels based on if the signal bandwidth is smaller or larger than the coherence bandwidth and if the symbol time is smaller or larger than the coherence time.

$$r_n = \sum_i h_i s_{n-i} + n_n = h_\delta s_{n-\delta} + \sum_{i \neq \delta} h_i s_{n-i} + n_n \tag{2.4}$$

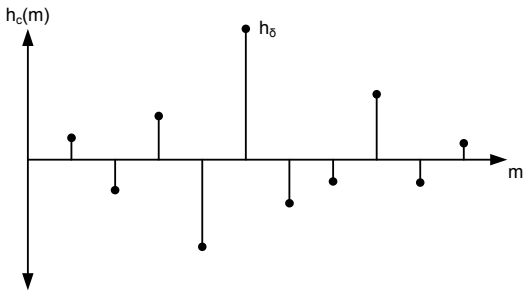

Figure 2.4: An example of a channel impulse response that would cause ISI. Tap marked by h_δ is the central tap seen in (2.4). The rest of the impulse response will then contribute to ISI.

Here n_n is the noise and h_i is the channel impulse response. The first term in the equation above now represents the desired symbol, delayed and with some gain h_δ. The second term is some undesired contribution from the surrounding signals multiplied with some channel gains, this part represents the ISI.

2.4 Microwaves

Frequencies higher than 6 GHz are considered to be unusable for mobile communication because of increased shadowing by obstruction during propagation [40]. These frequencies are

thus more useful when there is a LoS path between transmitter and receiver[1]. Another issue with these high frequencies is their increased attenuation. The received power is proportional to the square of the wavelength due to the electrical effective area of the receive antenna, as can be seen from the free space propagation equation [20, eq. 2.7]

$$\frac{P_r}{P_t} = \left[\frac{\sqrt{G}\lambda}{4\pi d}\right]^2 \tag{2.5}$$

where G is the product of the antenna gains, P_r is the received power and P_t is the transmitted power, d is the distance between the antennas and λ is the wavelength of the carrier. This means that going from 0.3 GHz to 30 GHz introduces 10.000 fold attenuation for the same setup. This can be compensated for in microwave links using highly directional antennas (with large G).

Another more serious phenomenon that is encountered when going up in frequency is the attenuation caused by rain. Figure 2.5 shows the attenuation per km in dB as a function of frequency and rain rates for a horizontally polarized signal. The attenuation will differ somewhat for different polarizations. For links operating at high frequencies even a short hop length can experience outage when there is heavy rain. A common requirement for microwave links is that they are operational 99.999% of the time (i.e. 5-9's availability) which corresponds to a downtime of less than 5 min per year. The link then needs to be able to cope with all rain conditions that appear on average for more than 5 min a year. Heavy rain that statistically only is seen for 5 min/year for a given location is commonly referred to as 5 min rain. For a certain location this sets an upper limit on the distance over which a microwave link can be reliably operated. For Europe the 5 min rain rarely exceeds 50 mm/hr while in south Asia it can exceed 100 mm/hr.

2.5 Dual Polarized Systems

Electromagnetic waves travel in 3D space along a straight line with orthogonal and oscillating electric and magnetic fields (plane wave approximation). The condition is that the fields are orthogonal to each other as well as the direction of propagation. A plane that is perpendicular to the propagation direction will thus contain all of the electromagnetic fields so that it is sufficient to describe them within that plane. For a given wave either of the field components (magnetic or electric) can be oscillating for example along the vertical axis requiring the other field component to oscillate along the horizontal axis.
Since most waves of interest for microwave links travel along the earth surface one can speak of a vertically- or horizontally polarized waves meaning that the electrical field is oscillating in the vertical or horizontal direction respectively. Naturally the wave can be polarized along any direction but the important thing is that each polarization can be broken down into these two components that form an orthogonal basis. A dipole antenna is a good example of a polarized antenna since it will only transmit and receive one polarization in the ideal case. Having two ideal polarized antennas rotated so that they are orthogonal to each other results

[1] Today's microwave links operate in frequency bands between 6 and 38 GHz

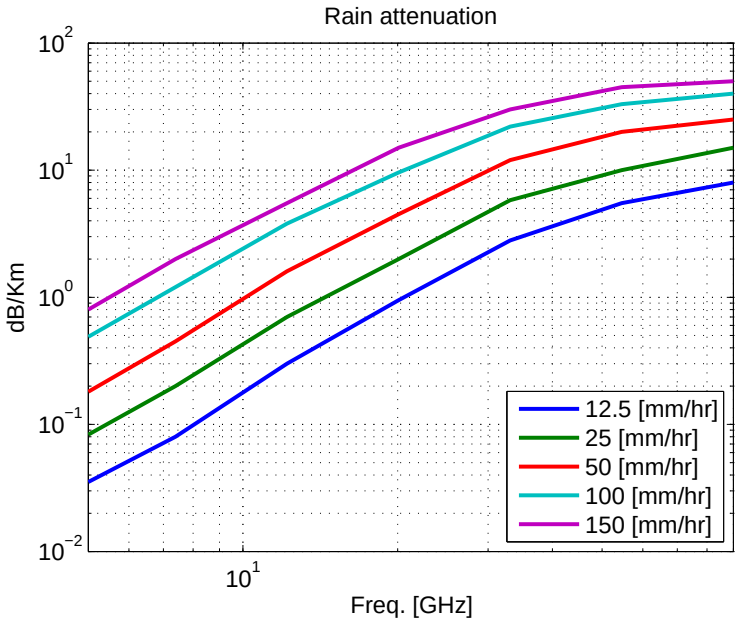

Figure 2.5: Signal attenuation caused by rain for different frequencies for horizontally polarized signals [12].

in two independent channels doubling the capacity of the system for a high SNR. A real system will always experience imperfections leading to crosstalk between polarizations. This is due to the fact that antennas can not be perfectly polarized and channel conditions may be in such a way that they treat the polarizations differently (*e.g.* rain) resulting in leakage between the channels. This leakage can be quantified using the channel cross-polarization discrimination (XPD) factor. It describes how much power from one polarization leaks into another polarization thus reducing the systems ability to separate between the two polarizations. It is defined for the vertical- and horizontal components respectively as

$$\mathrm{XPD}_V = \frac{\mathrm{E}\left\{|h_{V,V}|^2\right\}}{\mathrm{E}\left\{|h_{H,V}|^2\right\}} \quad \mathrm{XPD}_H = \frac{\mathrm{E}\left\{|h_{H,H}|^2\right\}}{\mathrm{E}\left\{|h_{V,H}|^2\right\}} \tag{2.6}$$

where for example $h_{V,H}$ is the flat channel impulse response between the vertically polarized Tx and horizontally polarized Rx. The higher the XPD the better isolation between different polarizations. Here these two XPDs are combined into one using the assumption that the they are the same for both polarizations, i.e. $\mathrm{XPD} = \mathrm{XPD}_V = \mathrm{XPD}_H$

Chapter 3

MIMO Systems

Multiple-input-multiple-output (MIMO) systems are those having (as the name suggests) more than one input and output, here this is taken to mean that both Tx and Rx have multiple antennas operating over the same bandwidth. There has been a great interest in research into wireless MIMO technologies for the last decade which was sparked by ground breaking work done by Winters [50] and Foschini [16] in 1992. These papers predicted remarkable spectral efficiencies for wireless communication systems with multiple transmitters and receivers. As time progressed interest would grow since the value of spectrum seemed to have no limits, this was reflected in the radio spectrum auctions in for example Germany and Britain during the height of the dot-com boom in 2000. There companies bought relatively small bandwidths for 100s of millions of pounds or Euros. The ability to squeeze even more bits through using smaller portions of spectrum became very valuable indeed. The interest subsided though slightly after the dot-com burst in 2001 but the technology never lost its appeal and now there are quite a few standards incorporating MIMO (*e.g.* LTE, WiMAX and IEEE 802.11n) and quite a few products using it. It can be said that MIMO is a proven technology with an abundance of published material, a good overview of MIMO can be found for example in [40]. A pre-condition for the great majority of this work is that the transmitter and/or the receiver are in a rich scattering environment unlike the line of sight links examined in this thesis. For a mobile scenario where the handset is surrounded by objects reflecting the signals from many different directions without any path dominating, the technology is at its best. In fact, the LoS MIMO path between multiple Tx's and Rx's have for practical mobile applications been considered useless as the difference in path lengths is too short to reach orthogonality between the received signals.
Moving the higher frequencies, *e.g.* microwaves, and requiring a fixed setup solves this problem, enabling MIMO to work even with only the direct paths present, but at the expense of larger antenna spacings as well as requirements on the distance between transmitter and receiver. It should be noted that the indoor environment can also be suitable since only short distances are needed. LoS MIMO is a fairly recent research topic, papers focusing on the indoor environment [25, 27] and outdoor environment [18, 14, 39] have been published on LoS MIMO over the years but the main attention has always been on the classical MIMO multipath environment. Excellent work on LoS MIMO has also been done by Bøhagen [5].

Besides spatial multiplexing, a second advantage of MIMO systems is that of adaptive directivity called beamforming or interference cancellation so that an array of non-directive

antennas can be electrically controlled to have a large gain in some direction while cancelling others (containing an interfering source for example). Diversity gain can also be obtained from the added antennas. These techniques are called smart antenna techniques and are discussed in [4, 23, 36].

3.1 Narrowband MIMO

A simple schematic view of a MIMO system can be seen in Figure 3.1. Here data enters the MIMO transmitter and is processed and distributed between the Tx antennas. The signal is transmitted over a channel described by the channel matrix **H**. The signals then arrive at the Rx antennas combined, it is then the job of the MIMO receiver to separate and process the incoming signal streams to reproduce (hopefully) the same data stream as at the Tx.

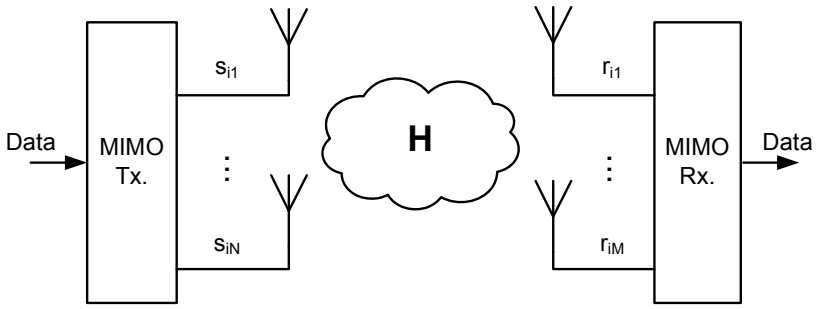

Figure 3.1: A block diagram of a simple MIMO system with N transmit antennas and M receive antennas.

Narrowband channels are called narrowband since they treat all the frequency components within the bandwidth of the signal the same (symbol duration is much larger than the multi-path delay spread $T_s >> T_m$), that is the frequency response is flat. That is to say that the received signals are only attenuated, delayed and phase shifted which means that each channel gain can be described (neglecting delay) by a single complex number. The whole channel which is made up of multiple paths can then be specified by a channel matrix **H**. Having N transmit antennas and M receive antennas and L_B symbols to be transmitted through each Tx antenna the system is described by

$$\begin{bmatrix} r_{11} & \cdots & r_{1M} \\ \vdots & \ddots & \vdots \\ r_{L_B1} & \cdots & r_{L_BM} \end{bmatrix} = \begin{bmatrix} s_{11} & \cdots & s_{1N} \\ \vdots & \ddots & \vdots \\ s_{L_B1} & \cdots & s_{L_BN} \end{bmatrix} \begin{bmatrix} h_{11} & \cdots & h_{1M} \\ \vdots & \ddots & \vdots \\ h_{N1} & \cdots & h_{NM} \end{bmatrix} + \begin{bmatrix} n_{11} & \cdots & n_{1M} \\ \vdots & \ddots & \vdots \\ n_{L_B1} & \cdots & n_{L_BM} \end{bmatrix} \tag{3.1}$$

where r_{im} is symbol number i from receive antenna m, s_{im} are the transmitted symbols, h_{nm} are complex values describing the channel between transmit antenna n and receive antenna

m and finally n_{im} represents the Gaussian noise. Using matrix notation (3.1) can simply be written as $\mathbf{r} = \mathbf{sH} + \mathbf{n}$. The scalar values of the channel matrix $\mathbf{H}$ can be written as $h_{nm} = \alpha_{nm} \exp(j\theta_{nm})$ where α_{nm} and θ_{nm} are the amplitude- and phase of the channel respectively.

The problem of the receiver is to counteract the effects of the channel, one way to do that is to find a matrix $\mathbf{B}$ so that $\mathbf{H} \cdot \mathbf{B} = \mathbf{I}$ if $N < M$ or $\mathbf{B} \cdot \mathbf{H} = \mathbf{I}$ if $N \geq M$. Each Rx antenna receives symbols from all Tx antennas so it is the job of the receiver to separate the data streams to obtain an estimate of what was actually transmitted. Assuming receiver channel knowledge, that is that $\mathbf{H}$ is known at the Rx, $\mathbf{B}$ can be found by using the Moore-Penrose Matrix Inverse

$$\mathbf{B} = \begin{cases} \left(\mathbf{H^H H}\right)^{-1} \mathbf{H}^{\mathrm{H}} & \text{if} \quad N \geq M \\ \mathbf{H}^{\mathrm{H}} \left(\mathbf{H H}^{\mathrm{H}}\right)^{-1} & \text{if} \quad N < M \end{cases} \tag{3.2}$$

This can then always be done given that the inverse exists which is always the case if $\mathbf{H}$ is full rank. The rank of $\mathbf{H}$, denoted R_H, defines how many linearly independent columns a matrix has which again corresponds to the number of achievable independent parallel channels that can be obtained. The rank always satisfies $R_H \leq \min(N, M)$ meaning that the number of independent channels obtainable from $\mathbf{H}$ is always equal or less than the lower antenna number at the Rx or Tx. The Pseudoinverse in (3.2) will enhance noise[1] and is not the optimal way if there is some prior knowledge about the noise distribution and power (*e.g.* MMSE estimate [2]).

When the channel is known at the receiver or transmitter it is called channel state information at the receiver (CSIR) or channel state information at the transmitter (CSIT) respectively. There are three basic schemes that are used to obtain CSIR and these are: Training based, semi-blind and blind channel estimations. Training based methods [45] send training symbols (symbols that are known at the Rx beforehand) and use them to compare what was received and what was sent to calculate an estimate of the channel. These training symbols can then be sent periodically in certain time slots within the symbol stream to keep track of the changing channel. Blind methods (*e.g.* [52]) are based on the fact that the Rx knows the modulation scheme and thus has some knowledge about how a transmitted signal should look like. It can thus compare the shape of the received symbols to what could have been transmitted. Since what was actually transmitted is unknown these methods can be slow to converge and may suffer from some phase ambiguity even after convergence. Semi-blind methods use some combination of training based and blind methods. The training data is sent only in the beginning [37, 10, 24] or is embedded within the data symbols called superimposed pilots (SIP) [8, 9, 48, 47, 26, 35]. They can get rid of the phase ambiguity as well as improving the convergence speed compared to blind methods.
CSIT is then usually obtainable by the Rx sending information about the channel to the Tx or the Tx using channel reciprocity where applicable.

[1] Since when removing the channel affects the noise is not considered.
[2] If $N \geq M$ then $\mathbf{B} = (\mathbf{H^H H} + \sigma_w^2 \mathbf{I})^{-1} \mathbf{H}^{\mathrm{H}}$ where σ_w^2 is the noise variance.

3.1.1 Singular Value Decomposition and Condition Numbers

As mentioned before not all environments are suitable for MIMO transmission. If for example the channel has one dominating path such as in a LoS environment then the capacity of the MIMO system should suffer. To see this we need to apply some mathematical method from linear algebra, namely singular value decomposition (SVD). For every $N \times M$ matrix $\mathbf{H}$ one can write

$$\mathbf{H} = \mathbf{U}\mathbf{\Sigma}\mathbf{V}^{\mathrm{H}} \tag{3.3}$$

where $\mathbf{U}$ and $\mathbf{V}$ are $N \times N$ and $M \times M$ unitary matrices [3] respectively. $\mathbf{\Sigma}$ is a $M \times N$ diagonal matrix of singular values σ_i of $\mathbf{H}$. If $\mathbf{V}$ is now known at the Tx (CSIT) and $\mathbf{U}$ at the receiver (CSIR) then the symbols at the Tx can be multiplied by $\mathbf{U}^{\mathrm{H}}$ before being transmitted and the received symbols multiplied by $\mathbf{V}$ after being received. This parallelizes the MIMO channel into R_H independent SISO channels with gains $\sigma_1,\ \sigma_2,\ ,\ldots\ ,\sigma_{R_H}$ (see Appendix B for further discussion). This can be seen in Figure 3.2. Since now these singular values represent the gain of each SISO channel the best channel matrix is the one that has equal gains or in other words the singular values should be identical. The larger the ratio between these singular values the worse the MIMO channel is. To describe the theoretical performance of a MIMO channel one needs to know all the singular values. It is though clear that it is always the smallest singular value that will affect the BER the most. In this thesis the condition number is introduced as a measure on how good a MIMO channel is. The condition number is the ratio between the largest- and the smallest singular value. When the channel is perfectly conditioned the condition number is one but it will grow as the channel condition worsen. The condition number is defined as

$$\kappa = \frac{\max(\sigma_i)}{\min(\sigma_i)} \tag{3.4}$$

The number has no mathematically rigorous coupling to BER or penalty but a rule of thumb is that if the condition number is large the penalty should be close to the square of the condition number. That is the SNR needs to be raised by κ^2 to achieve the same performance as if the condition number was one. One has also to remember that penalty is usually expressed in dB while condition number is in a linear scale.

As an example lets consider two 2x2 MIMO channels $\mathbf{H}_1$ and $\mathbf{H}_2$ given as

$$\mathbf{H}_1 = \begin{bmatrix} 1 & e^{j\pi/2} \\ e^{j\pi/2} & 1 \end{bmatrix} \quad \text{and} \quad \mathbf{H}_2 = \begin{bmatrix} 1 & 1 \\ 1 & 1 \end{bmatrix} \tag{3.5}$$

Doing the SVD so that $\mathbf{H}_1 = \mathbf{U}_1\mathbf{\Sigma}_1\mathbf{V}_1^{\mathrm{H}}$ and $\mathbf{H}_2 = \mathbf{U}_2\mathbf{\Sigma}_2\mathbf{V}_2^{\mathrm{H}}$ we get the following singular value matrices

$$\mathbf{\Sigma}_1 = \begin{bmatrix} \sqrt{2} & 0 \\ 0 & \sqrt{2} \end{bmatrix} \quad \text{and} \quad \mathbf{\Sigma}_2 = \begin{bmatrix} 2 & 0 \\ 0 & 0 \end{bmatrix}$$

The singular values for the first channel are $\sigma_{11} = \sigma_{12} = \sqrt{2}$ while the singular values for the second channel are $\sigma_{21} = 2$ and $\sigma_{22} = 0$. The condition numbers are thus

[3] A unitary matrix $\mathbf{H}$ satisfies $\mathbf{H}^{\mathrm{H}}\mathbf{H} = \mathbf{H}\mathbf{H}^{\mathrm{H}} = \mathbf{I}$

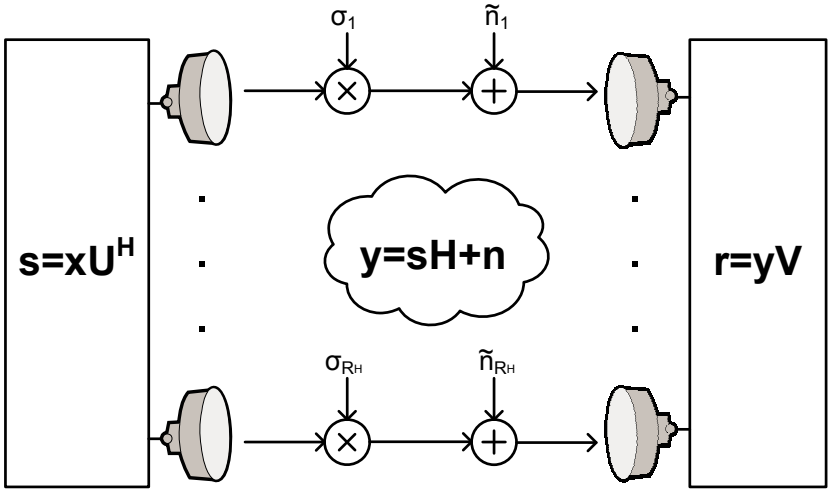

Figure 3.2: Using SVD the MIMO channel can be parallelized into R_H independent SISO subchannels with gains σ_k.

$$\begin{aligned} \kappa_1 &= \frac{\sqrt{2}}{\sqrt{2}} = 1 \\ \kappa_2 &= \frac{2}{0} \rightarrow \infty \end{aligned} \tag{3.6}$$

The second channel is rank deficient ($R_H = 1$) and does in fact not support MIMO transmission while the first one is full rank ($R_H = 2$) and is ideal for MIMO. This can also easily be seen if we try to invert $\mathbf{H}_1$ and $\mathbf{H}_2$ since $\mathbf{H}_2$ is singular and not possible to invert.

3.1.2 Channel Capacity

The capacity of a SISO system is given by the Shannon-Hartley theorem

$$C = \log_2 (1 + \bar{\gamma}) \tag{3.7}$$

where $\bar{\gamma}$ is the average SNR. The capacity of a MIMO system was derived by Telatar in 1995 [44]. The result is

$$C = \log_2 \left[\det \left(I_M + \frac{\bar{\gamma}}{N} \mathbf{H}\mathbf{H}^{\mathrm{H}} \right) \right] = \sum_{i=1}^{\min(N,M)} \log_2 \left(1 + \frac{\bar{\gamma}}{N} \lambda_i \right) \tag{3.8}$$

where λ_i is a eigenvalue of $\mathbf{H}\mathbf{H}^{\mathrm{H}}$. The eigenvalues and singular values are related by $\lambda_i = \sigma_i^2$. Looking back at the matrices defined in (3.5) the capacity can thus be calculated using the singular values obtained in the previous example for a given SNR. Setting the SNR to 20 dB the capacity becomes

$$\begin{aligned} C_1 &= \sum_{i=1}^{2} \log_2 \left(1 + 100 \cdot \sqrt{2}^2 \right) \approx 15.3 \ \ [\text{bps/Hz}] \\ C_2 &= \log_2 \left(1 + 100 \cdot 2^2 \right) + \log_2 \left(1 + 100 \cdot 0^2 \right) \approx 8.6 \ \ [\text{bps/Hz}] \end{aligned} \tag{3.9}$$

As can be seen the first channel has almost twice as high capacity compared to the second one. This is because $\mathbf{H}_2$ has rank 1 and only supports one data stream. If the SNR has a lower value the capacity gain of case 1 in the above equation will be reduced. Thus MIMO works best at high SNR which is most often readily available when there is LoS.
It is also noteworthy to mention that if the Tx knows the channel (CSIT) he can allocate more power to the better channel thus increasing the capacity (*e.g.* waterfilling). Assuming that the Tx in case 2 allocates double the power to the better channel and no power to the other one and the SNR has the relatively low value of 4 dB the result becomes

$$\begin{aligned} C_1 &= \sum_{i=1}^{2} \log_2\left(1 + 2.5 \cdot \sqrt{2}^2\right) \approx 5.2 \ \ [\text{bps/Hz}] \\ C_2 &= \log_2\left(1 + 2.5 \cdot 2 \cdot 2^2\right) \approx 4.4 \ \ [\text{bps/Hz}] \end{aligned} \tag{3.10}$$

3.2 Line-of-Sight MIMO

A properly designed MIMO system in a rich multipath environment will have a low correlation of phase and amplitude between different receive antennas. Replacing the rich multipath environment with one dominating LoS path will correlate the channels so that there will always be the same phase offset and amplitude between the Tx- and Rx antennas pairs over time. If the antennas are placed closely together the channel matrix will become a matrix with all elements identical which is singular reducing the capacity to a SISO system (3.7).

In LoS the phase of each channel gain h_{nm} is a function of the geometry and carrier frequency but is not governed by a statistical distribution as in non-LoS MIMO. By varying the separation between the transmitting and receiving antennas a static phase shift between the antennas can be introduced thus effecting the channel matrix. This is illustrated in Figure 3.3 where the different paths are marked h_{nm}. The phase of the received signal stream will depend on the length of the path (and carrier frequency) so different paths can have different phases. The normalized channel matrix can then be expressed as

$$\mathbf{H} = \begin{bmatrix} h_{11} & \cdots & h_{1M} \\ \vdots & \ddots & \vdots \\ h_{N1} & \cdots & h_{NM} \end{bmatrix} = \begin{bmatrix} \exp(jkd_{11}) & \cdots & \exp(jkd_{1M}) \\ \vdots & \ddots & \vdots \\ \exp(jkd_{N1}) & \cdots & \exp(jkd_{NM}) \end{bmatrix} \tag{3.11}$$

where $k = 2\pi/\lambda$ and d_{nm} represents the physical distances between the antennas.

3.2.1 Optimal Antenna Separation

As mentioned earlier the LoS channel is described by the geometry (in units of wavelengths) of the antenna placements. Finding the optimal configuration is thus a geometrical problem. To solve it some preferred antenna arrangement must be assumed. Here the antennas are considered to be organized in linear arrays where the Tx- and Rx antennas are separated by d_t and d_r respectively as shown in Figure 3.4. The total length of the arrays are then $(N-1)d_t$ and $(M-1)d_r$. The Tx and Rx antennas can be tilted in the plane of transmission by θ_t and θ_r respectively and the Rx array can be rotated out of plane by ϕ_r as is shown in the right

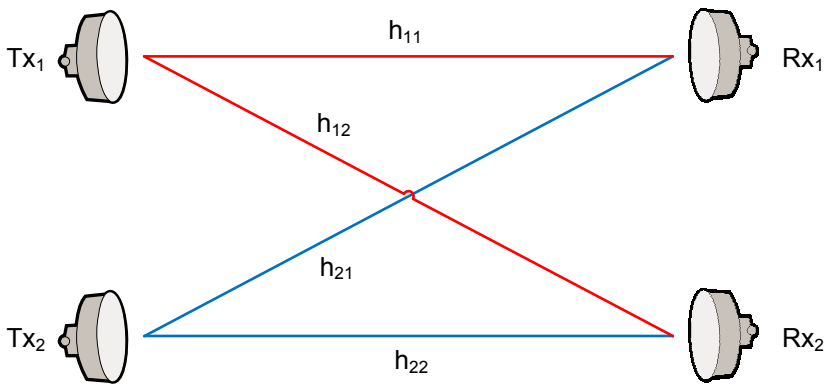

Figure 3.3: A schematic view of a 2x2 LoS MIMO system. There are four channels h_{ij} describing the phase and amplitude of each path.

side of Figure 3.4. Considering the origin to be at Tx_0 and denoting n and m to be the index of Tx and Rx antennas respectively, starting with zeros and going up to $N-1$ and $M-1$, then doing the derivation similar as in [5] the vectors describing the antenna placements are given by

$$\begin{aligned} \mathbf{a}_n^t &= nd_t \sin(\theta_t)\mathbf{n}_x + nd_t \cos(\theta_t)\mathbf{n}_z \\ \mathbf{a}_m^r &= [D + md_r \sin(\theta_r)\cos(\phi_r)]\mathbf{n}_x \\ &\quad + md_r \cos(\theta_t)\mathbf{n}_z + md_r \sin(\theta_r)\sin(\phi_r)\mathbf{n}_y \end{aligned} \tag{3.12}$$

where $\mathbf{n}_x$, $\mathbf{n}_y$ and $\mathbf{n}_z$ are unit vectors along the x-, y- and z-axis respectively. To calculate the distance between antenna m and n the absolute value of the difference of the vectors above can be taken. This corresponds then to the Euclidean distance between the antennas

$$\begin{aligned} d_{nm} &= |\mathbf{a}_m^r - \mathbf{a}_n^t| = [(D + md_r \sin(\theta_r)\cos(\phi_r) - nd_t \sin(\theta_t))^2 \\ &+ (md_r \sin(\theta_r)\sin(\phi_t))^2 + (md_r \cos(\theta_r) - nd_t \cos(\theta_t))^2\ ]^{1/2} \end{aligned} \tag{3.13}$$

Using the approximation $\sqrt{A^2+B} \approx A + \frac{B}{2A}$ if $A >> B$, which is true for the equation above since the distance D is much larger than the antenna spacing, then (3.13) can be written as

$$\begin{aligned} d_{nm} &\approx D + md_r \sin\theta_r \cos\phi_r - nd_t \sin\theta_t \\ &+ \frac{1}{2D}\left[(md_r \cos\theta_r - nd_t \cos\theta_t)^2 + (md_r \sin\theta_r \sin\phi_r)^2\right] \\ &= D + md_r \sin\theta_r \cos\phi_r - nd_t \sin\theta_t \\ &+ \frac{1}{2D}\left[m^2 d_r^2 \cos^2\theta_r + n^2 d_t^2 \cos^2\theta_t - 2mnd_t d_r \cos\theta_t \cos\theta_r + m^2 d_r^2 \sin^2\theta_r \sin^2\phi_r\right] \end{aligned}$$

Here another simplification has been made which is $D + md_r \sin(\theta_r) - nd_t \sin(\theta_t) \approx D$ for the denominator which is true since the distance between the Tx and Rx is much larger than the antenna separation and is also true for small angles.

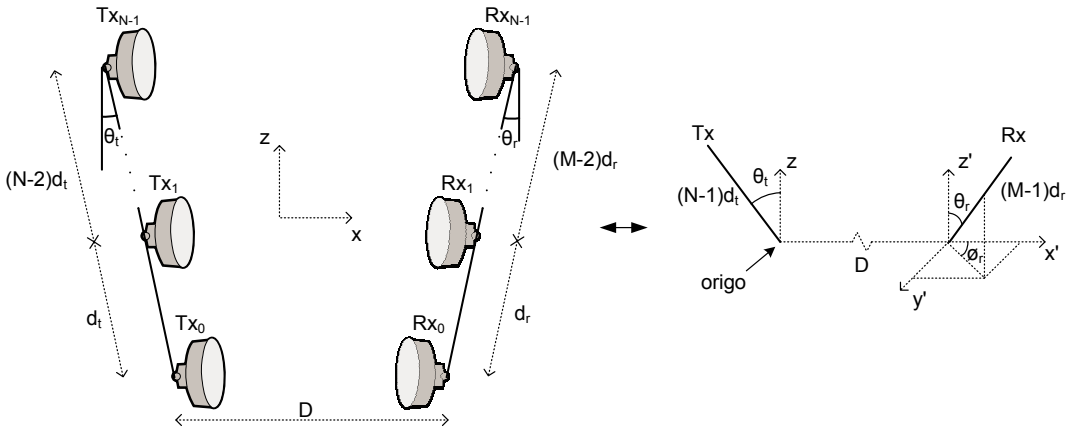

Figure 3.4: Tx antennas and Rx antennas organized in an array. The separation between the Tx and Rx antennas is d_t and d_r respectively, while θ_t and θ_r represents the angles of the antenna arrays with respect to the z axis. D is the distance between the antenna arrays.

Now that the distances between the antennas have been calculated a criteria for the optimal antenna separation should be found. One way to accomplish this is to note that the optimal separation should give the highest capacity or in other words should maximize (3.8). This corresponds to maximizing the product of the eigenvalues λ_i. It is known from linear algebra that trace$\{\mathbf{W}\} = \sum \lambda_i = NM$ for a normalized unit power matrix $\mathbf{H}$ if

$$\mathbf{W} = \begin{cases} \mathbf{H}\mathbf{H}^{\mathrm{H}}, & N \leq M \\ \mathbf{H}^{\mathrm{H}}\mathbf{H}, & N > M \end{cases}$$

Then it is easy to show that (3.8) is maximized by $\lambda_1 = \lambda_2 = \cdots = \text{constant}$. This is obtained if $\mathbf{H}$ has orthogonal rows for $N \leq M$ or orthogonal columns for $N > M$. Defining the rows of $\mathbf{H}_{LoS}$ as $\mathbf{h}_n$, orthogonality between them can be expressed as $< \mathbf{h}_n, \mathbf{h}_i >_{n \neq i} = 0$. This condition can then be used to produce the expression for the optimal antenna separation (if $N \leq M$)

$$\begin{aligned} < \mathbf{h}_n, \mathbf{h}_i >_{n \neq i} &= \sum_{m=0}^{M-1} \exp\left(jk(d_{nm} - d_{im})\right) \\ &= \sum_{m=0}^{M-1} \exp\left(j2\pi \frac{d_t d_r \cos(\theta_r)\cos(\theta_t)}{\lambda D}(i-n)m\right) \\ &\cdot \quad \exp\left(jk[(i-n)d_t \sin(\theta_t) + \frac{1}{2D}(i-n)^2 d_t \cos^2(\theta_t)]\right) = 0 \\ &\Rightarrow \quad \frac{\sin\left(k d_t d_r \cos(\theta_r)\cos(\theta_t)(i-n)M/2D\right)}{\sin\left(k d_t d_r \cos(\theta_r)\cos(\theta_t)(i-n)/2D\right)} = 0 \\ &\Rightarrow \quad d_t d_r = \frac{\lambda D}{M \cos(\theta_t)\cos(\theta_r)} K \end{aligned} \tag{3.14}$$

where K is a positive odd number usually chosen to be one since that gives the smallest optimal antenna separation. Doing a similar derivation for the case $N > M$ would yield

the same expression only with M replaced with N. Defining $V = \min(M, N)$ a general requirement on the antenna separation is given as

$$d_t d_r = \frac{\lambda D}{V \cos(\theta_t) \cos(\theta_r)} K \tag{3.15}$$

Looking at the optimal antenna spacings given in (3.15) it can be seen that the separation increases as the distance D increases and that it decreases as the carrier frequency f_c increases (since $\lambda = c/f_c$). From an installation point of view it is often practical to chose $\theta_t = \theta_r = 0$ and $K = 1$. This is done in Figure 3.5 where the optimum antenna separation is plotted against distance and for different carrier frequencies.

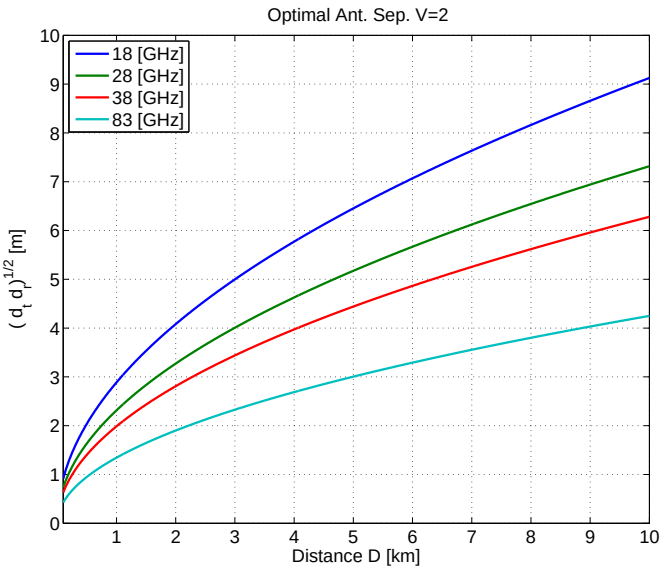

Figure 3.5: Optimal antenna separation for a 2x2 SS LoS MIMO system, plotted against distance for a few carrier frequencies. If the separation at both the Tx and Rx is chosen to be the same $d_t = d_r = d$ then the values on the y-axis correspond directly to d.

Other geometries of the antenna setup at Tx and Rx can be chosen as well. One such approach is to arrange the antennas in an equilateral rectangle (minimum of 4 antennas needed at Tx and Rx) also called uniform planar array. The calculations yield almost the same result as for the linear antenna array as is shown in reference [6].

There might be a few different reasons why the antennas are not placed with the optimal separation. The most common ones are perhaps that the required separation might be too large to accommodate at the site and that all transmission systems have some bandwidth, it is only possible to optimize for one frequency. Defining the parameter η as

$$\eta = \sqrt{\frac{d_t d_r}{(d_t d_r)_{\text{opt}}}} \tag{3.16}$$

to quantify the deviation from optimality. Choosing $d_t = d_r = d$, then (3.16) reduces to

$\eta = d/d_{\text{opt}}$. The condition number as a function of η for a 2x2 LoS MIMO is plotted in Figure 3.6. The condition number is at its lowest at $\eta = \sqrt{K}$ where $K = 1, 3, 5, \ldots$, the condition number approaches infinity for $K = 0, 2, 4, \ldots$.

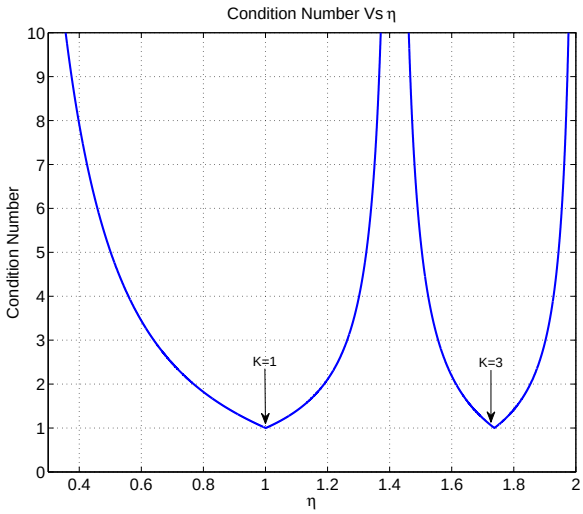

Figure 3.6: The condition number as a function of η defined in (3.16) for a 2x2 LoS MIMO system.

The condition number for a 2x2 LoS MIMO is derived analytically in Appendix A.1 and is given by

$$\kappa = \sqrt{\frac{2 + [2 + 2\cos(\pi\eta^2)]^{1/2}}{2 - [2 + 2\cos(\pi\eta^2)]^{1/2}}} \tag{3.17}$$

3.2.2 Vector Visualization for LoS MIMO

An alternative way of understanding a LoS MIMO system would be to use vector notation. For a 2x2 LoS MIMO system it can be seen that for the optimum case there should be a 90° phase shift at the carrier between Tx antenna n and Rx antennas $m \neq n$ (because of the condition $< \mathbf{h}_i, \mathbf{h}_n >_{i \neq n} = 0$). This can be visualized graphically using a vector representation of the signals. Consider first Figure 3.7a) where the Tx- and Rx antennas are phase locked and there is a 90° phase shift at the carrier frequency between paths d_{nn} and d_{nm} where $n \neq m$. Both receive antennas receive a signal that is a combination of both transmitted signals only with different phases. By rotating the received signals and combining them the combined signal streams can be separated. This is true even though the transmitters are not phase locked (Figure 3.7b-c). If however the phase difference between the direct- and diagonal paths is less than 90° as it is in Figure 3.7d the resulting signals will have less power and are thus more susceptible to noise. This corresponds to a suboptimal situation which can also be seen from the high condition number of the LoS channel matrix.

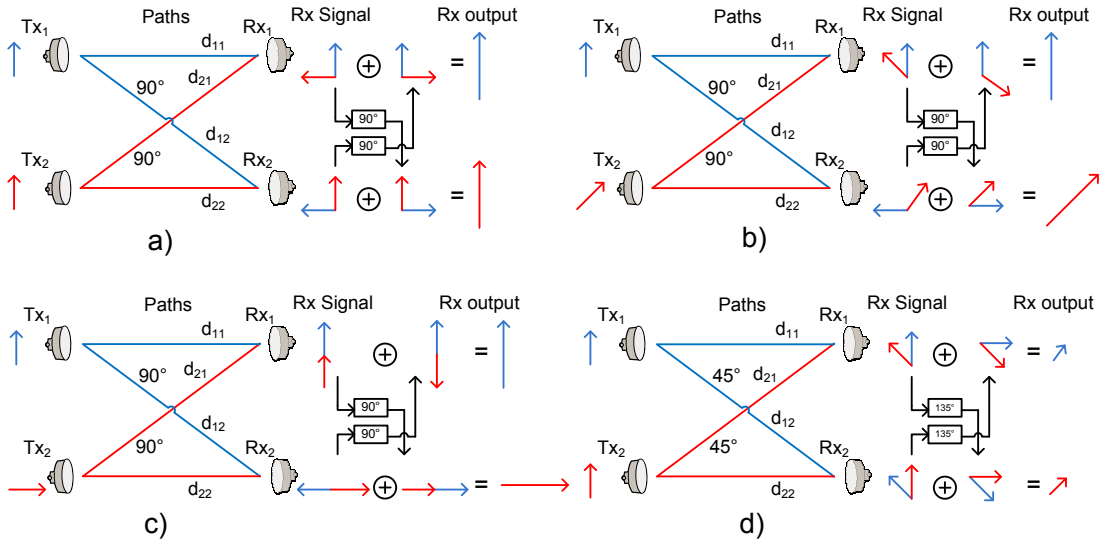

Figure 3.7: Separating the signals streams in a 2x2 LoS MIMO. All figures assume that the distances d_{ii} are a multiple of the wavelengths so that the received signal has the same phase rotation as the transmitted one. 90° difference between the direct- and diagonal paths for a-c, 45° for d. a) The Tx signals are phase locked (0° phase difference between them). b) 45° phase difference between Tx signals. c) 90° phase difference. It is interesting to note that there is no signal strength at Rx antenna 2. d) 0°.

Figure 3.7c) is an interesting special case. There Rx_2 receives no power while Rx_1 receives double, this happens because the signals combine constructively at Rx_1 while they combine destructively at Rx_2. Having a constant modulus signal constellation such as 4QAM the symbols will always have the same power but will instead be rotated differently. If Tx_2 transmits a symbol with a 90° phase shift compared to Tx_1 as is depicted in Figure 3.7c) Rx_2 receives no power. But if the receivers follows the simple procedure of rotating the received symbol back 90° and summing up between the branches the correct symbols will still be recovered.

3.2.3 Grating Lobes

A third approach for understanding LoS MIMO would be through grating lobes. Having two spatially separated transmitting antennas operating in the same bandwidth and carrier frequency will create gain patterns in the far field called grating lobes. For the setup in Figure 3.8 the receiver will see different signal strengths depending on the physical angle ϕ and electrical angle α for a fixed Tx antenna separation and frequency. We will start with the case when both Tx's are transmitting the same signal which will result in a static gain pattern.
Calculating the distances d_1 and d_2 using the law of cosines one gets

$$\begin{aligned} d_1^2 &= d_t^2/4 + D^2 - d_t D\cos(\phi) \\ d_2^2 &= d_t^2/4 + D^2 + d_t D\cos(\phi) \end{aligned} \tag{3.18}$$

The gain (relative to a single Rx antenna) can also be expressed as

$$
\begin{aligned}
G(\phi,\alpha) &= \frac{1}{T_{sc}}\int_0^{T_{sc}} \left(\sin(\omega t + d_1 k) + \sin(\omega t + d_2 k + \alpha)\right)^2 dt \\
&= \cos(d_1 k - d_2 k - \alpha) + 1 \\
&= \cos(k\Delta d + \alpha) + 1
\end{aligned} \tag{3.19}
$$

where $\Delta d = d_2 - d_1$.

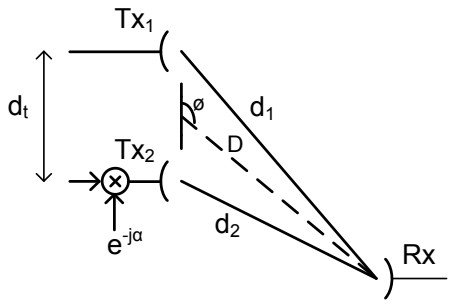

Figure 3.8: Two Tx antennas both transmitting the same signal. The observed signal strength or gain will depend on the angle between the Tx and Rx.

The grating lobes should have the same shape independent of D if the receiver is situated in the far field. For this to be true Δd needs to be constant if ϕ and d_t are constant.

$$
\begin{aligned}
(d_2 - d_1)^2 &= \left(d_1^2 + d_2^2 - 2d_1 d_2\right) \\
&= \frac{d_t^2}{2} + 2D^2 - \sqrt{\frac{d_t^4}{4} + 4D^4 + 2d_t^2 D^2 - 4d_t^2 D^2 \cos^2(\phi)} \\
&\approx \frac{d_t^2}{2} + 2D^2 - 2D^2 - \frac{d_t^4/4 + 2d_t^2 D^2 - 4d_t^2 D^2 \cos^2(\phi)}{2D^2} \\
&= d_t^2 \cos^2(\phi) - \frac{d_t^4}{16D^2}
\end{aligned} \tag{3.20}
$$

where the approximation $\sqrt{A^2 + B} \approx A + \frac{B}{2A}$ if $A^2 >> B$ was used in the third step. For $D >> d_t^2$ (3.20) can be written as

$$
\Delta d \approx d_t \cos(\phi) \tag{3.21}
$$

For two transmit antennas separated by a certain distance, (3.19) describes the power gain of the received signal for an observer in the far field. Envisioning an observer moving around the antenna array in the far field and measuring the signal strength it can be seen that as the physical separation in wavelengths between the transmit antennas grows the faster the signal strength will vary. Combining (3.19) and (3.21) it is easy to see how this is true

$$
G(\phi,\alpha) = \cos(k\Delta d + \alpha) + 1 \approx \cos\left(\frac{2\pi}{\lambda} d_t \cos(\phi) + \alpha\right) + 1
$$

As the ratio d_t/λ increases then the gain expressed above will vary faster as ϕ is varied. This can also be visualized looking at Figure 3.8, the larger d_t is the larger the change in Δd for some $\Delta\phi$. If now the transmitter would like to put the receiver in a null gain it can do so by varying α. α represents the electrical angle that is the phase of the signal and thus a full 180° degree phase offset is required to go from full gain to a null. The effects of changing α and varying the frequency (or antenna separation) can be seen in Figure 3.9.

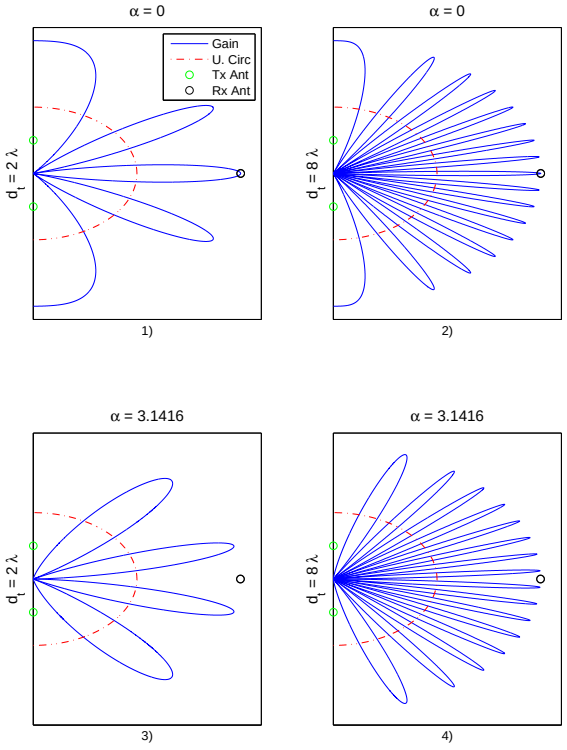

Figure 3.9: Gain pattern (grating lobes) for two antennas separated by d_t. The gain varies faster with angle as the antenna separation increases in wavelengths. 1) $\alpha = 0$ and $d_t = 2\lambda$. 2) $\alpha = 0$ and $d_t = 8\lambda$. 3) $\alpha = \pi$ and $d_t = 2\lambda$. 4) $\alpha = \pi$ and $d_t = 8\lambda$.

As the derivation in section 3.2.1 showed, the separation between Rx antennas and Tx antennas (denoted d_r and d_t respectively) should be in such a way that there is a 90° phase shifts between the direct- and diagonal paths. Setting the antenna separations so that (3.14) is satisfied and plotting the gain each Rx antenna sees while rotating the Tx antenna array an interesting pattern emerges. This can bee seen in Figure 3.10. When Rx_2 has a deep fade Rx_1 has maximum gain and vice versa. In LoS MIMO we are usually interested in spatially multiplexed systems so that each Tx antenna is transmitting different symbol streams. If the symbols on each Tx antenna have the same amplitude (by coincidence or because the modulation is constant amplitude) then their phase difference correspond to α. Since α only shifts the pattern seen in Figure 3.10 the situation can arise (for a 2x2 SS LoS MIMO) that one antenna receives no signal while the other receives a combination from both Tx antennas.

That situation is depicted also in Figure 3.7c and it is interesting to note that the signal streams are still easily separable at the receiver.

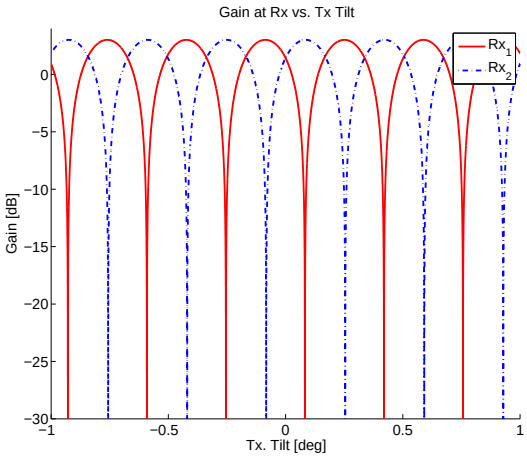

Figure 3.10: Gain pattern for an antenna arrangement satisfying (3.15). When one Rx has a null gain the second Rx will experience a peak gain.

3.3 Wideband MIMO Model

The discussion so far was limited to narrowband MIMO or flat channel MIMO, that is channels that could be described by a single complex number. Thus it was easy to express the MIMO channels in matrix form $\mathbf{H}$ so that the received signal was $\mathbf{r} = \mathbf{sH} + \mathbf{n}$. That can also be expressed in a series form as

$$r_m[j] = \sum_{n=1}^{N} h_{nm} s_n[j] \tag{3.22}$$

Here m represent the index of the Rx antenna and j is the discrete symbol timing. Now a wideband channel will act as a filter so that the gains in (3.22) need to be replaced by filters. This can be accomplished by

$$\begin{aligned} r_m[j] &= \sum_{n=1}^{N} \sum_{i=-L_t}^{L_t} h_{nm}[i,j] s_n[j-i] \Leftrightarrow \\ \mathbf{r}_m &= \sum_{n=1}^{N} \mathbf{h}_{nm} * \mathbf{s}_n \end{aligned}$$

where $\mathbf{h}_{nm}$ represents the channel filter between Tx antenna n and receive antenna m of length $2L_t + 1$ and $\mathbf{s}_n$ is the vector representation of the symbols sent from Tx antenna n. Expressing frequency selective MIMO channels in matrix form is a little bit more difficult and it requires some modifications to the channel matrix. In the most general case a $N \times M$

MIMO system has NM channels where each one of them is made up of a certain number of multipaths. The full channel is then considered to be made up of NM filters that are uncorrelated in the most general case. Equalizing such a channel is a much harder task than equalizing SISO channels since NM independent filters will be required in stead of just one. Transmitting L_B symbols (also called block length) the channel matrix can be expressed using Toeplitz matrices [4] such as

$$\mathbf{\Psi}_{nm} = \begin{bmatrix} h_{nm}[0] & \cdots & h_{nm}[-L_t] & 0 & \cdots & 0 \\ h_{nm}[1] & h_{nm}[0] & \cdots & h_{nm}[-L_t] & \ddots & 0 \\ \vdots & \ddots & \ddots & \ddots & \ddots & \vdots \\ 0 & \cdots & 0 & h_{nm}[L_t] & \cdots & h_{nm}[0] \end{bmatrix}^{\mathrm{T}}$$

where the $L_B \times L_B$ matrix $\mathbf{\Psi}_{nm}$ describes the channel from transmit antenna n to receive antenna m and $2L_t + 1$ is the length of the channel filter. Expressing the full MIMO channel in this way gives

$$\mathbf{\Psi} = \begin{bmatrix} \mathbf{\Psi}_{11} & \cdots & \mathbf{\Psi}_{1M} \\ \vdots & \ddots & \vdots \\ \mathbf{\Psi}_{N1} & \cdots & \mathbf{\Psi}_{NM} \end{bmatrix}$$

Defining the signal matrix $\mathbf{s}$ as

$$\begin{aligned} \mathbf{s} &= [\mathbf{s}_1, \ldots, \mathbf{s}_N] \\ \mathbf{s}_n &= [s_n[1], \ldots, s_n[L_B]] \end{aligned}$$

where $s_n[i]$ is the ith symbol transmitted from Tx antenna n. Here $\mathbf{s}$ will be a $1 \times NL_B$ vector. This enables the noise free received signal to be expressed as

$$\mathbf{r} = \mathbf{s}\mathbf{\Psi} \tag{3.23}$$

where $\mathbf{r}$ is the received signal and will have the dimensions $1 \times ML_B$. The matrix $\mathbf{\Psi}_{nm}$ arranges the channel filter taps in a convolutional matrix form. For a SISO channel there is only one filter so $\mathbf{\Psi}_{11}$ multiplied by the signal vector would represent the filtering operation of the channel. For a MIMO system there are multiple channel filters that operate on the Tx signal streams which are added up at the receiver. This may be conveniently expressed in matrix form by (3.23).

3.3.1 Channel Capacity

The channel capacity was defined for a narrowband MIMO channel in Section 3.1.2. For a frequency selective channel the capacity becomes frequency dependent. For a SISO channel the capacity becomes [33]

$$C = \int_{-\infty}^{\infty} \log_2\left(1 + \gamma |H(f)|^2\right) df$$

[4] A Toeplitz matrix is a square matrix with equal values on its left-to-right diagonals.

where $H(f)$ is the transfer characteristic of the channel (including Tx and Rx filters). A MIMO channel is described by a channel matrix so that the capacity can be expressed as [34]

$$C = \sum_{i=1}^{\min(N,M)} \int_{-\infty}^{\infty} \log_2 \left(1 + \gamma \lambda_i(f)\right) df$$

where $\lambda_i(f)$ is the ith eigenvalue of the positive definite matrix $\mathbf{C}(f) = \mathbf{H}^{\mathrm{H}}(f)\mathbf{H}(f)$. Here $\mathbf{H}(f)$ represents the frequency dependent narrowband channel matrix.

3.4 The LoS MIMO Channel

The LoS-MIMO channel differs from the non-LoS MIMO channel by the fact that there is one dominating path so that the incoming phases are dominated by the geometry of the channel and not scattering. Besides the LoS-path there can be secondary paths caused either by atmospheric scintillation or a reflection off the ground. This results in a frequency selective channel. A common model to use is the so called two ray model where the channel is described using one direct path and one path that reflects off the ground and is received with a random phase ϕ and a relative amplitude of $0 \leq b < 1$. The two paths have some delay difference τ that is commonly set to 6.3 ns as in Rummler's model [3]. The impulse response of such a channel is

$$\begin{aligned} h(t) &= \delta(t) + b\delta(t-\tau)e^{j\phi} \Leftrightarrow \\ H(s) &= \mathcal{L}\{h(t)\} = 1 + be^{-\tau s + j\phi} \end{aligned} \tag{3.24}$$

Remembering that $s = j\omega$ it can be seen from (3.24) that the channel introduces periodic notches in the frequency spectrum which are illustrated in Figure 3.11. The channel spans some bandwidth and will thus have a frequency response depending on where it is situated in the spectrum of Figure 3.11. If one of the notches happen to be within the bandwidth the channel will suffer from severe fading and ISI. The depth of the notches is given (in dB) by $B_n = 20\log_{10}(1-b)$.

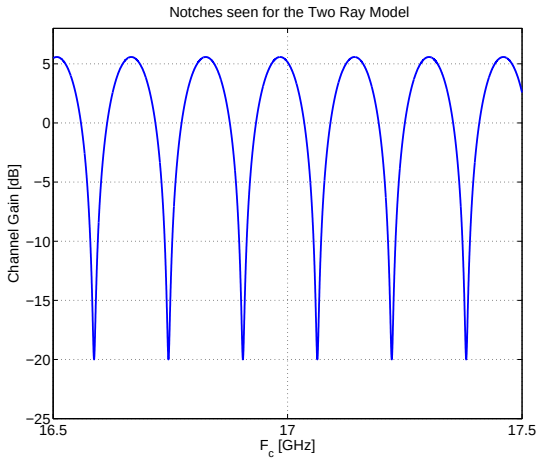

Figure 3.11: Periodic notches for the Two Ray Model. $\tau = 6.3$ ns, $\phi = 0$ and $b = 0.9$ in (3.24).

A LoS 2x2 SS-MIMO system with four frequency selective channels, denoted $\mathbf{h}_{nm}$ is illustrated in Figure 3.12. By varying the phase ϕ_{nm} of the ground reflection the properties of the channel filters $\mathbf{h}_{nm}$ are changed. Each channel can act as a lowpass- highpass or notch filter for example depending on ϕ_{nm}.
The $N \times M$ LoS MIMO channel is made up of NM such filters, each with its own realization of ϕ_{nm}.

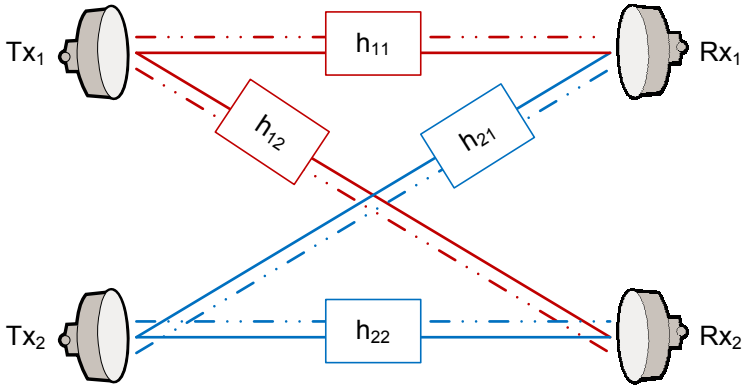

Figure 3.12: A LoS 2x2 SS-MIMO system with four frequency selective channels.

3.4.1 Mast Swing

A common installation arrangement for backhaul links is that they are mounted on a tall mast along with the mobile base stations which are placed on the top with the backhaul antenna disks a little bit below. In heavy wind the mast might rock back and forth resulting in periodic movement of the antennas. As the antennas move, the channel between Tx and Rx will change since the channels are partly described by geometry. As long as the Rx does not move out of the main beam of the Tx antenna the signal strength between any pair of Tx- and Rx antennas should be relatively unaffected. By moving the mast the channel notches can be seen across the bandwidth of each channel forcing the STE to adapt. Another effect is that the movement at such high carrier frequencies will cause some differential frequency offset at the Rx. Since all real systems have to have some carrier recovery this is usually not such a large problem.

3.5 Dual Polarized MIMO

Dual polarized MIMO systems make use of two orthogonal polarization states, often described as vertical and horizontal polarization. The interference between the two states is called cross-polarization discrimination (XPD) (defined in (2.6)) and depends both on the transmission channels and the polarization mismatch between Tx and Rx. XPD is usually expressed in dB and the larger it is the more isolation there is between the states.

The channel can lower the XPD and there have been quite a few papers on how the channel treats the polarizations, *e.g.* [2, 30]. The results indicate that even in a scattering environment the XPD should be high (at least 5-15 dB) and for a non-scattering LoS channel it is even higher. Thus DP MIMO schemes can provide high rank MIMO channels with good condition numbers. References [15, 42] show the benefits of using DP MIMO in a Ricean fading environment when the antennas are not configured for LoS. This is though not the optimal comparisons for the purpose of this discussion since the antenna placements for a SS MIMO system should be optimized for the LoS environment. In Ref. [7] this is done

with the result that SS-SP MIMO outperforms its DP counterpart in low SNR because of the added 3 dB array gain. The difference is reduced when the SNR is high which is common in LoS environments. The SS-SP MIMO was also found to be more sensitive to polarization mismatch than DP MIMO. Reference [12] shows that the XPD is not lowered significantly even for heavy rain which suggests that SS-SP MIMO should have superior performance even while it rains because of reduced SNR. A benefit of the DP MIMO system is that the antennas may be combined, thus there is no need for spatial separation at the Tx and Rx site.
The largest benefit for DP MIMO systems is though the relaxed requirements on antenna separation, DP antennas can be situated as close together as the installation allows.

It is interesting to analyze 4x4 SS-DP MIMO systems since these can produce 4 fold capacity compared to a SISO system (at a high SNR) while relaxing somewhat the requirements for the separation. The narrowband channel matrix can be written as

$$\begin{aligned}\mathbf{H} &= \begin{bmatrix} h_{1\mathrm{V},1\mathrm{V}} & h_{1\mathrm{V},1\mathrm{H}} & h_{1\mathrm{V},2\mathrm{V}} & h_{1\mathrm{V},2\mathrm{H}} \\ h_{1\mathrm{H},1\mathrm{V}} & h_{1\mathrm{H},1\mathrm{H}} & h_{1\mathrm{H},2\mathrm{V}} & h_{1\mathrm{H},2\mathrm{H}} \\ h_{2\mathrm{V},1\mathrm{V}} & h_{2\mathrm{V},1\mathrm{H}} & h_{2\mathrm{V},2\mathrm{V}} & h_{2\mathrm{V},2\mathrm{H}} \\ h_{2\mathrm{H},1\mathrm{V}} & h_{2\mathrm{H},1\mathrm{H}} & h_{2\mathrm{H},2\mathrm{V}} & h_{2\mathrm{H},2\mathrm{H}} \end{bmatrix} = \begin{bmatrix} \mathbf{H}_{11} & \mathbf{H}_{12} \\ \mathbf{H}_{21} & \mathbf{H}_{22} \end{bmatrix} \\ &= \begin{bmatrix} \sqrt{1-\alpha}e^{jkd_{11}} & \sqrt{\alpha}e^{jkd_{11}} & \sqrt{1-\alpha}e^{jkd_{12}} & \sqrt{\alpha}e^{jkd_{12}} \\ \alpha e^{jkd_{11}} & \sqrt{1-\alpha}e^{jkd_{11}} & \sqrt{\alpha}e^{jkd_{12}} & \sqrt{1-\alpha}e^{jkd_{12}} \\ \sqrt{1-\alpha}e^{jkd_{21}} & \sqrt{\alpha}e^{jkd_{21}} & \sqrt{1-\alpha}e^{jkd_{22}} & \sqrt{\alpha}e^{jkd_{22}} \\ \alpha e^{jkd_{21}} & \sqrt{1-\alpha}e^{jkd_{21}} & \sqrt{\alpha}e^{jkd_{22}} & \sqrt{1-\alpha}e^{jkd_{22}} \end{bmatrix} \end{aligned} \tag{3.25}$$

or using the Kronecker product $\otimes$ as

$$\mathbf{H} = \mathbf{H}_{\mathrm{LoS}} \otimes \mathbf{W}_{XPD} = \begin{bmatrix} e^{jkd_{11}} & e^{jkd_{12}} \\ e^{jkd_{21}} & e^{jkd_{22}} \end{bmatrix} \otimes \begin{bmatrix} \sqrt{1-\alpha} & \sqrt{\alpha} \\ \sqrt{\alpha} & \sqrt{1-\alpha} \end{bmatrix}$$

where $\alpha = \mathrm{E}\left\{|h_{i\mathrm{H},i\mathrm{V}}|^2\right\} = \mathrm{E}\left\{|h_{i\mathrm{V},i\mathrm{H}}|^2\right\}$. Here $h_{n\mathrm{V},m\mathrm{H}}$ denotes the gain between the vertically polarized Tx antenna n and the horizontally polarized Rx antenna m. α measures the ratio of the power for one polarization that is transferred to the other polarization and is constrained by $0 < \alpha \leq 1$. In terms of the XPD defined in (2.6) α can be expressed as

$$\alpha = \frac{1}{\mathrm{XPD}+1}$$

The condition number of (3.25) is plotted against XPD in Figure 3.13. As can be seen the condition number drops off quickly with increased XPD. If the antenna placement is suboptimal the system can be seen to be more sensitive to the XPD. Comparing this result to Figure 3.6 it can be seen that the condition numbers converge to the same value.

To calculate the condition number of (3.25) analytically, the eigenvalues of $\mathbf{H}\mathbf{H}^{\mathrm{H}}$ should be calculated first. The result is (given that $\theta_t = \theta_r = 0$)

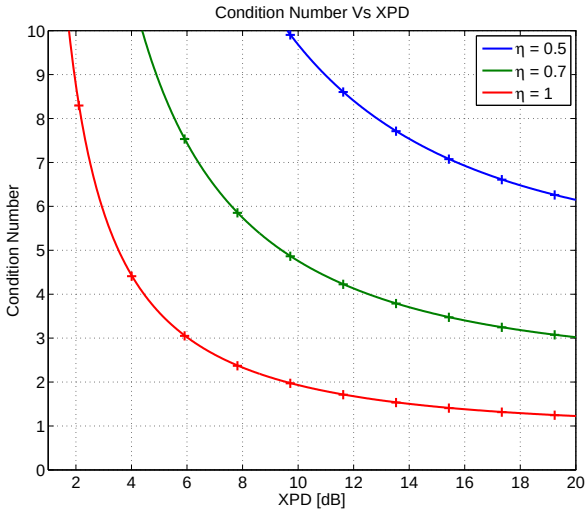

Figure 3.13: The condition number κ as a function of XPD for a 4x4 SS-DP MIMO as is described in (3.25). This is done for $\eta = 0.5,\ 0.7,\ 1$ (see (3.16) for the definition of η). The dots represent values calculated using (3.27).

$$\begin{aligned} c_1 &= (2 - f_a(a))\left[1 - \cos(\pi\eta^2/2)\right] \\ c_2 &= (2 - f_a(a))\left[\cos(\pi\eta^2/2) + 1\right] \\ c_3 &= (2 + f_a(a))\left[\cos(\pi\eta^2/2) + 1\right] \\ c_4 &= (2 + f_a(a))\left[1 - \cos(\pi\eta^2/2)\right] \end{aligned} \tag{3.26}$$

where η is defined by (3.16) and $f_a(a) = 4\sqrt{\alpha - \alpha^2}$. The condition number is thus

$$\kappa = \sqrt{\frac{\max(c_1, c_2, c_3, c_4)}{\min(c_1, c_2, c_3, c_4)}} \tag{3.27}$$

Looking at (3.26) and (3.27) there are a few things to note. When $\alpha = 1/2$ (XPD= 0 dB) then $c_1 = c_2 = 0$ meaning that the channel can only support 2 data streams. This can perhaps be seen intuitively since then there is no discrimination between the polarization states, that is the 4x4 SS-DP MIMO has been reduced to a 2x2 equivalent.

3.6 Penalty

A perfect system setup, that is a full rank MIMO channel and a system that only introduces white Gaussian noise, will have a certain BER for a given SNR. If a target BER is set then the SNR that achieves that can be computed. If any imperfections are then introduced in the system a higher SNR should be needed to get the same target BER. The difference in SNR values is here termed as penalty. It is the penalty in power that has to be paid if this imperfection is introduced. For example if there is a penalty of 3 dB present in a system the

Tx power will have to be raised by 3 dB to achieve the same BER.

Assuming Gray coding and a square M-QAM constellation the BER can be calculated for a SISO system as

$$P_b = \left(1 - \frac{1}{\sqrt{\mathrm{M}}}\right) Q\left(\sqrt{\frac{3k}{\mathrm{M}-1}\frac{E_b}{N_0}}\right)$$

where $k = \log_2(\mathrm{M})$. For a MIMO system such as is depicted in Figure 3.2 there are M Rx antennas [5] and equally many parallelized SISO channels with singular values $\sigma_1, \ldots, \sigma_{R_H}$. The BER for a MIMO system using SVD is thus given as (similar as in [49, eq. 3.50])

$$P_b = \frac{1}{R_H}\sum_{i=1}^{R_H}\left(1 - \frac{1}{\sqrt{\mathrm{M}}}\right) Q\left(\sqrt{\frac{3k}{\mathrm{M}-1}\frac{E_b}{N_0}\sigma_i^2}\right) \tag{3.28}$$

The singular values (or gains) σ_i are calculated for 2x2 SS-SP LoS MIMO in (A.1) and for 4x4 SS-DP LoS MIMO in (3.26) (since the singular values are the square root of the eigenvalues of $\mathbf{HH}^{\mathrm{H}}$). Selecting the BER $P_b = 10^{-3}$ and $\mathrm{M} = 16$ (16QAM) the penalty can be numerically calculated for a 2x2 SS-SP LoS MIMO and a 4x4 SS-DP LoS MIMO against η and XPD. This has been done in Figure 3.14.

[5] M represents the constellation dimension while M represents the number of Rx antennas.

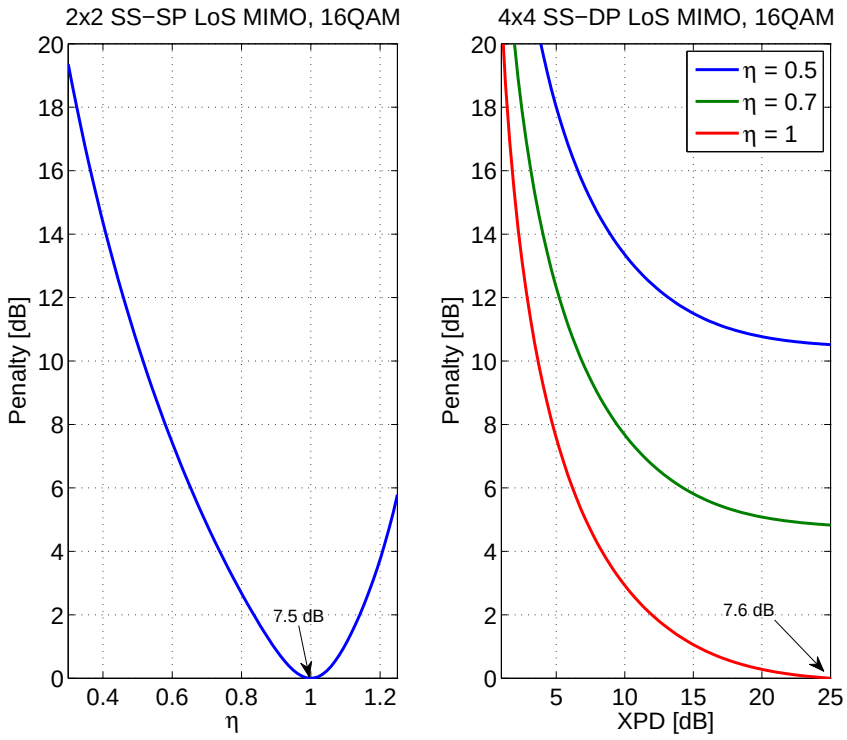

Figure 3.14: The penalty plotted against η and XPD for 2x2 SS-MIMO and 4x4 SSDP-MIMO respectively assuming the SVD method. The target BER is 10^{-3}.

Chapter 4

MIMO Equalization

This chapter introduces MIMO equalizers, one of the most important components in MIMO receivers. MIMO equalizers, on one hand, work as a typical equalizer to remove the Inter-Symbol-Interference (ISI) which is a common phenomenon mainly caused by a frequency selective channel, such typical equalization techniques, especially for SISO equalizers, have been extensively investigated in the literature [53], [20], [43]. On the other hand, in addition to removing the ISI, MIMO equalizers cancel the Inter-Stream-Interference. Figure 4.1 shows a schematic view of a 2x2 LoS MIMO system h_{21} and h_{12} interferes with h_{11} and h_{22} at Rx_1 and Rx_2 respectively.

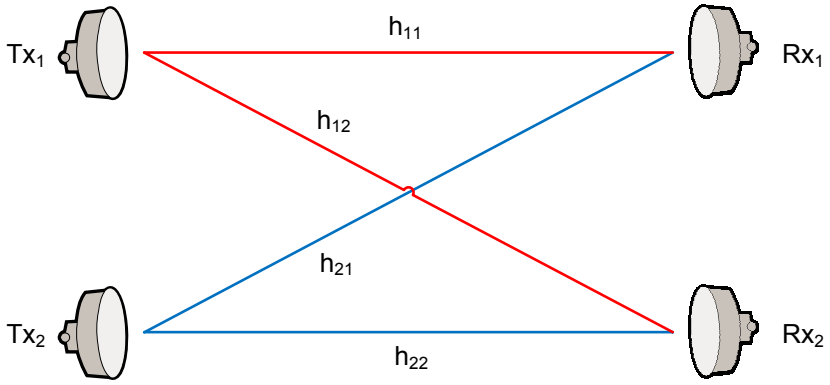

Figure 4.1: A schematic view of a 2x2 LoS MIMO system. There are four channels h_{ij} describing the phase and amplitude of each path.

Figure 4.2 shows how a MIMO Space Time Equalizer (STE) uses Constant Modulus Algorithm (CMA) to remove both the ISI and Inter-Stream-Interference for a 2x2 SS-SP MIMO system using 16QAM modulation. As shown in the figure, the received signals are wildly distributed before equalization. The right figures show how the transmitted signals are recovered using equalization. It is noteworthy that the recovered signals are shown after the phase recovery loop is turned on otherwise these recovered signals might have a random rotation.

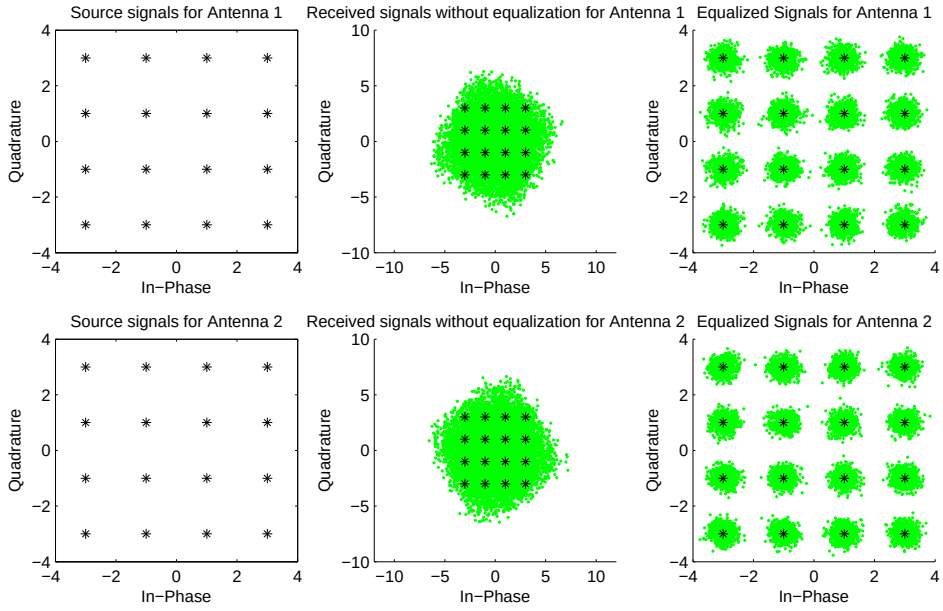

Figure 4.2: 16-QAM constellation. Left figures: The constellation of the transmitted symbols. Middle figures: The received symbols distorted by ISI and Inter-Stream-Interference. Right figure: The equalized symbols.

4.1 Equalizer types

Equalization techniques fall into two broad categories: linear- and non-linear equalizers. Compared to non-linear equalizers, linear equalizers have larger noise enhancement which will be discussed in the following section but they are more easily understood and simpler to implement. Due to the complexity of non-linear equalizers from a practical standpoint, only linear equalizers are discussed and compared in this report. We look into MIMO linear equalizers consisting of trained algorithms such as Least Mean Square (LMS), and Recursive Least Square (RLS) and blind algorithms such as Constant Modulus Algorithm (CMA), Modified Constant Modulus Algorithm (MCMA), Simplified Constant Modulus Algorithm (SCMA) and their variants. Figure 4.3 shows the categories of equalization techniques. All the equalizers in this thesis use a symbol-by-symbol transversal filter structure which is shown in Figure 4.4 where w_0 stands for the central tap.

4.2 Linear Equalizers

4.2.1 Linear equalizers structure and noise enhancement

Figure 4.5 illustrates a block diagram of a linear equalizer. As discussed above, linear equalizers typically suffer from noise enhancement hence they should balance ISI mitigation and noise amplification. Since the overall system is seen as a linear system in which the received signal can be expressed as an addition of distorted signals caused by ISI and additive white

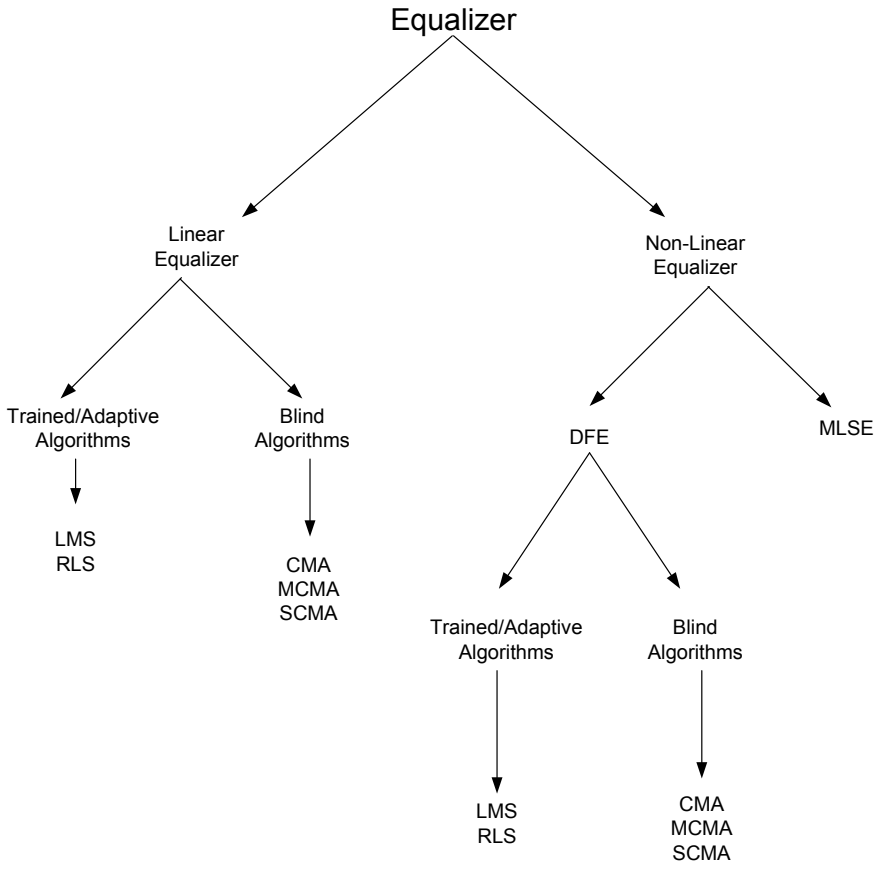

Figure 4.3: Equalizer types, algorithms.

Gaussian noise (AWGN). This is expressed as

$$r(k) = \sum_{i=-L_c}^{L_c} h(i)s(k-i) + n(k) \tag{4.1}$$

where $r(k)$ is the kth sample of the discrete received signals at the receiver front end, $s(k)$ is the transmitted signal and $n(k)$ is the Gaussian noise. Using the discrete time Fourier transform (DTFT) and passing the received signals through the equalizer, the following equation is derived

$$Y(\omega) = R(\omega)H_{eq}(\omega) = S(\omega)H(\omega)H_{eq}(\omega) + N(\omega)H_{eq}(\omega) \tag{4.2}$$

where the capital letters of the signals and channel response denote their discrete time Fourier transform, ISI introduced by channel $H(\omega)$ can be removed by introducing an equalizer $H_{eq}(\omega)$, in the frequency domain, defines as

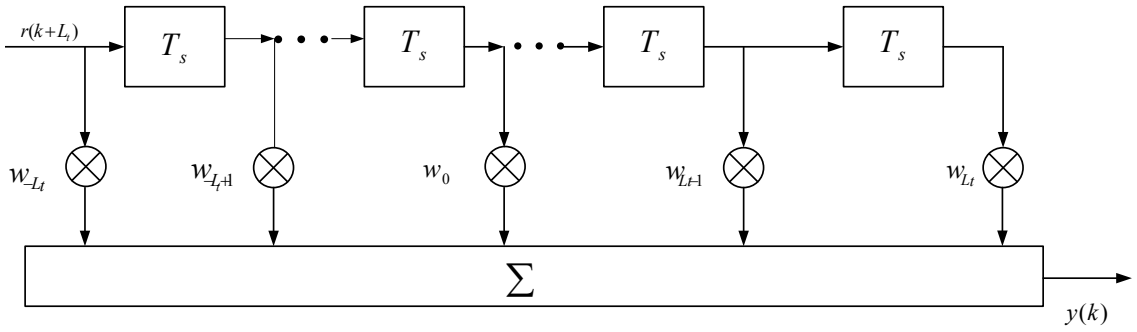

Figure 4.4: Transversal Filter Structure.

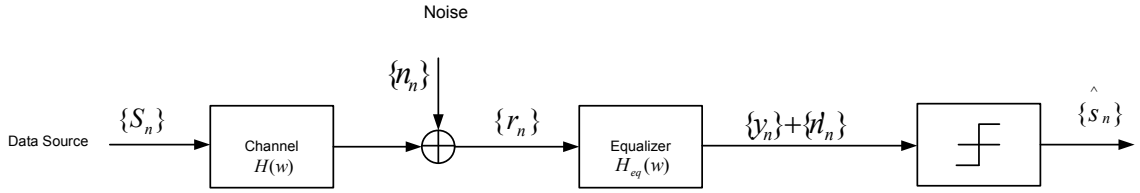

Figure 4.5: The diagram of a linear equalizer.

$$H_{eq}(\omega) = \frac{1}{H(\omega)} \tag{4.3}$$

$$Y(\omega) = S(\omega) + \frac{N(\omega)}{H(\omega)} \tag{4.4}$$

Here the last term is the colored Gaussian noise (frequency dependent), and all the ISI has been successfully removed from the received signal. The inverse equalizer which has a frequency response of $H_{eq}(\omega)$ is often approximated by a finite-impulse or transversal filter as illustrated in Figure 4.4 impulse responses are the filter taps w_i and the length of the filter taps L is expressed as $L = 2L_{\mathrm{t}} + 1$. As can be seen in the figure, the structure looks like a convolution operation which convolves the equalizer taps with the received signals in order to invert the CIR (Channel Impulse Response) and cancel the ISI. However, if $H(\omega)$ has deep attenuation at any frequency within the bandwidth of transmitted signals, $H_{eq}(\omega)$ will have a high gain in the same range and the noise power range will be greatly enhanced. In this case, even though the ISI is removed by the equalizer the system may still perform poorly due to a reduced SNR. Thus the goal of equalization is not only to remove the ISI but also to prevent enhancing the noise power too much. Conventional linear equalizers process equalization approximately by inverting the channel response and the noise power will be enhanced. Equalizers based on the minimum mean square error (MMSE) algorithms have the benefit that they are balancing ISI removal and noise enhancement as they are trying to minimize the error between the estimated- and desired symbols. Both LMS and RLS are kind of MMSE equalizers.

4.2.2 MIMO Space Time Equalizer (STE)

In order to cancel both the ISI and the Inter-Stream-Interference, a MIMO STE has been considered. A STE has to be able to not only initialize filter taps but also to update the taps iteratively as the channel change over time using some adaptive algorithm. A STE for both 2x2 SS-SP and 4x4 SS-DP MIMO systems are considered they can easily be extended into a MIMO system with N transmitting and M receiving antennas. The channel between each Tx and Rx antenna pair is considered to be an independent frequency selective channel with additive white Gaussian noise (AWGN).

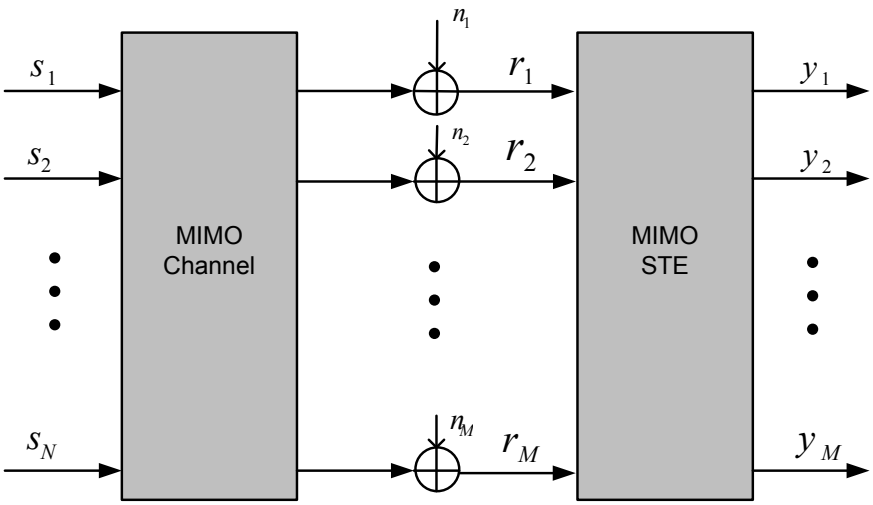

Figure 4.6: MIMO Space Time Equalizer diagram.

Figure 4.6 shows a block diagram of a MIMO STE where the overall system can be modeled as a linear system shown in Figure 4.7. Here N and M denote the number of transmitting and receiving antennas respectively. $\mathbf{h}$ and $\mathbf{w}$ denote the channel filters and the equalizer filters respectively. The following equation shows the discrete output of the mth receiving antenna

$$\mathbf{r}_m(k) = \sum_{m=1}^{M} \mathbf{s}_n(k) * \mathbf{h}_{n,m}(k) + \mathbf{n}_m(k) \tag{4.5}$$

here $\mathbf{r}_m(k)$ is the discrete output of the mth receiving antenna at sampling time k and $\mathbf{n}_m(k)$ is the AWGN added at mth receiving antenna at sampling time k. $\mathbf{s}_n(k)$ is the discrete input to the nth transmitting antenna, $\mathbf{h}_{n,m}(k)$ is the discrete channel response from the nth transmitting antenna to mth receiving antenna. The above equation can be rewritten in matrix form as follows

$$\mathbf{r} = \mathbf{s}\mathbf{\Psi} + \mathbf{n} \tag{4.6}$$

where $\mathbf{r}$ is the received signal with the dimension 1xML_{B}. $\mathbf{s}$ and $\mathbf{\Psi}$ are defined in (3.23) and (3.3) respectively. The equalized signal can be described by the following matrix

$$\mathbf{y}(k) = \mathbf{r}_k \mathbf{W}(k) \tag{4.7}$$

here $\mathbf{y}(k)$ is a vector with M equalized symbols at sample time k, $\mathbf{W}(k)$ is the equalizer tap matrix that is defined in (4.14), $\mathbf{r}_k$ is the kth row vector of receiving matrix $\mathbf{R}$ that defined in (4.18). Figure 4.8 shows how the real and imaginary part of the magnitudes of STE filter taps looks like after the equalizer converges. The first 43 taps are the coefficients of the equalizer w_{11} and the remaining 43 taps belong to the canceler w_{21} that cancels Inter-Stream-Interference from Tx_2.

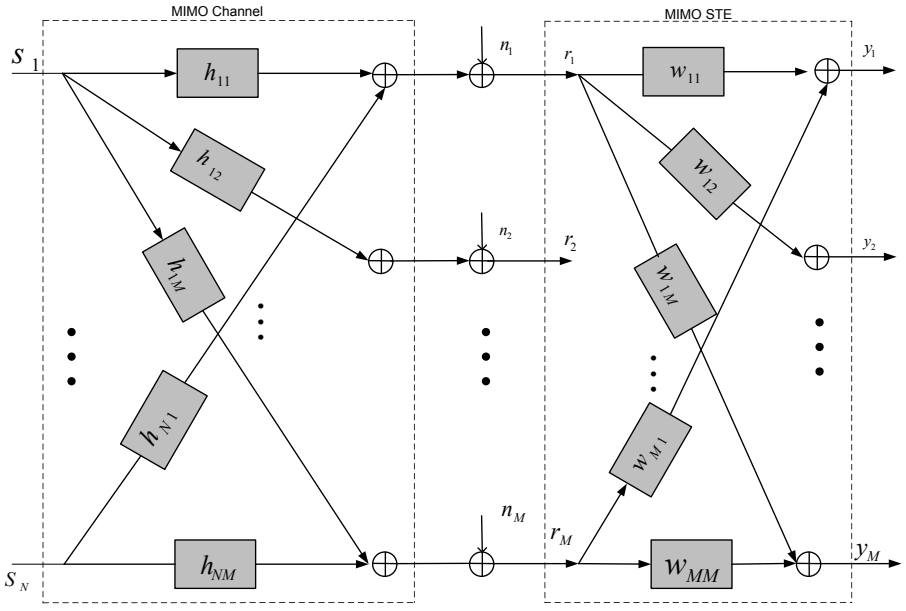

Figure 4.7: Structure of the MIMO space time equalizer.

4.3 Trained Equalization

There are two different equalizer setting approaches, *preset* and *adaptive*. For the *preset* approach, the information of the channel response is obtained from the channel measurement or channel estimation to set the equalizer filter taps. For the latter approach, instead of estimating the channel, equalizer taps are automatically adjusted by periodically sending training symbols and allowing the equalizer taps to adjust its parameters in response to these known symbols and corresponding received signals.

Figure 4.9 illustrates how training sequences are organized in a transmission sequence. A training sequence with L_{TR} symbols is stored in front of the data package and sent together with data repeatedly. Then filter taps are adjusted per iteration by solving the error function between these known training symbols and corresponding received signals. A 2x2 SS-SP MIMO STE under training mode is shown in Figure 4.10. Where the equalizer w_{11} and w_{22} are used to cancel the ISI that is introduced in the direct path channel between Tx_1,Rx_2 and

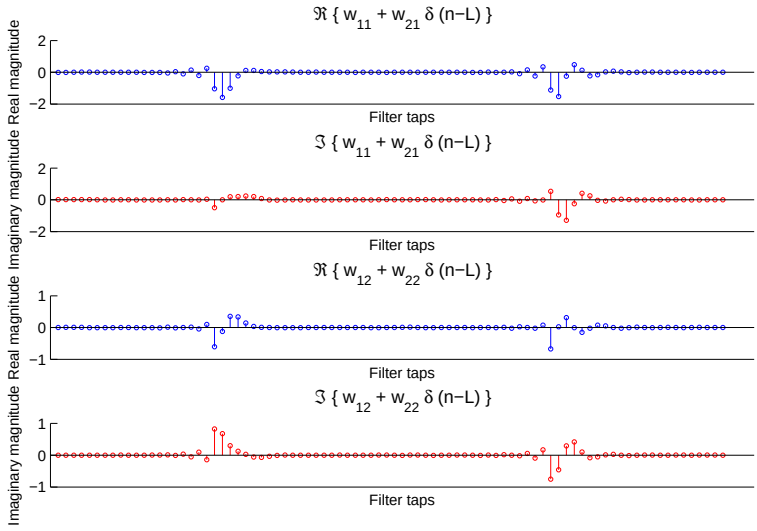

Figure 4.8: Filter taps of a converged equalizer for 2x2 SS-SP MIMO

Tx_2,Rx_2 respectively. w_{12} and w_{21} cancel the Inter-Stream-Interference between Tx_1,Rx_2 and Tx_2,Rx_1 respectively. They work together to recover the desired symbols at both receiving antennas.

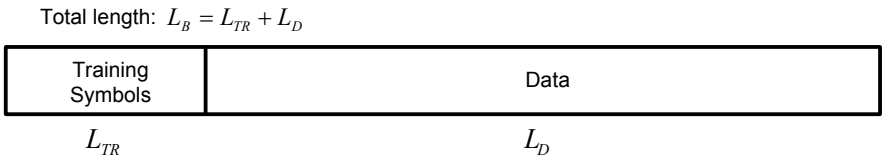

Figure 4.9: Package structure of trained equalization.

4.3.1 Zero-Forcing Algorithm (ZF)

SISO system

The signal we desire after the equalization operation is the transmitted symbol with an integer delay. In other words, after removing both the ISI and Inter-Stream-Interference, an equalized signal $s_{eq}(k) = s(k-\delta)$ where δ is a time delay with an integer number is obtained. Received signal can be expressed in a discrete time domain as

$$r(k) = \sum_{i=-L_c}^{L_c} h(i)s(k-i) + n(k) \tag{4.8}$$

where $s(k)$ and $r(k)$ are the kth sample of the transmitted- and received signals and $2L_c+1$ is the channel length. The ZF (Zero Forcing) algorithm works by forcing the impulse response

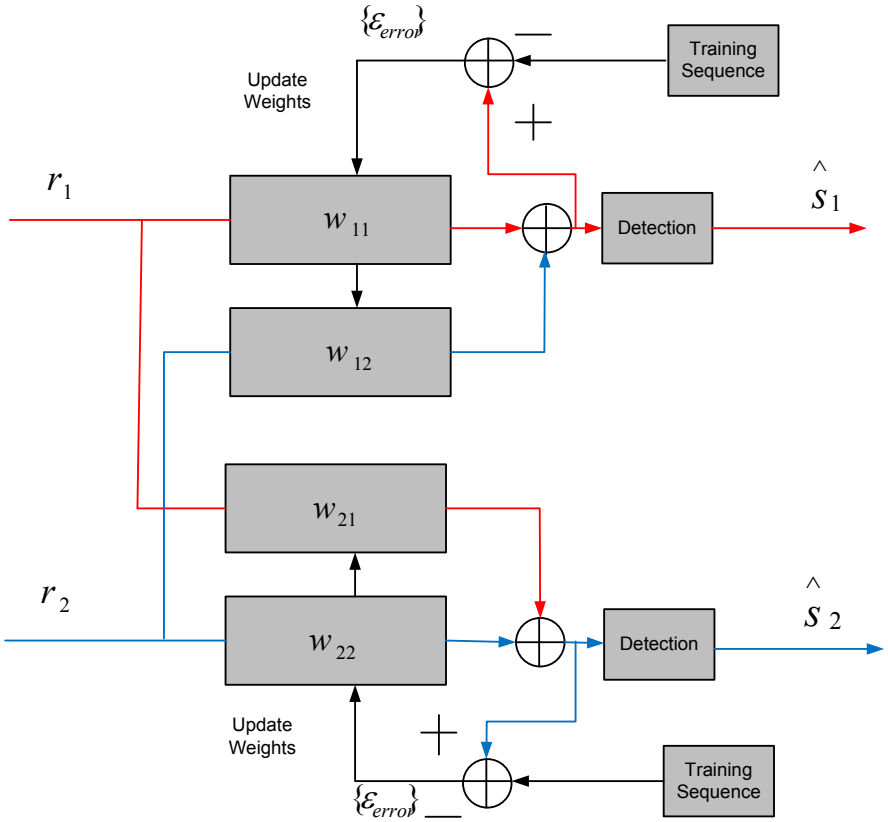

Figure 4.10: The structure for a 2×2 MIMO STE under training mode.

of the equalized channel to a delta function. In theory, any channel response can be perfectly equalized by a ZF equalizer with infinite number of taps. The upper plot in Figure 4.11 shows the channel response through which signals are transmitted. The lower plot is the equalized samples which are forced by the equalizer to zeros ($2<n<8$) except the center tap. From Figure 4.4 the equalizer response, due to the channel response $\mathbf{H}_c$, can be expressed as [20]

$$\mathbf{h}_{eq} = \mathbf{H}_c\mathbf{w} \tag{4.9}$$

$$\mathbf{w} = \mathbf{H}_c^{-1}\mathbf{h}_{eq} \tag{4.10}$$

where $\mathbf{h}_{eq}$ and $\mathbf{w}$ are column vector given by

$$\mathbf{h}_{eq} = \begin{bmatrix} 0 \\ \vdots \\ 0 \\ 1 \\ 0 \\ \vdots \\ 0 \end{bmatrix} \quad \mathbf{w} = \begin{bmatrix} w_{-L} \\ w_{-L+1} \\ \vdots \\ w_0 \\ w_1 \\ \vdots \\ w_L \end{bmatrix} \tag{4.11}$$

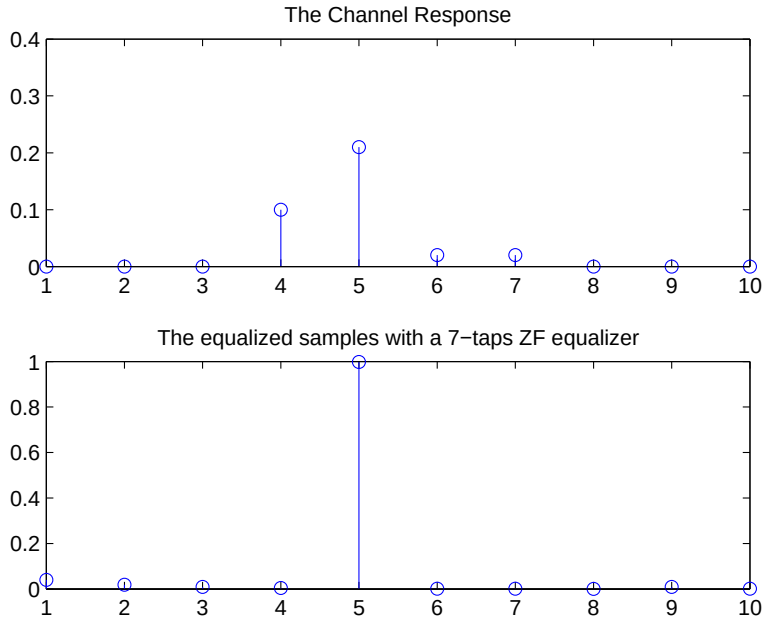

Figure 4.11: The upper plot: Channel response samples. The lower plot: Equalized samples using a seven taps ZF algorithm.

$\mathbf{H}_c$ is the matrix of channel responses of the form

$$\mathbf{H}_c = \begin{bmatrix} h_c(k) & h_c(k-1) & \cdots & h_c(k-2L) \\ h_c(k+1) & h_c(k) & \cdots & h_c(k-2L+1) \\ h_c(k+2) & h_c(k+1) & \cdots & h_c(k-2L+2) \\ \vdots & \vdots & \ddots & \vdots \\ h_c(k+2L) & h_c(k+2L-1) & \cdots & h_c(k) \end{bmatrix}$$

Thus $4L$ samples of the channel response can be used to determine a Zero-Forcing equalizer with $2L+1$ filter taps. Although the Zero-Forcing algorithm is conceptually simple and easy to implement, the impact of the noise enhancement impact is not taken into account. Any noise added after the channel gets amplified by a large factor if the channel has a deep attenuation and this destroys the overall signal-to-noise ratio. Thus the zero-forcing equalizer is not commonly used in most applications.

4.3.2 Least Square Algorithm (LS)

MIMO system

The least square algorithm is widely used to solve over-determined systems, i.e. systems with more equations than unknowns. A STE with usage of LS algorithms is for considered and equalized signal can be expressed as

$$y_m(k) = \sum_{j=1}^{M} \mathbf{r}_j(k)\mathbf{w}_{j,m}(k) \tag{4.12}$$

where M denotes the number of receiving antennas, $\mathbf{r}_j$ is the vector of received symbols at jth receiving antenna and $\mathbf{w}_{j,m}$ is the filter taps for cancelling the ISI or Inter-stream-Interference of the channel $h_{j,m}$. The error function for the mth equalizer output is defined as

$$e_m(k) = s_m(k) - y_m(k) \tag{4.13}$$

The index m stands for the mth receiving antenna, (4.12) is repeated for each of L_B outputs of mth equalizer corresponding to L_B input signals. Now, collecting L_B samples from the mth receiving antenna, which is expressed as $\mathbf{r}_m = [r_m(1) \quad r_m(2) \quad \dots \quad r_m(L_\mathrm{B})]$. Then, L_B samples of input signals from the nth transmitting antenna is collected and expressed as $\mathbf{s}_n = [s_n(1) \quad s_n(2) \quad \dots \quad s_n(L_\mathrm{B})^\mathrm{T}]$. Furthermore, the linear equalizer matrix can be written as

$$\mathbf{W} = \begin{bmatrix} \mathbf{w}_{1,1} & \mathbf{w}_{2,1} & \dots & \mathbf{w}_{M,1} \\ \mathbf{w}_{1,2} & \mathbf{w}_{2,2} & \dots & \mathbf{w}_{M,2} \\ \vdots & \vdots & \ddots & \vdots \\ \mathbf{w}_{1,M} & \mathbf{w}_{2,M} & \dots & \mathbf{w}_{M,M} \end{bmatrix} \tag{4.14}$$

where M denotes the number of receiving antennas. In matrix (4.14) the i,jth element of the linear equalizer matrix is a linear transversal filter with maximum length of $2L+1$ as described in Figure 4.4. Thus the minimization problem over a block of L_B samples is expressed as

$$\mathbf{w}_m = \arg \ \min \|\mathbf{s}_m - \mathbf{R}\mathbf{w}_m\|^2 \tag{4.15}$$

where $\mathbf{w}_m$ denotes the mth column vector of filter matrix $\mathbf{W}$ and $\|\cdot\|$ is the vector norm operation.$\mathbf{s}_m$ is the mth column of $\mathbf{S}$ matrix as defined in (4.22) and $\mathbf{R}$ is introduced below. This minimization problem has a unique solution, given by solving (4.16)

$$\mathbf{w}_m = (\mathbf{R}^\mathrm{H} \cdot \mathbf{R})^{-1} \cdot \mathbf{R}^\mathrm{H} \cdot \mathbf{s}_m \tag{4.16}$$

$\mathbf{s}_m$ is a vector of source signals of mth transmitting antenna, and $\mathbf{R}$ is formed as

$$\mathbf{R} = [\mathbf{R}_1, \dots, \mathbf{R}_M] \tag{4.17}$$

where,

$$\mathbf{R}_m = \begin{bmatrix} r_m(L_t) & r_m(L_t-1) & \dots & r_m(1) & 0 & \dots & 0 \\ r_m(L_t+1) & r_m(L_t) & \dots & r_m(2) & r_m(1) & \dots & 0 \\ \vdots & \vdots & & \vdots & \vdots & \ddots & \vdots \\ r_m(L) & r_m(L-1) & \dots & r_m(L-L_t) & r_m(L-L_t-1) & \dots & r_m(1) \\ \vdots & \vdots & \ddots & \vdots & \vdots & \ddots & \vdots \\ 0 & \dots & 0 & r_m(L_\mathrm{B}) & r_m(L_\mathrm{B}-1) & \dots & r_m(L_\mathrm{B}-L_t-1) \end{bmatrix} \tag{4.18}$$

where $r_m(k)$ is the kth sample received at Rx antenna m. $2L_t+1$ is the equalizer filter length and L_t is the index of central tap of the equalizer. M is the number of receiving antennas. A derivation of the least square algorithm based on the MIMO equalizer can be found in the Appendix A.

4.3.3 Least Mean Square Algorithm (LMS)

MIMO system

The LMS (Least Mean Square) algorithm was invented in 1959 by Stanford university professor Bernard Widrow and his first Ph.D student, Ted Hoff. It uses *stochastic gradient descent* to start at some arbitrary initial point and iteratively moves towards the optimal point in small steps. Due to its simplicity, the LMS algorithm becomes very popular in practical applications. Furthermore, it can be applied in both training and DD (Decision-Directed) modes. In training mode, as shown in Figure 4.9, by-the-receiver known symbols are added and transmitted in front of the data in order to update the equalizer using LMS. In DD mode, it assumes that the hard decisions of the received signals are correct and those estimated symbols can be treated as training symbols to update the filter. Using the SGD (stochastic gradient descent) the filter updating process is expressed as

$$\mathbf{W}(k+1) = \mathbf{W}(k) - \mu \nabla_w J^{\text{lms}} \tag{4.19}$$

where $\nabla_w J^{\text{lms}}$ is the gradient of the cost function that is to be minimized, and μ is the step-size parameter that controls the convergence speed of the LMS algorithm. The remaining part to compute is the MSE cost function of LMS algorithm J^{lms}. The basic idea behind the LMS algorithm is to minimize the MSE (Mean Square Error) between the estimated signal and desired signal (for simplicity, the system delay δ is ignored)

$$e_m(k) = y_m(k) - s_n(k) \tag{4.20}$$

where n,m stands for the nth transmitting and mth receiving antenna respectively. Here $n = m$ is set then the MSE cost function can be written as

$$\begin{aligned} J^{\text{lms}} &= \mathrm{E}\left\{|e_m(k)|^2\right\} \\ &= \mathrm{E}\left\{|y_m(k) - s_n(k)|^2\right\} \\ &= \mathrm{E}\left\{|\mathbf{r}_k \mathbf{w}_i - s_n(k)|^2\ \right\} \end{aligned}$$

where $\mathbf{r}_k$ is the kth row vector of receiver matrix $\mathbf{R}$ which is the same as (4.18) and $\mathbf{w}_m$ is mth column vector of equalizer matrix defined in (4.14). It is worthwhile to note that the LMS algorithm suffer from noise enhancement problems since noise impact is included within the criterion so that the minimization of MSE includes the minimization of ISI terms plus noise power [43]. The following equations can be derived based on the above J^{lms} cost function

$$
\begin{aligned}
J^{\text{lms}} &= \mathrm{E}\left\{|e_m(k)|^2\right\} \\
&= \mathrm{E}\left\{e_m(k)e_m(k)^*\right\} \\
&= \mathrm{E}\left\{(\mathbf{r}_k\mathbf{w}_m - s_n(k))\,(\mathbf{r}_k\mathbf{w}_m - s_n(k))^*\right\} \\
&= \mathrm{E}\left\{(\mathbf{r}_k\mathbf{w}_m - s_n(k))\left(\mathbf{r}_k^{\mathrm{H}}\mathbf{w}_m^{\mathrm{H}} - s_n^*(k)\right)\right\} \\
&= \mathrm{E}\left\{\mathbf{r}_k\mathbf{w}_m\mathbf{r}_k^{\mathrm{H}}\mathbf{w}_m^{\mathrm{H}} - \mathbf{r}_k\mathbf{w}_m s_n^*(k) - s_n(k)\mathbf{r}_k^{\mathrm{H}}\mathbf{w}_m^{\mathrm{H}} + s_n(k)s_n^*(k)\right\} \\
&= \mathbf{w}_m\mathrm{E}\left\{\mathbf{r}_m\mathbf{r}_m^{\mathrm{H}}\right\}\mathbf{w}_m^{\mathrm{H}} - \mathbf{w}_m\mathrm{E}\left\{\mathbf{r}_k s_n^*(k)\right\} \\
&\quad -\mathbf{w}_m^{\mathrm{H}}E\left\{s_n(k)\mathbf{r}_k^{\mathrm{H}}\right\} + \mathrm{E}\left\{s_n(k)s_i^*(k)\right\}
\end{aligned}
$$

$\mathrm{E}\left\{\mathbf{r}_k\mathbf{r}_k^{\mathrm{H}}\right\}$ is the received signal autocorrelation matrix and $\mathrm{E}\left\{s_n(k)s_n^*(k)\right\}$ is desired signal variance. Finally, substitution of later term in (4.19) for MSE cost function is done by following equations

$$
\nabla_w J^{\text{lms}} = \mathrm{E}\left\{\mathbf{r}_k\mathbf{r}_k^{\mathrm{H}}\right\}\mathbf{W} - \mathrm{E}\left\{\mathbf{s}(k)\mathbf{r}_k^{\mathrm{H}}\right\}
$$

$$
\mathbf{W}(k+1) = \mathbf{W}(k) - \frac{1}{2}\mu\mathbf{r}_k^{\mathrm{H}}(\mathbf{r}_k\mathbf{W}(k) - \mathbf{s}(k)) \tag{4.21}
$$

where the matrix $\mathbf{R}$ and $\mathbf{W}$ are defined in (4.18) and (4.14) respectively. $\mathbf{s}(k)$ is the kth row vector of the matrix $\mathbf{S}$ that is defined as

$$
\mathbf{S} = \begin{bmatrix}
s_1(1) & s_2(1) & \dots & s_N(1) \\
s_1(2) & s_2(2) & \dots & s_N(2) \\
\vdots & \vdots & \vdots & \vdots \\
s_1(k) & s_2(k) & \dots & s_N(k)
\end{bmatrix} \tag{4.22}
$$

where, N denotes the number of transmitting antennas.

Stability

The above equation (4.21) is achieved using LMS (Least Mean Square) algorithm, the step size value μ has to be chosen so that it satisfies some condition to assure stability of the algorithm [21]. This condition is

$$
0 < \mu < \frac{2}{\lambda_{max}} \tag{4.23}
$$

where λ_{max} stands for the largest eigenvalue of the autocorrelation matrix $\mathrm{E}\left\{\mathbf{r}_{\mathrm{k}}\mathbf{r}_{\mathrm{k}}^{\mathrm{H}}\right\}$. μ determines the convergence speed, a large step-size value leads to a fast convergence but high residual MSE. On the other hand, a small step-size makes the algorithm converge to relatively low MSE but slowly. Therefore, one has to be careful when choosing the step-size, as a wrong setting might ruin convergence due to a possible divergence problem.

4.3.4 Recursive Least Square Algorithm (RLS)

SISO system

The Recursive Least Square algorithm, which is similar to the Least Mean Square algorithm, aims for minimizing the sum of the squares of the error (the error between the equalized and desired signal). By adding a weighting factor, RLS has much faster convergence speed and lower MSE compared to LMS [17]. The error between the equalized and desired signal is written as

$$e(k+1) = s(k+1) - \mathbf{w}^{\mathrm{H}}(k)\mathbf{r}(k+1) \tag{4.24}$$

where the equalizer filter vector $\mathbf{w}$ and the received signal vector $\mathbf{r}$ have L (filter length) elements. s is the transmitted symbol and $w(k)$ denotes the filter taps for the kth iteration. Then, the cost function for RLS can be written as

$$J^{\mathrm{rls}}(k) = \sum_{i=1}^{k} \lambda^{k-i}[s(i) - \mathbf{w}^{\mathrm{H}}(k)\mathbf{r}(i)]^2 \tag{4.25}$$

where $0 < \lambda \leq 1$ is the weighting factor and it is fixed for all k. The cost function is minimized by taking the derivatives for all entries of vector $\mathbf{w}$ and setting the equation equal to zero [17].

$$\frac{\partial J^{\mathrm{rls}}(k)}{\partial \mathbf{w}(\mathrm{H})} = \sum_{i=1}^{k} \lambda^{k-i}(s(i) - \mathbf{w}^{\mathrm{H}}(k)\mathbf{r}(i))\mathbf{r}(i) = 0 \tag{4.26}$$

In short, $\mathbf{w}(k)$ can be achieved and written from above equation as

$$\mathbf{w}(k) = \mathbf{R}_{corr}(k)^{-1}\mathbf{r}_{corr}(k) \tag{4.27}$$

where,

$$\begin{aligned} \mathbf{R}_{corr}(k) &= \sum_{i=1}^{k} \lambda^{k-i}\mathbf{r}(i)\mathbf{r}^{\mathrm{H}}(i) \\ \mathbf{r}_{corr}(k) &= \sum_{i=1}^{k} \lambda^{k-i}s(i)\mathbf{r}(i) \end{aligned}$$

The basic goal of the recursive algorithm is to derive the equalizer filter $\mathbf{w}(k+1)$ based on $\mathbf{w}(k)$ which leads to the following recursive relations [17]

$$\mathbf{R}_{corr}(k+1) = \lambda\mathbf{R}_{corr}(k) + \mathbf{r}(k+1)\mathbf{r}^{\mathrm{H}}(k+1) \tag{4.28}$$

and,

$$\mathbf{r}_{corr}(k+1) = \lambda\mathbf{r}_{corr}(k) + s(k+1)\mathbf{r}(k+1) \tag{4.29}$$

From (4.27) it can be obtained that

$$\mathbf{w}(k+1) = \mathbf{R}_{corr}^{-1}(k+1)(\lambda \mathbf{r}_{corr}(k) + s(k+1)\mathbf{r}(k+1))$$

where,

$$\lambda \mathbf{r}_{corr}(k) = (\mathbf{R}_{corr}(k+1) - \mathbf{r}(k+1)\mathbf{r}^{\mathrm{H}}(k+1))\mathbf{w}(k)$$

and,

$$\mathbf{w}(k+1) = \mathbf{w}(k) + \mathbf{R}_{corr}^{-1}(k+1)\mathbf{r}(k+1)\left[(s(k+1) - \mathbf{r}^{\mathrm{H}}(k+1)\mathbf{w}(k))\right]$$

The matrix $\mathbf{R}_{corr}^{-1}(k+1)$ in the above equation can be updated recursively with the help of the matrix inversion lemma [17]. Given matrices $\mathbf{A}$, $\mathbf{U}$, $\mathbf{B}$ and $\mathbf{V}$

$$(\mathbf{A} + \mathbf{UBV})^{-1} = \mathbf{A}^{-1} - \mathbf{A}^{-1}\mathbf{U}(\mathbf{B}^{-1} + \mathbf{VA}^{-1}\mathbf{U})^{-1}\mathbf{VA}^{-1} \tag{4.30}$$

By using the matrix inversion lemma, no matrix inverse process is needed in (4.30) which reduces the computation and complexity. $\mathbf{A}$, $\mathbf{U}$, $\mathbf{B}$ and $\mathbf{V}$ are chosen by the following equations

$$\begin{aligned}\mathbf{A} &= \lambda \mathbf{R}_{corr}(k)\\ \mathbf{U} &= \mathbf{r}(k+1)\\ \mathbf{B} &= \mathbf{I}\\ \mathbf{V} &= \mathbf{r}^{\mathrm{H}}(k+1)\end{aligned}$$

then the matrix inverse lemma yields [17]

$$\mathbf{R}_{corr}^{-1}(k+1) = \frac{1}{\lambda}\left[\mathbf{R}_{corr}^{-1}(k) - \frac{\mathbf{R}_{corr}^{-1}(k)\mathbf{r}(k+1)\mathbf{r}^{\mathrm{H}}(k+1)\mathbf{R}_{corr}^{-1}(k)}{\lambda + \mathbf{r}^{\mathrm{H}}(k+1)\mathbf{R}_{corr}^{-1}(k)\mathbf{r}(k+1)}\right] \tag{4.31}$$

In order to update the filter taps by following (4.31), an invertible matrix $\mathbf{R}_{corr}^{-1}(0)$ is needed.

MIMO system

In the 2x2 MIMO system, the above equations are modified as

$$\mathbf{R}_{corr}^{-1}(k+1) = \frac{1}{\lambda}\left[\mathbf{R}_{corr}^{-1}(k) - \frac{\mathbf{R}_{corr}^{-1}(k)\mathbf{r}_{k+1}^{\mathrm{H}}\mathbf{r}_{k+1}\mathbf{R}_{corr}^{-1}(k)}{\lambda + \mathbf{r}_{k+1}\mathbf{R}_{corr}^{-1}(k)\mathbf{r}_{k+1}^{\mathrm{H}}}\right] \tag{4.32}$$

$$\mathbf{W}(k+1) = \mathbf{W}(k) + \mathbf{R}_{corr}^{-1}(k+1)\mathbf{r}_{k+1}^{\mathrm{H}}\left[s(k+1) - \mathbf{r}_{k+1}\mathbf{W}(k)\right] \tag{4.33}$$

where $\mathbf{r}_k$ stands for the kth row vector of matrix $\mathbf{R}$ that has the same format as the matrix in (4.18) and $\mathbf{W}$ is the equalizer filter taps matrix that has the same format as the matrix in (4.14).

4.4 Blind Equalization

Sending training symbols at the beginning to initialize the receiver can be impractical and not effective for some applications [19]. The correct sampling point has to be known in order to extract the training symbols before the equalizer converges. However, trained algorithms need information from training sequences to converge. In addition to the above issues, the training sequence will also consume bandwidth. So, in some cases, it is desirable to equalize the channel without the aid of training sequence and it is called *blind* equalization ([51], [13], [28], [38], [46]). Figure 4.12 illustrates the structure of a 2x2 MIMO equalizer using blind algorithms.

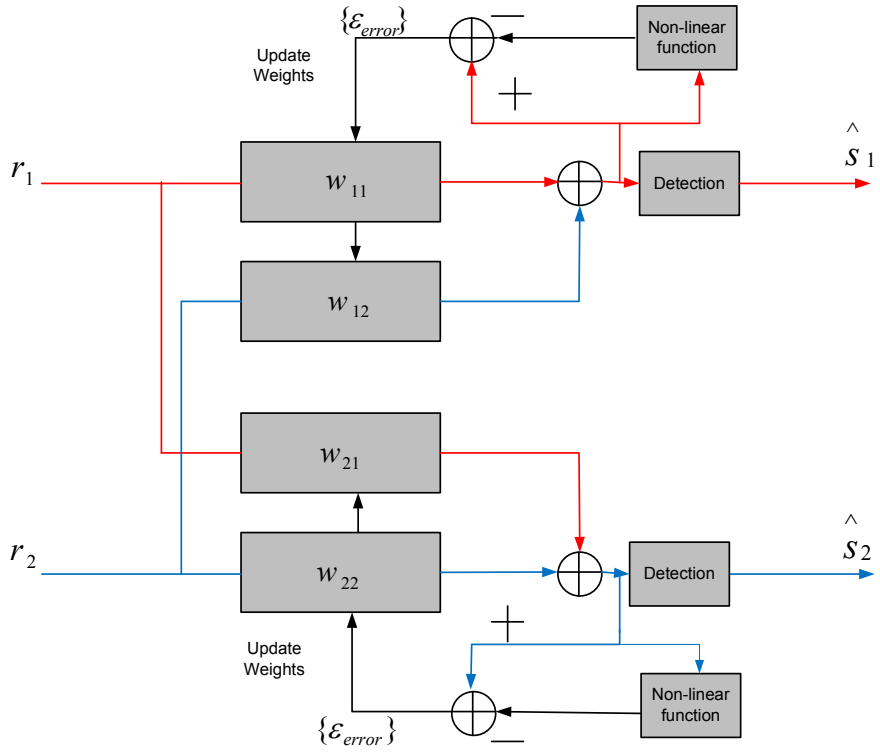

Figure 4.12: MIMO Equalizer using blind algorithm.

4.4.1 Constant Modulus Algorithms (CMA)

SISO system

Many modulation format have the constant modulus property such as PSK, FSK. The received signal $r(k)$ may then be described by

$$r(k) = \sum_{i=1}^{L_c} h(i)s(k-i) + n(k) \tag{4.34}$$

where $s(k)$ is the transmitted signal and $r(k)$ is the received distorted signal plus noise and L_{c} is the channel length. The source is unknown but it has a constant amplitude value $|s| = C$ for all k. So, the objective is to construct a receiver weight matrix $\mathbf{w}$ such that equalized signal $y(k)$ can be denoted by

$$y(k) = \mathbf{w}^{\mathrm{H}}(k)\mathbf{r}(k) \tag{4.35}$$

where $\mathbf{w}(k)$ is defined as $\mathbf{w}(k) = [w(k-\frac{L}{2}), w(k-\frac{L}{2}+1), ...w(k), w(k+1), ...w(k+\frac{L}{2})]^{\mathrm{T}}$ and L is the filter length. $\mathbf{r}(k)$ is defined as $\mathbf{r}(k) = [r(k-\frac{L}{2}), r(k-\frac{L}{2}+1), ...r(k), r(k+1), ...r(k+\frac{L}{2})]^{\mathrm{T}}$ Thus the possible solution is to compute a $\mathbf{w}$ such that $|y(k)| = C$ for all k where $y(k)$ is the output of equalizer. Again, a stochastic gradient descent (SGD) method is considered

$$\mathbf{w}\,(k+1) = \mathbf{w}\,(k) - u\nabla_{w} J^{\mathrm{cma}}\,(\mathbf{w}) \tag{4.36}$$

$$J^{\mathrm{cma}} = \frac{1}{4}\mathrm{E}\left\{\left(|y(k)|^2 - R_{cma}\right)^2\right\} \tag{4.37}$$

where R_{cma} is known as Godard radius [43] and it is a real constant and the value is chosen based on source alphabet and p factor. It was noted [43] that by setting $R_{\mathrm{cma}} = \mathrm{E}\left\{|s(k)|^{2p}\right\}/\mathrm{E}\left\{|s(k)|^{p}\right\}$ and $p = 2$ the existence of a local minima of $\nabla_{\mathbf{w}} J^{\mathrm{cma}}$ that perfectly equalizes the distorted signals with an arbitrary phase rotation is assured in a SISO system. By computing the gradient of the cost function we obtain (4.39) for updating the weights [38] [41]

$$\nabla_{\mathbf{w}} J^{\mathrm{cma}} = y(k)(|y(k)|^2 - R_{\mathrm{cma}})\mathbf{r}^{\mathrm{H}}(k) \tag{4.38}$$

$$\mathbf{w}\,(k+1) = \mathbf{w}\,(k) - \mu y(k)(|y(k)|^2 - R_{\mathrm{cma}})\mathbf{r}^{\mathrm{H}}(k) \tag{4.39}$$

MIMO system

In the MIMO case filter taps are updated independently based on different equalized signals from each receiving antennas

$$y_m(k) = \mathbf{r}_k \mathbf{w}_m(k) \tag{4.40}$$

$$\mathbf{w}_m(k+1) = \mathbf{w}_m(k) - \mu y_m(k)(|y_m(k)|^2 - R_{cma})\mathbf{r}_k^{\mathrm{H}} \tag{4.41}$$

where $\mathbf{w}_m(k+1)$ is the mth column vector of the equalizer matrix that is defined in (4.17), and $y_m(k)$ is the mth equalized signal for mth receiving antenna. $\mathbf{r}_k$ is the kth row vector of receiving matrix $\mathbf{R}$ that is defined in (4.18). It is noteworthy that the CMA not only removes ISI but is phase blind. So, the equalized signals after CMA equalizer might have a constant phase rotation that needs to be rotated back. Additionally, as shown in [11], the CM criterion of (4.37) also works well for non-constant modulus cases such as 16QAM or 64QAM. But the minimization of (4.37) does not ensure the recovery of all source signals in a MIMO system because it may converge to recover the same source signal at many outputs. In order to solve this problem, a cross-correlation term is introduced due to its computational simplicity [32]. Then (4.38) is rewritten as

$$\nabla_{\mathbf{w}_m} J^{\mathrm{cma}}(\mathbf{w}_m) = (1-\alpha) y_m(k)(|y_m(k)|^2 - R)\mathbf{r}_k^{\mathrm{H}} + \alpha \sum_{i=1}^{m-1} \hat{r}_{mi}(k) y_i(k) \mathbf{r}_k^{\mathrm{H}}, (m = 1, 2, ...M) \tag{4.42}$$

equation (4.39) will be modified as

$$\mathbf{w}_m(k+1) = \mathbf{w}_m(k) - \mu y_m(k)[(1-\alpha)(|y_m(k)|^2 - R) + \alpha \sum_{i=1}^{m-1} \hat{r}_{mi}(k) y_i(k)]\mathbf{r}_k^{\mathrm{H}} \tag{4.43}$$

$$\hat{r}_{mi}(k+1) = \lambda \hat{r}_{mi}(k) + (1-\lambda) y_m(k) y_i^*(k) \tag{4.44}$$

where α is the mixing parameter which is chosen between 0 and 1. $\hat{r}_{mi}(k) = \mathrm{E}[y_m(k)y_i^*(k)]$ is the cross-correlation between the mth and the ith equalizer outputs and prevents the extraction of the same signal at many outputs. $\lambda \in [0, 1]$ is a parameter that controls the length of the effective data window in the estimation. The first term in (4.42) ensures the recovery of only one signal at each equalizer output and the cross-correlation term ensures that each equalizer output is different from other ones. α has to be selected carefully for its optimum value in different channel conditions. For example, higher α value is chosen if equalizers are more likely to converge the same channel. Here if we assume a 2x2 Los MIMO system with an optimal separation (Inter-Stream-Interference from Tx_2 has a 90° phase shift compared with desired transmitted signals at Tx_1). Initial filter taps are set up by the following matrix

$$\begin{array}{ccc} \uparrow & \begin{bmatrix} 0 & 0 \\ \vdots & \vdots \\ 0 & 0 \end{bmatrix} & \uparrow \\ w_{11} & \begin{bmatrix} e^0 & e^{-j\frac{\pi}{2}} \end{bmatrix} & w_{21} \\ \downarrow & \begin{bmatrix} 0 & 0 \\ \vdots & \vdots \\ 0 & 0 \end{bmatrix} & \downarrow \\ \uparrow & \begin{bmatrix} 0 & 0 \\ \vdots & \vdots \\ 0 & 0 \end{bmatrix} & \uparrow \\ w_{12} & \begin{bmatrix} e^{-j\frac{\pi}{2}} & e^0 \end{bmatrix} & w_{22} \\ \downarrow & \begin{bmatrix} 0 & 0 \\ \vdots & \vdots \\ 0 & 0 \end{bmatrix} & \downarrow \end{array} \tag{4.45}$$

where $\mathbf{w}_1 = [w_{11} \quad w_{12}]^{\mathrm{T}}$ and $\mathbf{w}_2 = [w_{21} \quad w_{22}]^{\mathrm{T}}$. Each column vector w_{ij} has a length of L taps. $e^0, e^{-j\frac{\pi}{2}}, e^{-j\frac{\pi}{2}} and e^0$ are the central taps for $w_{11}, w_{12}, w_{21} and w_{22}$ respectively. There is another algorithm that uses the Gram-Schmidt orthogonalization procedure to force this separation, more detailed discussion can be found in paper [31] for reader's interest. Figure 4.13 shows the initial filters setting in the simulation system (also given in 4.45), where it is assumed that the 2x2 SS-SP MIMO system starts with an optimal antenna separation.

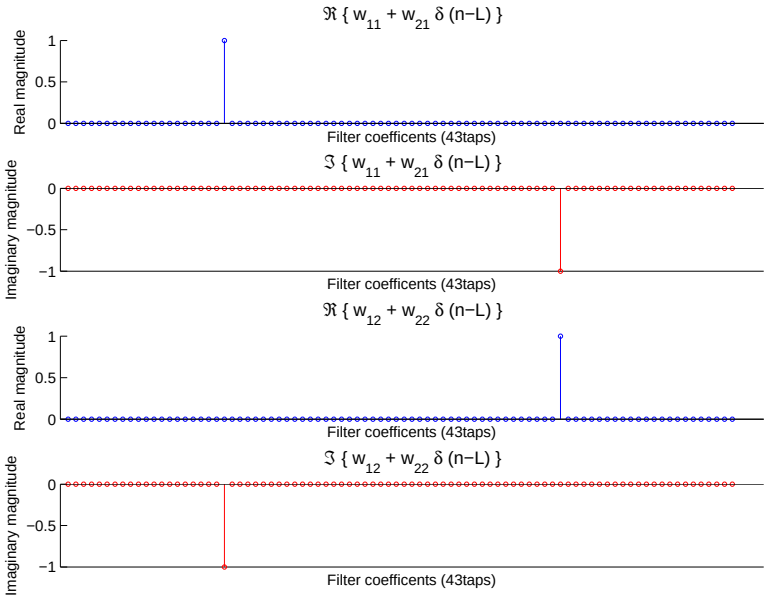

Figure 4.13: Filter initialization of STE for the 2 × 2 SS-SP MIMO

4.4.2 Modified Constant Modulus Algorithm (MCMA)

SISO system

The CMA (Constant Modulus Algorithm) algorithm expects constellations with a constant amplitude, which degrades the equalization performance when a M-QAM (M>4) modulation is used since it has multi-modulus property. In order to improve the performance of the CMA for M-QAM (M>4), a multi-modulus algorithm, called MCMA (Modified Constant Modulus Algorithm), has been proposed in [29]. In this algorithm the cost function for CMA (4.38) is modified to consider the real and imaginary parts separately. The modified cost function is written as

$$J^{\text{mcma}}(k) = J_R(k) + J_I(k) \tag{4.46}$$

where $J_R(k)$ and $J_I(k)$ are the cost functions for the real- and imaginary parts of the equalizer output $y(k) = y_R(k) + j \cdot y_I(k)$ respectively and they are defined as

$$J_R(k) = \mathrm{E}\left\{\left(|\Re\{y(k)\}|^2 - R_{\mathrm{R}}\right)^2\right\} \tag{4.47}$$

$$J_I(k) = \mathrm{E}\left\{\left(|\Im\{y(k)\}|^2 - R_{\mathrm{I}}\right)^2\right\} \tag{4.48}$$

Assuming the input data is complex numbers with two dimensions, R_{R} and R_{I} are the real constants determined for the real and imaginary parts of the source signals respectively

$$R_R = \frac{E\left\{|\Re\{s(k)\}|^4\right\}}{E\left\{|\Re\{s(k)\}|^2\right\}} \tag{4.49}$$

$$R_I = \frac{E\left\{|\Im\{s(k)\}|^4\right\}}{E\left\{|\Im\{s(k)\}|^2\right\}} \tag{4.50}$$

where $\Re\{s(k)\}$ and $\Im\{s(k)\}$ denote the real and imaginary part of source signals $s(k)$ respectively. The tap weights vector is updated using SGD to optimize the cost function

$$\mathbf{w}(k+1) = \mathbf{w}(k) - \mu\nabla_w J^{\text{cma}}(\mathbf{w}) \tag{4.51}$$

$$= \mathbf{w}(k) - \mu e(k)\mathbf{r}^{\text{H}}(k) \tag{4.52}$$

where the error signal $e(k) = e_R(k) + j * e_I(k)$ is given by

$$e_{\text{R}}(k) = \Re\{y(k)\}\left(|\Re\{y(k)\}|^2 - R_{\text{R}}\right)$$
$$e_{\text{I}}(k) = \Im\{y(k)\}\left(|\Im\{y(k)\}|^2 - R_{\text{I}}\right)$$

MIMO system

For MIMO systems, equalizer taps are updated independently for different receiving antennas which is similar to the Simplified Constant Modulus Algorithm (SCMA) method. This processing is expressed as

$$y_m(k) = \mathbf{r}_k\mathbf{w}_m(k) \tag{4.53}$$

$$e_{m,\text{R}}(k) = \Re\{y_m(k)\}\left(|\Re\{y_m(k)\}|^2 - R_{\text{R}}\right) \tag{4.54}$$

$$e_{m,\text{I}}(k) = \Im\{y_m(k)\}\left(|\Im\{y_m(k)\}|^2 - R_{\text{I}}\right) \tag{4.55}$$

$$e_m(k) = e_{m,\text{R}}(k) + j * e_{m,\text{I}}(k) \tag{4.56}$$

$$\mathbf{w}_m(k+1) = \mathbf{w}_m(k) - \mu e_m(k)\mathbf{r}_k^H \tag{4.57}$$

here $\mathbf{r}_k$ is the kth row vector of receiving matrix $\mathbf{R}$ that is defined in (4.18) and $y_m(k)$ is the kth sample of equalized signals on the mth receiving antenna. This algorithm modifies the CMA cost function so that the resulting cost functions becomes dependent of the phase rotation. Hence, the MCMA can correct for some carrier frequency offset and remove the ISI simultaneously. As a result MCMA results in a performance improvement in convergence speed and residual MSE floor [29].

4.4.3 Simplified Constant Modulus Algorithm (SCMA)

MIMO system

A Simplified Constant Modulus Algorithm (SCMA) has recently been proposed in [32]. Instead of projecting signal points onto a M-QAM constellation based on both real and imaginary part, it only considers one dimension (either real or imaginary part due to their symmetry) which is more flexible and less complicated compared to CMA or MCMA from practical implementation point of view. This algorithm suggests to minimize the following cost function for the mth Rx output and based on the real-part of signal in this thesis

$$J_m^{\text{scma}} = \mathrm{E}\left\{(|\Re\{y_m(k)\}|^2 - R_{\text{scma}})^2\right\} \tag{4.58}$$

where $\Re\{\cdot\}$ stands for the real-part operation. R is given as

$$R_{\text{scma}} = \frac{\mathrm{E}\left\{|\Re\{s(k)\}|^4\right\}}{\mathrm{E}\left\{|\Re\{s(k)\}|^2\right\}} \tag{4.59}$$

In order to force the separation of equalized signals at different outputs, the same cross-correlation term is used here as in (4.42) and the gradient of (4.58) is rewritten as

$$y_m(k) = \mathbf{r}_k \mathbf{w}_m(k)$$

$$\begin{aligned}
\nabla J_{\mathbf{w}_m}^{scma} &= (1-\alpha)\Re\{y_m(k)\}\left[(|\Re\{y_m(k)\}|^2 - R) + \alpha \sum_{i=1}^{m-1} \hat{r}_{mi}(k) y_i(k)\right]\mathbf{r}_k^{\mathrm{H}} \\
\mathbf{w}_m(k+1) &= \mathbf{w}_m(k) - \mu\Re\{y_m(k)\}\left[(1-\alpha)(|\Re\{y_m(k)\}|^2 - R) + \alpha \sum_{i=1}^{m-1} \hat{r}_{mi}(k) y_i(k)\right]\mathbf{r}_k^{\mathrm{H}}
\end{aligned}$$

where α is the mixing parameter which is chosen between 0 and 1. And $\hat{r}_{mi}(k) = \mathrm{E}\left[y_m(k) y_i^*(k)\right]$ is the cross-correlation between the mth and the ith equalizer outputs and prevents the extraction of the same signal at many outputs. $y_m(k)$ is the kth equalized signal of mth receiving antenna. $\mathbf{r}_k$ is the kth row vector of receiving matrix $\mathbf{R}$ that is defined in (4.18). The criterion of SCMA leads to the converge of the signal constellation that, in absence of noise, corresponds to recovery of desired signal with a constant phase rotation that differs between modulation formats. For QAM this rotation is $\frac{\pi}{2}$. It is shown in [32] that the proposed algorithm presents a lower computational complexity compared to the MCMA without any loss in performance but it can be less stable than the other two algorithms in some specific channel conditions.

4.5 Decision-Directed Mode (DD)

In addition to blind and training mode, there is another mode called Decision-Directed mode that is commonly used. The DD (Decision-Directed) mode that has been implemented for a 2x2 MIMO system is illustrated in Figure 4.14. The structure only shows the output of the equalizer for the first receiving antenna. The main idea of DD mode is that it assumes the current hard decision of equalized symbol from previous iteration is correct and the channel

is not changed during this iteration period so that filter taps from previous iteration can be used to equalize the received signals for the current iteration and treating equalized symbols as training symbols to update the filter taps for the current iteration. Then the training mode algorithms such as LMS and RLS processes equalization without receiving any training sequence from the transmitter. This is why blind equalization is normally followed by a DD mode in order to significantly improve the MSE of the estimation. Thus in DD mode perfect initial convergence is not needed for the equalizer to converge to the optimal setting as long as estimated signals are correct most of the time.

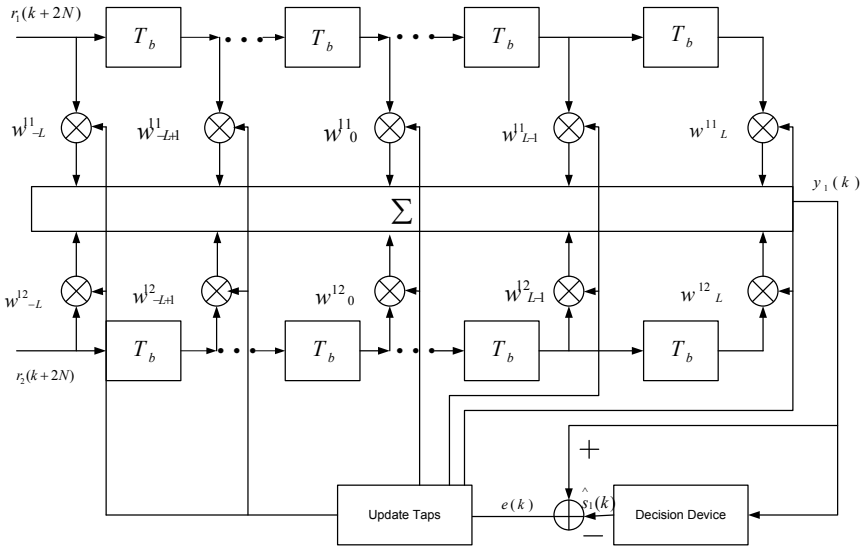

Figure 4.14: 2×2 MIMO-STE under Decision-Directed Mode.

MIMO system

For RLS algorithm the error function of (4.24), in DD mode, can be rewritten as

$$e_m(k+1) = \hat{s}_m(k+1) - \mathbf{r}_{k+1}\mathbf{w}_m(k)$$

where $\mathbf{r}_{k+1}$ is the $k+1$th row vector of $\mathbf{R}$ that defined in (4.18). $\mathbf{w}_m(k)$ is the mth column vector of $\mathbf{W}$ matrix that is defined in (4.14). $\hat{s}_m(k+1)$ is the hard decision of equalized signal $y_m(k+1)$ at sample time $k+1$ on the mth receiving antenna. Then, filter taps can be updated by following equation

$$\mathbf{W}(k+1) = \mathbf{W}(k) + \mathbf{R}^{-1}_{corr}(k+1)\mathbf{r}^{\mathrm{H}}_{k+1}[\hat{\mathbf{s}}(k+1) - \mathbf{r}_{k+1}\mathbf{W}(k)]$$

For LMS algorithm, the error function is modified as

$$e_m(k) = \hat{s}_m(k) - \mathbf{r}_k\mathbf{w}_m(k)$$

where $\hat{s}_m(k)$ is the hard decision of equalized signal $y_m(k)$ at sample time k for the mth receiving antenna. Equation (4.21) is rewritten as

$$\mathbf{W}(k+1) = \mathbf{W}(k) - \frac{1}{2}\mu \mathbf{r}_k^{\mathrm{H}}(\mathbf{r}_k \mathbf{W}(k) - \hat{\mathbf{s}}(k))$$

4.6 Complexity comparison of different algorithms

Since there is always a trade off between the performance of the algorithms and their computation complexity. It is important and necessary to make a complexity comparison between different algorithms [31] and try to find a algorithm that might achieve the best balance.

Algorithm	**Multiplications**	**Additions**
CMA	$2(4M \cdot L + 3) \cdot M$	$(9M \cdot L + 2) \cdot M$
$MCMA$	$2(4M \cdot L + 3) \cdot M$	$(9M \cdot L + 5) \cdot M$
$SCMA$	$(4M \cdot L + 3) \cdot M$	$(6M \cdot L + 1) \cdot M$
LMS	$(8M \cdot L + 2) \cdot M$	$(9M \cdot L + 2) \cdot M$
RLS	$4M^2 \cdot L(1 + 6L + M \cdot L)$	$22M^2 \cdot L^2 + 2M + 1 + 10M^2 \cdot L + 4M \cdot L$

Table 4.1: Comparison of complexity of different algorithms per weight update.

In Table (4.1), L denotes the order of equalizers (number of filter taps) and M is the number of receiving antennas. From this table it can be seen that SCMA has the lowest computational complexity. It is noteworthy that (as shown in the simulation section), SCMA has almost the same performance as the MCMA algorithm but lower computation complexity. This might be a big benefit for the real implementation since SCMA only use the information from one-dimension of signals to update weights instead of two. Compared with LMS, the RLS algorithm has a faster convergence speed but much higher complexity which is shown in the above table.

Chapter 5

Simulations

The simulation software was written in Matlab using a modular architecture to enable easy selection and combination of different blocks. A graphical user interface (GUI) was constructed alongside the code to ease block selection and simulation parameters selection. The simulator handles both 2x2 SS-SP LoS MIMO and 4x4 SS-DP LoS MIMO. All the simulations are done at baseband using Matlabs 64 bit floating point numbers making quantization errors negligible. A block diagram of the entire 2x2 SS-SP LoS MIMO system can be seen in Figure 5.1. It gives a good overview of the system design and makes it easier to visualize how data is processed in the system. Both branches generate independent data which remain separate until being combined by the MIMO channel. At the Rx the data streams are processed separately with the exception of the STE which needs both data streams in order to cancel the inter-stream interferences. Each Rx branch then outputs its estimate of the transmitted symbol- and bit sequence and thus the branches have their own BER and MSE values.

Following the sequence of events necessary to generate and process a block of data bits gives a better insight into the design. Data bits are generated using a uniform random distribution which are modulated in the modulator into a Gray coded M-QAM constellation. The resulting symbol sequence is then filtered using a oversampled root-raised-cosine filter. The filter emulates an analog signal by an oversampling rate of 16, resulting in a symbol time of $T_{Qs} = (Q \cdot F_s)^{-1} = 1.25$ ns, and a roll-off factor of $\beta = 0.35$. The signal then passes through the LoS MIMO channel which will be discussed in Section 5.3. At the receiver additive white Gaussian noise with zero mean is added to the signal. Independent realizations of the AWGN is added to each signal stream. This is then followed by a matched filter that is not oversampled as in the Tx. Phase noise with a certain spectral density $S_{ph}(\omega)$ is then generated once (new realization for each symbol) and multiplied to both signal streams which is consistent with the assumption of a synchronous system (one phase noise realization for the whole system). The analog to digital converter then samples the signal at baud rate without any timing errors. The signal then enters the space time equalizer (STE) where it is equalized and the inter-stream interferences are cancelled. The STE tunes its equalizers by using the error signals generated by the detectors. The detectors have phase trackers that rotate the signal so to alleviate some of the phase noise. The sliced signal is then finally feed to the demodulator which outputs the estimated data sequence.

The following approximations where made for the design of the system (most of which can

easily be dropped in future versions).

- The system is considered to be completely synchronous so that there is no need for a symbol timing estimation at the ADC and no need for any phase adjustments between the Rx signal streams in the STE. There is also no carrier frequency offsets between Tx and Rx.
- There are no quantization errors introduced to the system. The simulation is done at a 64 bit floating point number representation making it highly accurate.
- Between every Tx and Rx pair there are only two paths considered, one direct LoS path and one ground reflection. The direct paths all have the Rx power of one and all the ground reflected paths have the same amplitude b. All the ground reflections have the same delay as well $\tau = 6.3$ ns. This is the Two Ray model.
- The Tx and Rx antennas can only move back and forth in a plane that is parallel to the masts.

These assumptions ease the design of the simulation and allow for more easily interpretable results.

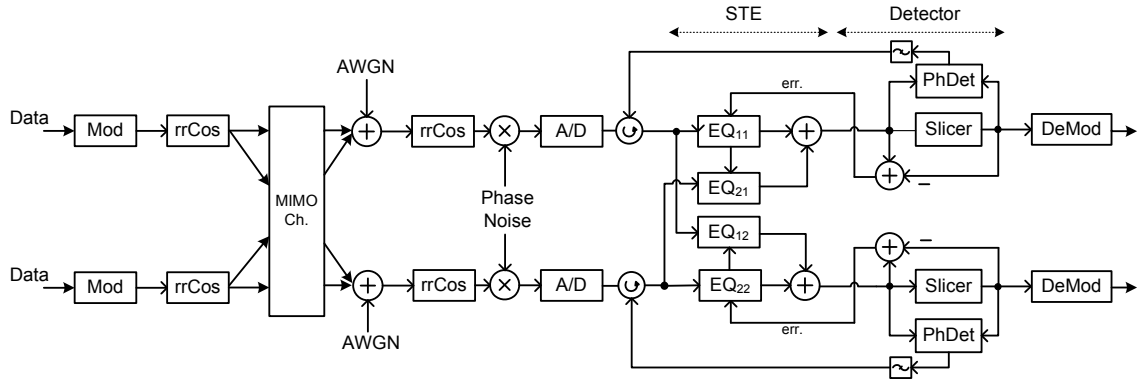

Figure 5.1: A block diagram representing the tentative design of the simulator for a 2x2 SS-SP LoS MIMO.

A 4x4 SS-DP LoS MIMO system will also be investigated. The design is almost the same as shown in Figure 5.1 with the exception that there are four branches now at the Tx and Rx and the design of the STE now includes 16 equalizers (including 8 XPICs). This is shown for one polarization at the Rx in Figure 5.2. The dual polarized 4x4 channel matrix is modeled using (3.25) which assumes that both the Tx and Rx have two dual polarized antennas (both polarized antennas collocated). Each ground reflection has though an independent phase offset creating 16 independent frequency selective channels.

For convenience some basic simulation constants are summarized in Table 5.2. All of them are kept constant during the simulations unless otherwise stated.

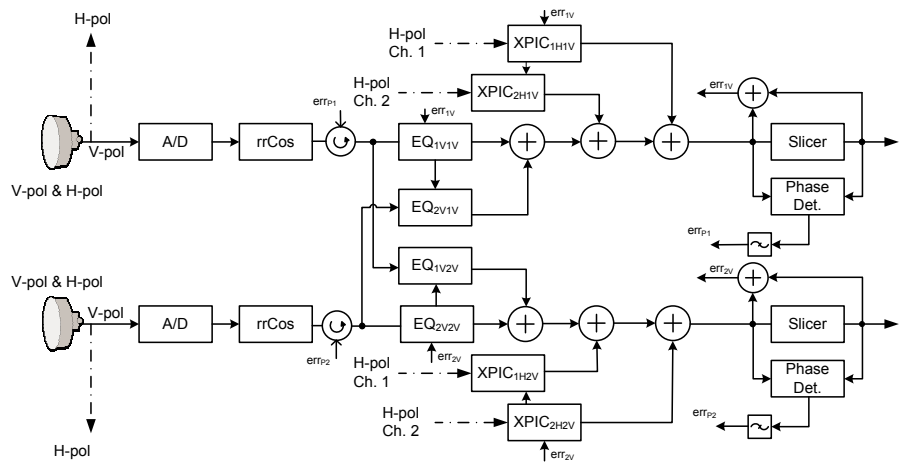

Figure 5.2: A block diagram representing the tentative design of the vertically polarized Rx for a 4x4 SS-DP LoS MIMO. The block diagram neglects all noise sources.

5.1 Goals

The goal of the simulation is to evaluate the performance of a LoS MIMO system, both 2x2 SS-SP and 4x4 SS-DP, subjected to different conditions and using different adaptive algorithms. The results should then work as a guideline for an implementation of a real system and help to select algorithms and give an understanding of the impact of certain suboptimalities in the installation of the system as well as response to different channel conditions. To be more specific the desired results are given in Table 5.1.

Section	Description
6.2	Tolerance to low XPD
6.2	Tolerance to suboptimal antenna placements
6.6	Tolerance to phase noise
6.1	Tolerance to frequency selective channels
6.5	Tolerance to mast swing
6.4, 6.3	Evaluation of different algorithms for STE

Table 5.1: Desired results obtained by simulation and the section where they are published in the report.

The evaluation of different adaptive algorithms (STE's) is perhaps the biggest task. For that part the main focus will be on blind equalizers as well as training based methods to initialize the system followed by Decision Directed (DD) adaptive algorithms to track the channel. For these methods there are mainly three attributes that are investigated

- Convergence speed
- MSE- and/or BER-floors
- Tolerance to mast swing and phase noise

5.2 Quantifying Performance

Comparing performance requires some measurable quantities that can be used to evaluate different setups and different channel conditions. There will be mainly three quantities used for comparison. The first one is the bit-error-rate (BER) defined as the ratio between the number of bits received in error to the total number of bits received or more precisely

$$\text{BER} = \frac{\sum_{n=1}^{L_b} |b_n - \hat{b}_n|}{L_b}$$

where b_n is the nth transmitted bit (0 or 1) and $\hat{b}_n$ is the nth estimated bit at the receiver. L_b is the total length of the bit sequence. This is a very practical quantity to measure for a real system since that will define for a large part the actual performance of a real system. Since the simulator does not use any error correction coding the BER can easily be lowered by using a good coding scheme. The target BER is though often very low requiring very long simulation times to get obtain reliable estimates. Another quantity that does not require such long simulation times is the mean-square-error (MSE). It averages the square error between the soft estimate of a symbol and the actual symbol transmitted

$$\text{MSE} = \frac{\sum_{n=1}^{L_B} |s_n - \hat{r}_n|^2}{L_B}$$

Where s_n is the nth transmitted symbol and $\hat{r}_n$ is the soft estimate of the nth received symbol. L_B is then the number of symbols transmitted.

The final quantity is the penalty described in Section 3.6. It quantifies how much more the Tx power needs to be increased between different scenarios to achieve the same BER and is usually specified in dB. The target BER for the penalty will be 10^{-3}. A baseline SNR needs to be established for the penalty, that is usually the lowest achievable SNR for a certain BER. For a SISO system with a flat channel and using 16QAM modulation the SNR is about 10.5 dB for a BER of 10^{-3}. A 2x2 MIMO system will have a 3 dB array gain[1] so the baseline SNR will be considered to be 7.5 dB. Finding the penalty using simulation software can be a challenge since the BER is an output and is a function of great many variables. The SNR needed for a certain BER is desired to be found for a certain setup. For these simulations a search algorithm inputs the SNR into the simulator and runs it successively until the desired BER has been found. That SNR minus the baseline SNR is then the penalty.

5.3 The Channel

The frequency selective channels used by the simulator is the Two Ray channel described in Section 3.4. The Tx and Rx antenna discs are mounted on two masts of height L_T and L_R respectively. The Rx mast is situated on a hill of height L_L and the horizontal distance between the base of the masts is L_H. The masts can then have a time varying tilt of β_T for the Tx and β_R for the Rx to simulate mast movement in heavy wind. The setup can be seen in Figure 5.3. Unless otherwise specified the parameters for the channel setup are the same as given in Table 5.2.

[1] Two Rx antennas doubles the received power.

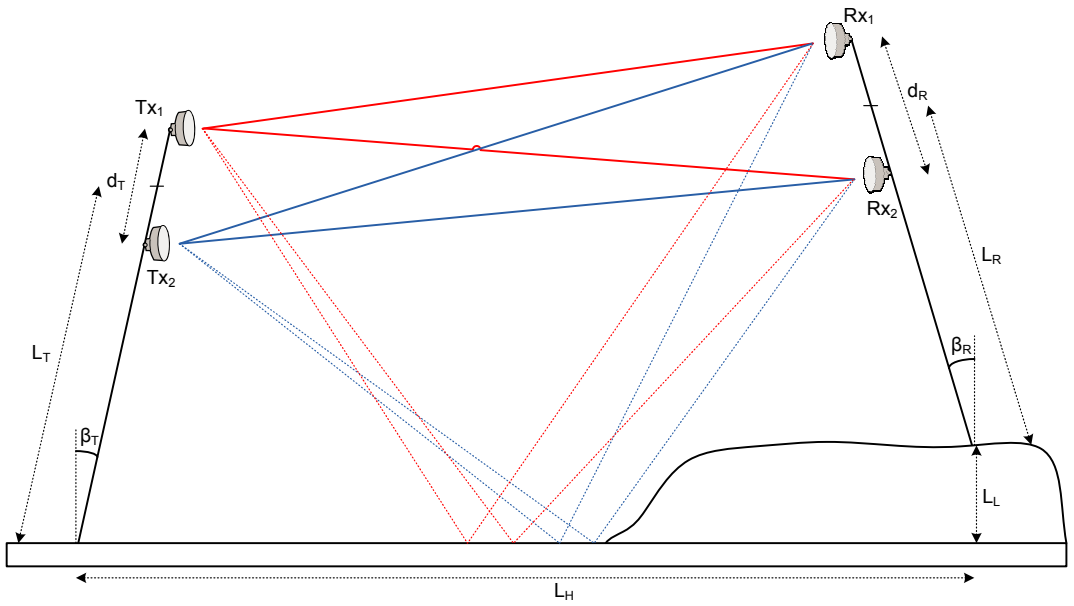

Figure 5.3: The setup of the Tx and Rx antennas. β_T, β_R, d_T, d_R, L_T, L_R, L_L and L_H can all be varied.

The amplitude of the reflected waves is b and for the purpose of the simulation it is bounded between zero and one where one is the amplitude of the direct wave. Each ground reflection must traverse a longer path so there is a delay difference between the ground reflection and the direct path. This delay is set to be fixed in accordance to Rummler's model at 6.3 ns which is a common standard but the phase offset of the arriving direct path and ground reflection is random. For a 2x2 MIMO system there are 4 channels where each one has an independent phase offset between ground reflection and direct path but otherwise share the same parameters. For example the channel between Tx_2 and Rx_1 will have the same delay and same ground reflection amplitude as any other channel but it has an independent phase offset ϕ_{21}. This phase offset is enough to determine how the channel behaves. It can be relatively flat or it can act as a lowpass-, highpass- or bandpass filter. If the channels have a deep notch then noise will be amplified but attenuating channels do not necessarily represent the worst case scenario. Since the channels produce collectively some frequency dependent MIMO channel with some frequency dependent singular values as is discussed in 3.3 which influence the performance it is not always easy to identify the worst case channel.

Since there are infinitely many channel realizations it is necessary to narrow down the selection to a few cases. Selecting the most interesting channels can be challenging since it is not even clear what represents a worst case. The selection process thus becomes somewhat ad-hoc. The channel responses displayed for the MIMO channels are obtained by measuring the impulse responses seen between each Tx- and Rx antenna pair. This is done by transmitting an impulse on one transmitter at a time instant and measuring the output from each receiver. The impulse responses include the Tx- and Rx filters as well as the ADC. Selecting the channels for the 4x4 MIMO is clearly even harder since there are 16 independent channel responses making up the whole MIMO channel. To ease the selection the 4x4 MIMO

channels are constructed from the 2x2 channels making the following simplifications that both the polarizations and corresponding cross-polarized paths see the same channels as the single polarized case. That is the channels between Tx_n and Rx_m are the same for the SP and DP cases independent of polarization ($\mathbf{h}_{nVmV} = \mathbf{h}_{nHmH} = a\mathbf{h}_{nHmV} = a\mathbf{h}_{nVmH}$ where a is some constant related to the XPD). This is made more apparent in the following sections where the two channels chosen for use in the simulations are described (frequency plots are obtained using DTFT). They are denoted A and B and both have their defining attributes.

These channels are also realized as SISO channels by removing the paths $\mathbf{h}_n m$ where $n \neq m$. The BER for the resulting parallel channels are then averaged for penalty calculations.

5.3.1 Channel A: All Notches

2x2 SS-SP LoS MIMO: This channel has a notch between all Tx- and Rx pairs. This will attenuate part of the spectrum of the signal by the full notch depth with a subsequent SNR reduction at the receiver. The placement of the notches can be seen in Figure 5.4(a) where the amplitude response is plotted from $-F_s/2$ to $F_s/2$ where F_s is the sampling frequency. The depth of these notches depend on the amplitude of the ground reflection selected here to be $b = 0.9$. The channels act as FIR filters and have thus a guaranteed linear phase response which can be seen in Figure 5.4(b). Looking at the pole zero plot for the z-transform of the impulse responses in Figure 5.4(c) it is noteworthy that all of the channels have a zero rather close to the unit circle making them harder to invert at the Rx. Finally the condition number along with the singular values is plotted in Figure 5.4(d) as a function of frequency.

4x4 SS-DP LoS MIMO: This channel is now significantly more complex even though it is constructed from the channel in Figure 5.4. The magnitude of the impulse response is plotted in Figure 5.5 while the condition number and singular values are plotted in Figure 5.6.

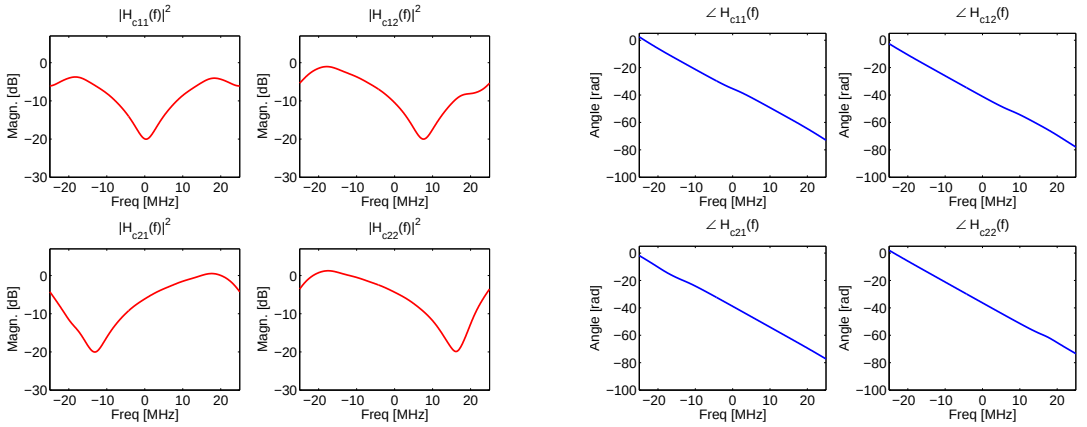

(a) Magnitude

(b) Phase

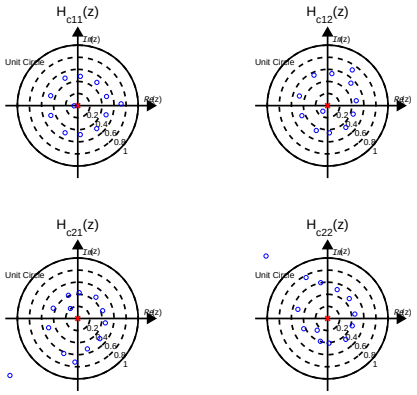

(c) Pole Zero Plots

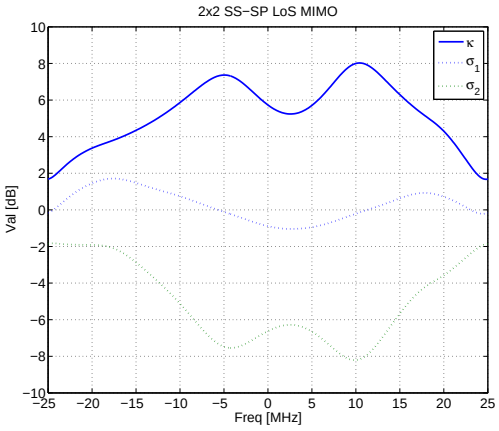

(d) Condition Number and Singular Values

Figure 5.4: Channel A: Frequency response of the four SISO channels making up the 2x2 SS-SP LoS MIMO channel along with pole zero plots and a plot of the condition number and singular values as a function of frequency. For these plots $b = 0.9$.

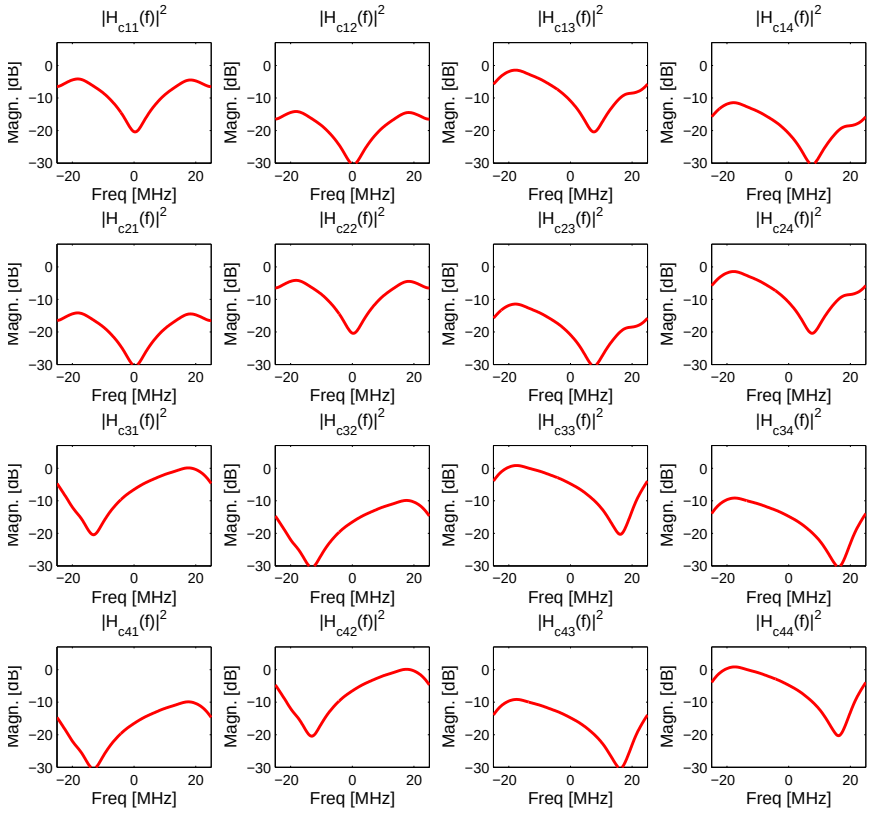

Figure 5.5: Channel A: The magnitude of the impulse responses for the 4x4 SS-DP LoS MIMO channel.

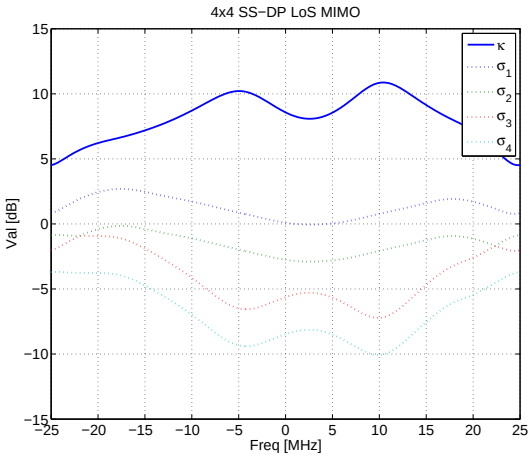

Figure 5.6: Channel A: The condition number and singular values for the 4x4 SS-DP LoS MIMO channel.

5.3.2 Channel B: Ill conditioned

2x2 SS-SP LoS MIMO: This channel has only one deep notch but is very ill conditioned since the condition number becomes very high for some part of the spectrum as is shown in Figure 5.7(d). The magnitude response is seen to contain only one deep notch while the other channels are relatively flat (Figure 5.7(a)). The phase is again linear as is expected and as can be seen from Figure 5.7(b). Finally the pole zero plot shows that the channel containing the notch has a zero closest to the unit circle (Figure 5.7(c)).

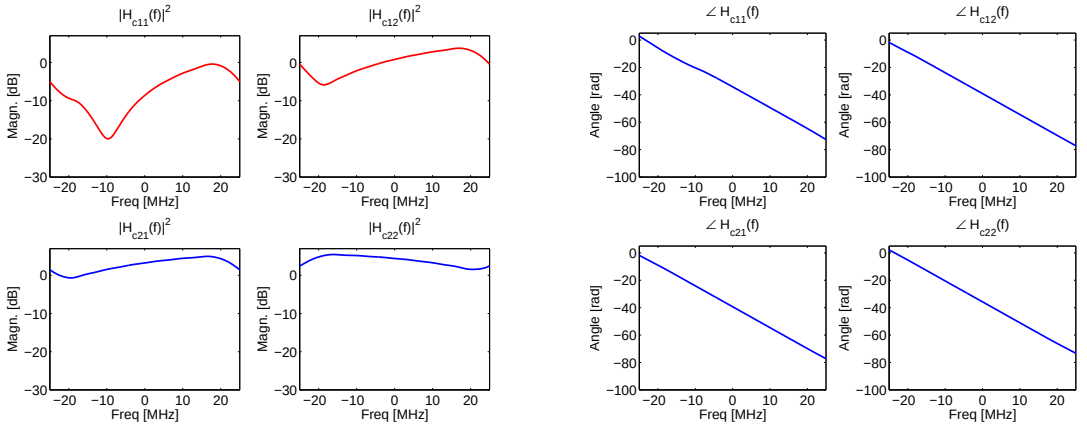

(a) Magnitude

(b) Phase

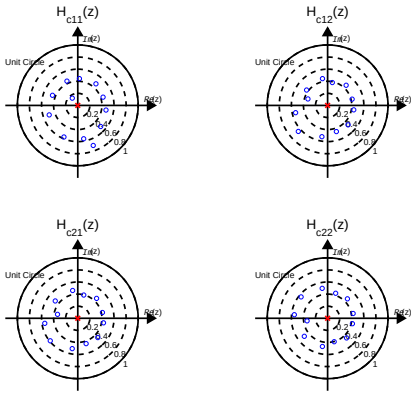

(c) Pole Zero Plots

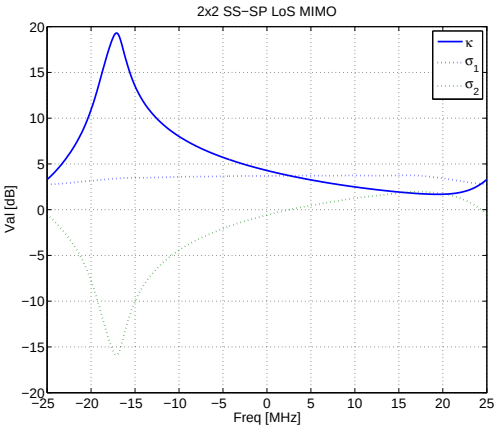

(d) Condition Number and Singular Values

Figure 5.7: Channel B: Frequency response of the four SISO channels making up the 2x2 SS-SP LoS MIMO channel along with pole zero plots and a plot of the condition number and singular values as a function of frequency. For these plots $b = 0.9$.

4x4 SS-DP LoS MIMO: The magnitude of the impulse responses is plotted in Figure 5.8 while the condition number and singular values are plotted in Figure 5.9. Some of the notches in Figure 5.8 seem to be deeper than others, this is because of the XPD chosen to be 10 dB for the plots.

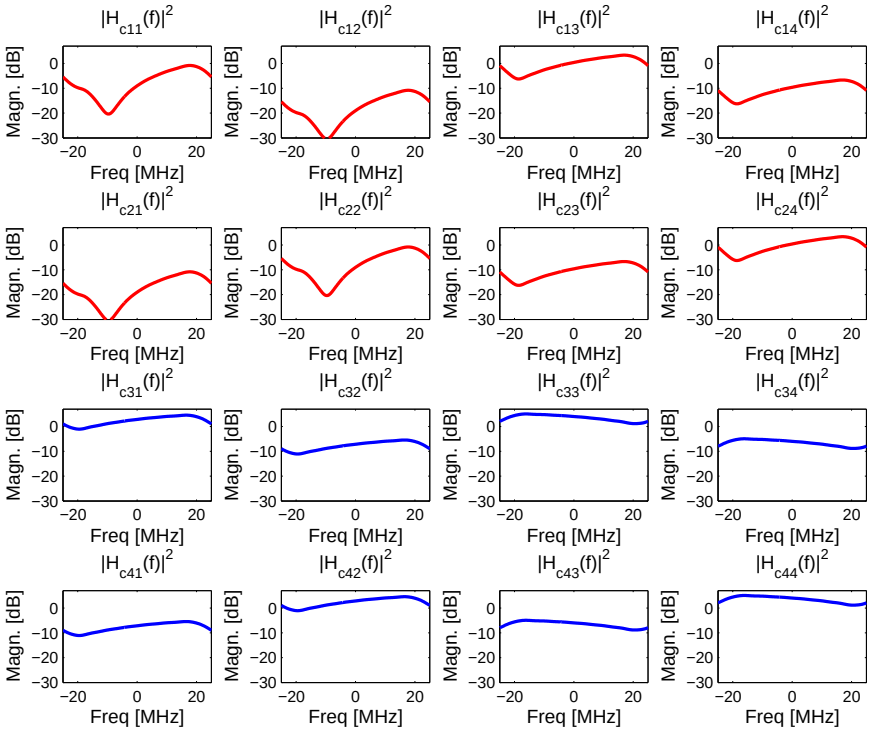

Figure 5.8: Channel B: The magnitude of the impulse responses for the 4x4 SS-DP LoS MIMO channel. Here XPD is 10 dB.

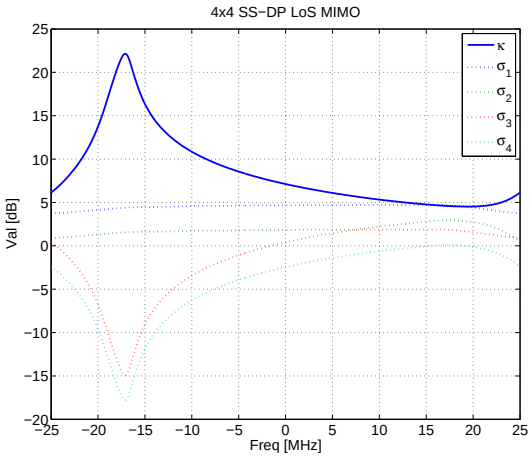

Figure 5.9: Channel B: The condition number and singular values for the 4x4 SS-DP LoS MIMO channel.

5.3.3 Mast Swing

Mast swing will cause the antennas to move and this movement will change the channel. The length of the direct path will change which in turn changes the phase of the direct path. Since the ground reflection phase is modeled as static this will change the offset between the phase of the ground reflection path and the direct path causing the notches seen in Figure 3.11 to move across the channel. This forces the STE to adapt continuously to new channel conditions and this movement sets a lower limit for the convergence speed of the adaptive filters.

How the channel behaves with mast swing in reality is poorly understood since the phase offset between the LoS path and the ground reflection path evolves with an unknown distribution as the antennas moves. If the model was entirely calculated from the geometry then the conclusion could easily be drawn that the phase offset hardly changes at all. A millimeter wave reflecting off some unknown surface will though experience a phase shift that can differ even for only slight changes. This is enough to motivate that it is not prudent to assume a static channel when the antennas are moving. Fixing the phase of the ground reflection while varying the LoS paths according to geometric calculations seems to be an intuitive compromise representing a "bad enough" scenario. This is further motivated by the fact that the ground reflected path is modeled as having a static relative delay. Quantifying how much a standard mast might move in heavy wind can also be quite difficult. The values chosen in table 5.2 are only motivated compromises explained below.

There have been measurements of the width (in degrees) of half of the 3-dB beam widths for parabolic antennas commonly used for microwave links. There is quite a selection of antennas with different gains intended for different frequency bands. A high half 3-dB beam width is here considered to be 2.3°. The value 2.3° is thus chosen to represent the highest possible tilt of a mast. It is a well known fact that the frequency of oscillation for a pendulum made up of a solid uniform rod of length L is

$$f = \frac{1}{2\pi}\sqrt{\frac{3g}{2L}}$$

where g is the acceleration of gravity (9.8 [m/s^2]). For a 10 m long rod the result is $f \approx 0.2$ Hz. This value is used as the maximum frequency of mast swing for the simulations.

5.4 Space Time Equalizers

A space time equalizer is implemented at the receiver in order to compensate for inter-symbol-interference, inter-stream-interference, cross-polarization-distortion and also to track the channel changes. One scope of this master thesis is to analyze and evaluate different adaptive algorithms for space time equalizers. Due to the complexity of implementation issues, only MMSE (Minimum mean square error) algorithms are analyzed and evaluated in this thesis.

According to the properties of the chosen channels, a discrete-time baseband FIR equalizer with 43 taps is set up in all simulations and the 21st tap is set as the center tap.

5.4.1 Trained Decision Directed Equalization

The scheme used by the space time equalizers fall into two categories: Blind followed by Decision Directed mode and Trained followed by Decision Directed mode. The trained algorithms are mainly LS (Least Square) but LMS (Least Mean Square) and RLS (Recursive Least Square) can also be applied in training mode. The Decision-Directed algorithms include LMS (Least Mean Square) and RLS (Recursive Least Square) along with some variants.

The trained algorithms use 200 and 400 training symbols for 2x2 SS-SP and 4x4 SS-DP MIMO systems respectively to obtain the initial convergence. The weights update of equalizers will then be switched to DD (Decision Directed) mode. The training sequences are modulated from the same pseudorandom binary sequence (PRBS) so that each realization of the filter taps generated by training and the same algorithm should be similar (noise will also affect the filter).

5.4.2 Blind Equalization

Three different blind algorithms will be compared and they are CMA (Constant Modulus Algorithm), MCMA (Modified Constant Modulus Algorithm), and SCMA (Simplified Constant Modulus Algorithm). Since the blind algorithms are phase independent it is assumed that the blind algorithms are accompanied by a phase-recovery loop that rotates the constellation into its correct place and this rotation acts per 100 symbols. It is also assumed that there is no carrier frequency offset between the transmitter and the receiver. After the initial convergence of the blind algorithms, the STE will switch into Dicision-Directed mode to be able to track the channel changes and improve the MSE.
The initial filter taps are set based on the assumption of optimal antenna separation which leads the inter stream interference from another transmitting antenna (2×2 MIMO) to have a 90° phase shift compared to the desired signal. The initialization of the filters are based on this assumption. Thus all the central taps of the equalizers will be set to one or $e^{-j\pi/2}$ as is shown in Figure 5.10.

5.5 Noise and Phase Tracking

White Gaussian noise is added to each Rx signal stream separately with a relative power measured from one LoS signal stream. Thus the actual noise power is independent of ground reflections and how the LoS signals add at each Rx (if it is destructive or constructive addition). This results in a 3 dB array gain for a 2x2 MIMO system compared to a SISO system.

Phase noise is generated in the time domain and is applied on a symbol-to-symbol basis. The system is considered to be synchronous and driven only by one oscillator at the Rx. Thus only one realization of the phase noise is generated and applied to each stream. The streams will thus have fully correlated phase noises. The Welch power spectrum of the phase noise is shown in Figure 5.11. It is a $1/f^2$ noise with -85 dBrad^2/Hz^2 power at 100 kHz from the

[2] B dB[rad^2]/Hz $= B - 3$ dBc/Hz

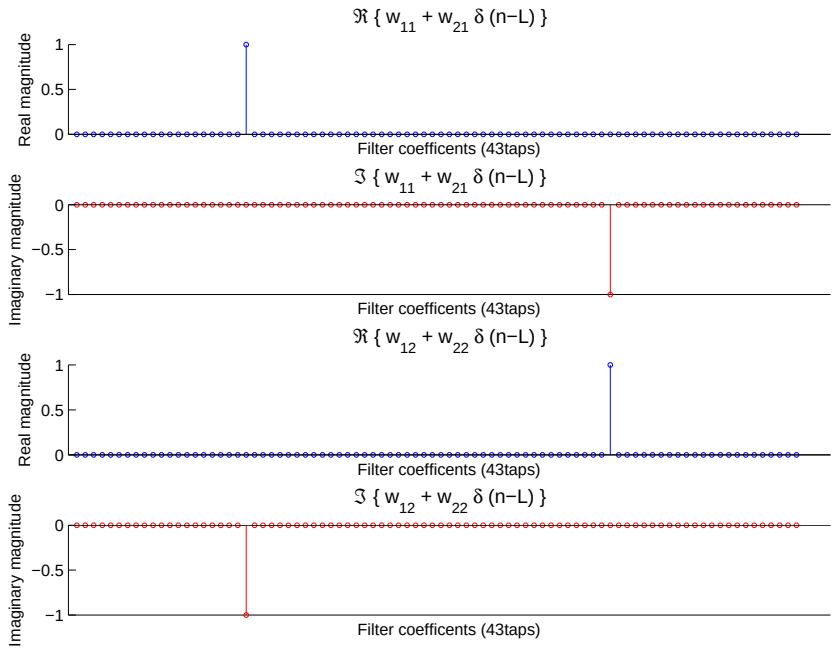

Figure 5.10: Filter initialization of STE for the 2 × 2 SS-SP MIMO.

carrier.

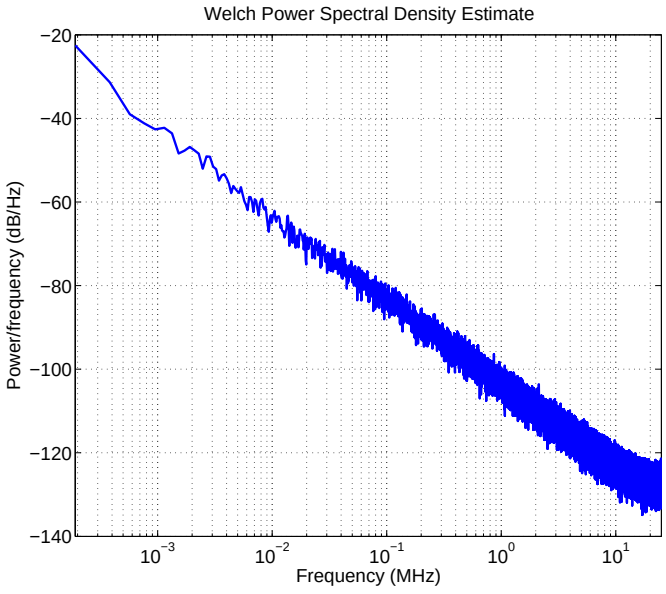

Figure 5.11: The Welch power spectrum for the phase noise.

The phase tracker used to compensate for phase noise is shown in Figure 5.12. It is applied for

each Rx branch as is shown in Figure 5.1. For handling differential phase noise (independent phase noise realization for each Rx branch)[3] NM phase trackers and phase rotators are needed. One in front of every equalizer, inter-stream canceler and XPIC. This is due to the relatively low bandwidth of these filters.

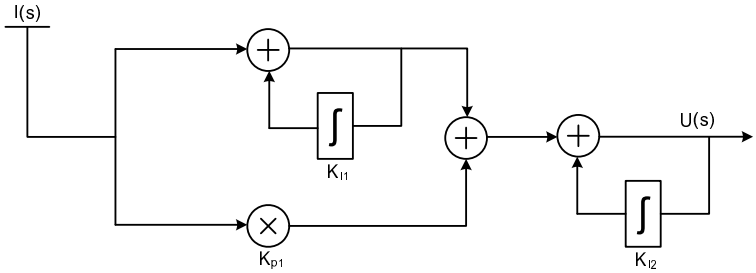

Figure 5.12: Schematic view of the phase tracker.

The gains of the phase tracker were found by brute force search. The actual values chosen can be seen in Table 5.2.

5.6 Simulation Parameters

The parameters used for the simulations are summarized in Table 5.2. They will be kept constant during all simulations unless otherwise stated.

[3] In a microwave link with radios separated several meters the phase noise will be differential.

Symbol	Value	Description
F_s	50 MHz	The sampling frequency
Q	16	Oversampling rate at the Tx filter
F_c	17 GHz	Carrier frequency
β	0.35	Roll-off-factor for the root-raised Cosine filters
M	16	Modulation order for M-QAM
L_T	10 m	Tx antenna mast height
L_R	10 m	Rx antenna mast height
L_H	1 km	Tx and Rx antenna mast horizontal distance
d_T	2.97 m	Tx antenna separation
d_R	2.97 m	Rx antenna separation
L_L	0 m	Rx landscape height
$\beta_{\mathbf{max}}$	2.3°	Maximum tilt of antenna masts
$F_{\mathbf{MS}}$	0.2 Hz	Frequency of mast swing
L	43	Number of filter taps for each filter in the STE
L_t	21	The placement of the central tap in each filter in the STE
K_{I1}	0.35	A gain for the phase tracker
K_{I2}	10^{-4}	A gain for the phase tracker
K_{P1}	0.015	A gain for the phase tracker
μ_{cma}	5e-6	The stepsize of the CMA.
μ_{mcma}	5e-6	The stepsize of the MCMA
μ_{lms}	1e-4	The stepsize of the LMS in the Decision-Directed Mode
α	1	The mixing parameter for SCMA
b	0.9	The ground reflection factor
SNR	35dB	Signal-to-noise ratio
L_{tr22}	200 symbols	Number of training symbols for 2x2 MIMO system
L_{tr44}	400 symbols	Number of training symbols for 4x4 MIMO system
R	13.2	The average constant magnitude of Blind algorithm (16QAM)
W	0.98	Forgetting factor for RLS algorithm
BER_t	10^{-3}	Target BER for penalty calculations

Table 5.2: Parameters used during the simulations.

Chapter 6

Results

Here the simulation results will be presented. When a relevant value used for a particular simulation is not stated in the text the reader is referred to Table 5.2 for a list of default values.

6.1 Frequency Selective Channels

Two MIMO channels are selected for the simulations, those are discussed in Section 5.3. It is interesting to see how the system responds to these channels and try to get a feeling for what requirements they put on the design. The length of the STE equalizer filters will heavily affect the performance since a too short filter will lead to high- or even infinite penalty.
Figure 6.1(a) plots the penalty versus filter length for a 2x2 SS-SP LoS MIMO while Figure 6.1(b) does this for a 4x4 SS-DP LoS MIMO with three different values of XPD. The channels were static during the simulations and a long (600 and 2400 symbols for the 2x2 and 4x4 systems respectively) training sequence was used to initialize the STE using the LS algorithm, the filter taps were kept static after the training sequence. Looking at the plots it can be seen that at a certain number of filter taps a penalty floor is reached. The penalty then slowly grows as the number of filter taps are increased since each tap introduces a slight estimation error. For channel A the penalty floor is reached at about 15 taps while for channel B it takes about 43 taps. The penalty floors for channel A and B are then at about 14- and 19 dB respectively. For a low XPD value it is even beneficial to have more taps but for the sake of complexity the number is chosen to be 43 for the simulations. Removing the ground reflection completely ($b = 0$) a penalty of 0.8 dB for the 2x2 MIMO is still observed. This is due to the fact that the taps of the STE introduce some estimation errors which add up. Increasing the number of training symbols to 6000 reduces this penalty to 0.2 dB.

It is interesting to see what kind of penalties are expected for a random channel realization, that is random phase offsets between the direct paths and ground reflections while the b-values and delays are kept fixed. This is done in Figures 6.2(a) and 6.2(b) for 50 random channel realizations for 2x2- and 4x4 MIMO respectively.
The penalty can be negative since the ground reflection can enforce the direct path which is seen in some cases. None of the channel realizations exceed the penalty of channel B.

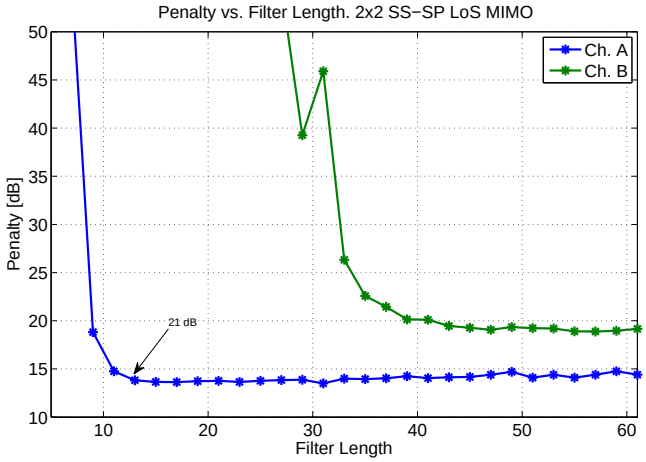

(a) 2x2 SS-SP LoS MIMO

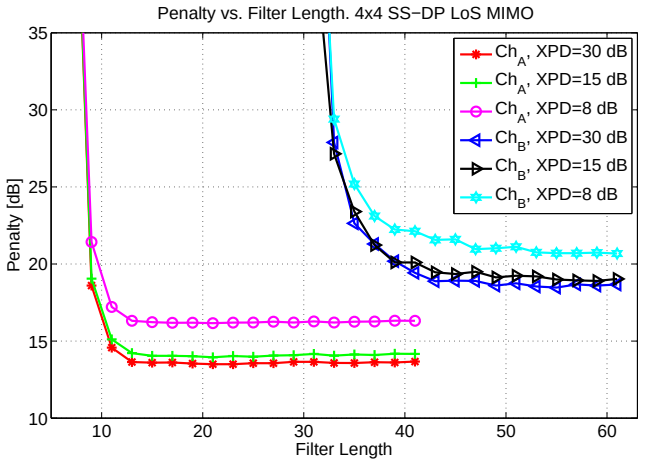

(b) 4x4 SS-DP LoS MIMO

Figure 6.1: Penalty (at BER of 10^{-3}) as a function of filter length for the STE.

Figure 6.3 shows how the penalty changes as a function of the ground reflection amplitude for both channel A and B. Channel A behaves as might be expected but channel B reaches its highest penalty at $b = 0.89$ and then the penalty reduces as b increases. An explanation for this is that the frequency dependent condition number has a peak at $b = 0.89$. Increasing the strength of the ground reflection further starts to improve the condition number.
It is interesting to compare these results to a SISO system. By removing the diagonal paths of the 2x2 MIMO channels (that is removing $\mathbf{h}_{12}$ and $\mathbf{h}_{21}$) two parallel SISO channels are obtained. The BER is then calculated as the mean of the two streams. Penalty is then plotted against the number of filter taps in Figure 6.4. For 13 filter taps the penalty is seen to be 9- and 8 dB for channel A and B respectively. This is a much lower penalty than seen for the MIMO channels and with the added benefit of smaller equalizer filters.

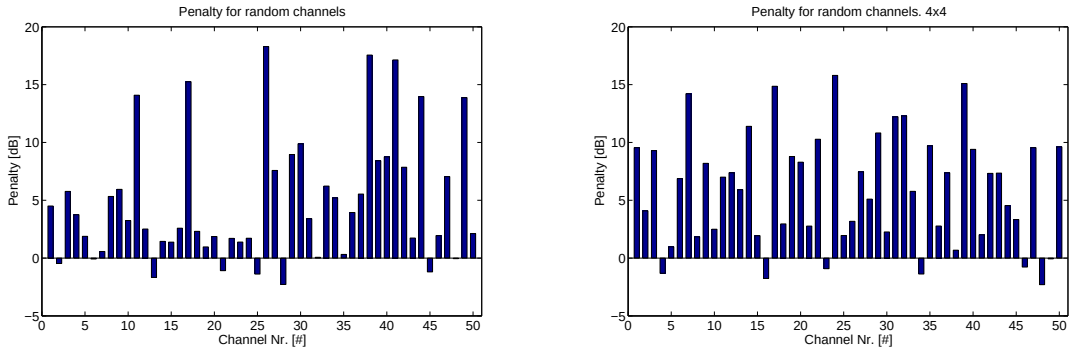

(a) 2x2 SS-SP LoS MIMO

(b) 4x4 SS-DP LoS MIMO

Figure 6.2: Penalty (at BER of 10^{-3}) for a random channel realization.

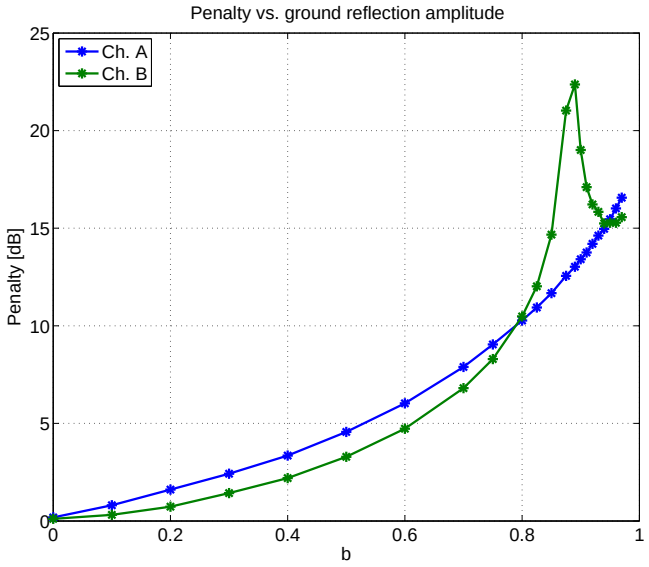

Figure 6.3: Penalty (at BER of 10^{-3}) as a function of the ground reflection amplitude.

6.2 Suboptimal Antenna Placements and XPD

Installing the Tx- or Rx antennas with suboptimal separation will negatively affect the performance of the MIMO system since it lowers the condition number of the channel matrix. There is thus a penalty associated with $\eta \neq 1$ (see (3.16)) and that is plotted for a flat channel ($b = 0$) in Figure 6.5(a) for a 2x2 SS-SP LOS MIMO as a function of η. The system is not so sensitive to changes in η if it is close to one. For $\eta = 0.9$ a penalty of less than one dB is observed but the penalty grows quicker as η becomes smaller. This results is not in good agreement with Figure 3.14 since direct matrix inversion and SVD are fundamentally different approaches (see Appendix B for further clarification).
In Figure 6.5(b) the penalty is given as a function of XPD for 3 different η for a 4x4 SS-DP LoS MIMO. As the XPD and η are lowered the penalty increases as expected.

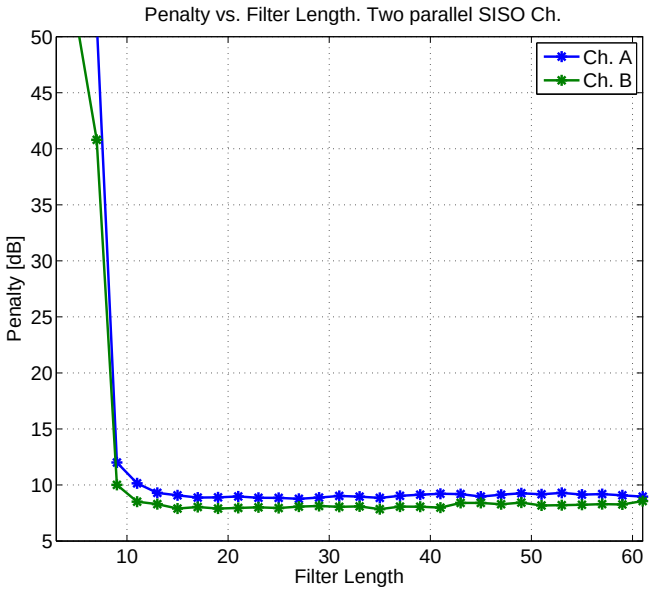

Figure 6.4: Penalty (at BER of 10^{-3}) as a function of filter length for the SISO representation of channel A and B. Here the un-penalized SNR is considered to be 10.5 dB while it is 7.5 dB for the MIMO systems (array gain).

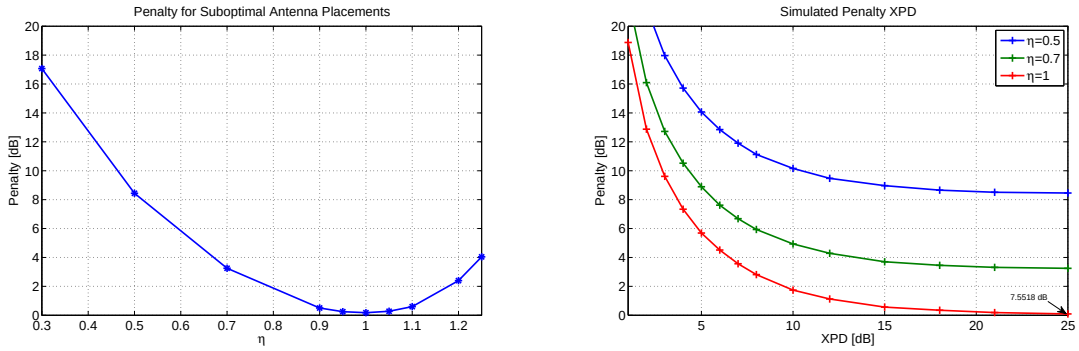

(a) Penalty Vs. η

(b) Penalty Vs. XPD for different η

Figure 6.5: Penalties (at BER of 10^{-3}) for suboptimal antenna placement η and low XPD values.

Added penalty is also expected for the frequency selective channels A and B when lowering the XPD. This added penalty caused by low XPD values should as well grow similarly independent of the channel realization. This can be seen in Figure 6.6 where the penalty is plotted against XPD for channels A and B. The penalty difference between the channels is seen to be almost constant at 5 dB.

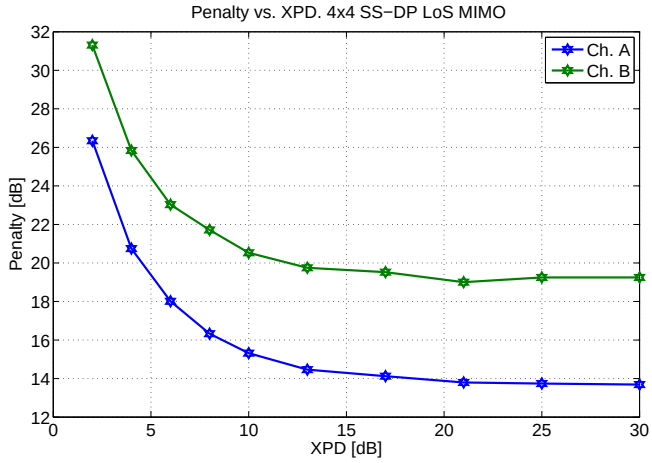

Figure 6.6: Penalty as a function of XPD for channel A and B.

6.3 Decision Directed Algorithms

It is important that an adaptive algorithm responds sufficiently fast to changes, that is that it has fast enough convergence speed. For WRLS and LMS it is apparent that the weighting factors and step-sizes will play an important role in determining the adaptation speed. Selecting a static channel and setting the SNR to the very high value of 95 dB the convergence speed can be seen by counting how many symbols it takes for the algorithm to reach its residual MSE floor. LMS and WRLS are analyzed in DD-mode, both started with the same channel estimate obtained using LS and training.
Figure 6.7(a) shows the DD-LMS algorithm converging to its residual MSE of channel A. As the step-size is increased the convergence becomes faster, in fact if the step-size is doubled only half the symbols are needed to reach the noise floor. A trade off is that the actual MSE floor reached is higher if the step-size is larger. If the step-size is chosen too large the algorithm becomes unstable and might diverge. The LMS with the step-size of $\mu_{\text{LMS}} = 6 \cdot 10^{-4}$ needs about 25 thousand symbols to reach the MSE-floor.
Figure 6.7(b) shows how the WRLS algorithm behaves for the same setup. Three different weighting factors are chosen, $\lambda_1 = 0.98$, $\lambda_2 = 0.99$ and $\lambda_3 = 0.995$. A lower weighting factor means that the algorithm is able to adapt faster but with the penalty of a less refined autocorrelation matrix which means that the residual MSE reached will lie higher. A higher weighting factor will give a slower convergence but a more precise autocorrelation matrix resulting in a better convergence. This can be seen by looking at Figure 6.7(b). λ_3 results in slower convergence than using λ_1 but a lower MSE floor. About 500 symbols were needed to reach the MSE floor for WRLS with λ_1. A huge improvement compared to the LMS algorithm.

6.4 Blind Algorithms

The convergence of blind algorithms such as CMA, MCMA or SCMA is quite sensitive to their step-sizes. The step-size has to be carefully chosen in order to avoid divergence of the

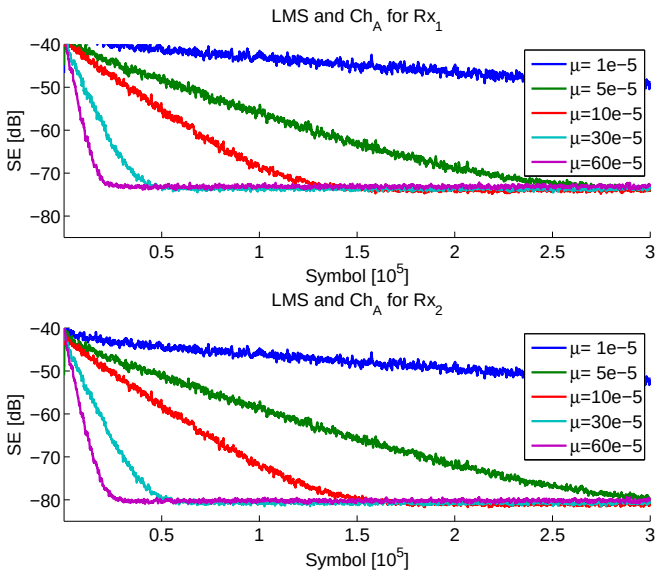

(a) LMS

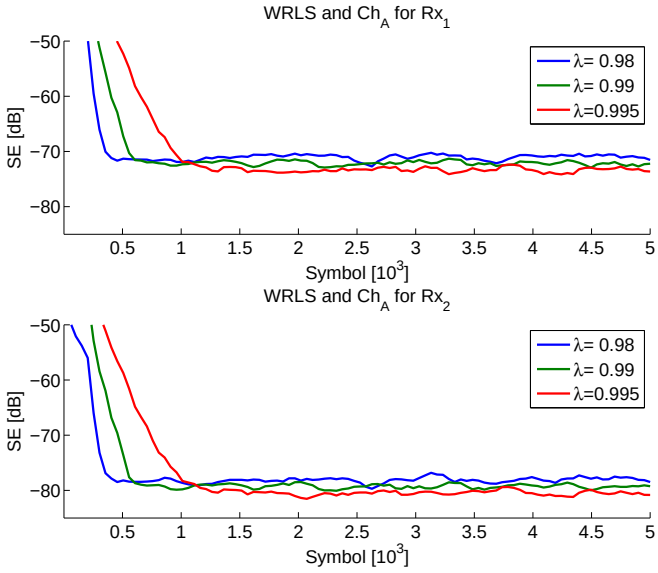

(b) WRLS

Figure 6.7: Convergence of the WRLS and LMS to their MSE-floor.

algorithms. There is a trade off between convergence speed and the residual MSE floor, a large step-size value leads to a fast convergence speed but relatively high residual MSE or even instability and vice versa. In order to make a fair comparison, the same step-size is set for all the blind algorithms when comparing the performance. This step-size is chosen by simply searching for a suitable step-size for all the algorithms. A step-size of $5 \cdot 10^{-6}$ is set for the following simulations.

The convergence of blind algorithms is simulated using a static channel (no mast swing) for a few ground reflection amplitudes (b factor). A larger b factor leads to a stronger inter-symbol-interference. All the blind algorithms converge for both Rx_1 and Rx_2 when $b = 0$ as shown in Figure 6.8(a), both channels behave exactly the same and the convergence performances are the same. However, when $b = 0.5$ convergence is not always reached. Comparing the performance for channel A and B (Figure 6.8(b) and 6.8(c) respectively) it can be seen that it takes a longer time for algorithms in channel A to converge but a lower residual MSE floor is achieved. Channel B converges faster for MCMA and SCMA but CMA does not converge for Rx_2.
A much stronger Inter-symbol-Interference is introduced in Figures 6.8(d) and 6.8(e) by setting $b = 0.9$. Both channel A and B become too difficult for the STE to converge, convergence fails for such a strong ground reflection value and inter-symbol-interference.

6.5 Mast Swing

Mast swing will cause the channel to vary as the antennas move. A changing channel will require adaptive algorithms that can adjust fast enough to compensate in real time. At high carrier frequencies only a small change in the distance between the Tx and Rx will rotate the constellation. This rotation in the LoS paths will cause a fast change in the frequency selective channels. The mast swing velocities are given in the unit λ/s so that the results are independent of the carrier frequency. Another reason for using that unit is that the affects of the velocity of the mast swing depends on how the phases between the ground reflection and direct paths are changing in relation to the actual mast movement. A change of one wavelength can be considered to be a change of 2π for those phases. Assuming a varying direct path but a static ground reflection then for the carrier frequency selected here (17 GHz) the relation 1 λ/s $\approx$ 0.02 m/s is valid[1].

6.5.1 Decision Directed

Decision directed algorithms will diverge if they are fed with sufficiently many wrong symbol decisions. If such an algorithm loses track once, the errors will saturate and the algorithm will diverge to some false realization. If the algorithm adapts too fast then fewer decision errors are needed to get it to diverge, if the algorithm on the other hand adapts too slowly more decision errors will be made in a varying channel resulting again in divergence. Thus for a particular system setup and channel there is an optimum selection of parameters for the algorithm chosen. As the velocity of the mast increases it gets harder to adapt sufficiently fast until the algorithm diverges for any parameter selection. To evaluate the performance of the algorithms the squared-errors (SE) are plotted against the number of symbols received. A moving average filter is applied to the SE to smooth out the symbol-to-symbol variations making it a moving mean-squared-error. The initial channel estimate is obtained by sending training symbols in the beginning. For a BER of 10^{-3} a MSE of about -7 dB is needed for 16QAM and a pure Gaussian noise channel.

[1] The antennas move with slightly different velocities because the mast is tilting.

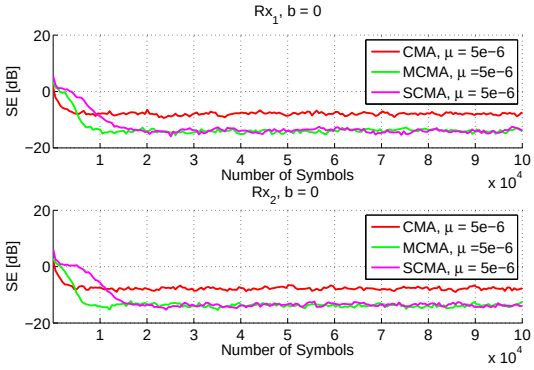

(a) $b = 0, V_{\mathrm{MS}} = 0\ \lambda/\mathrm{s}$

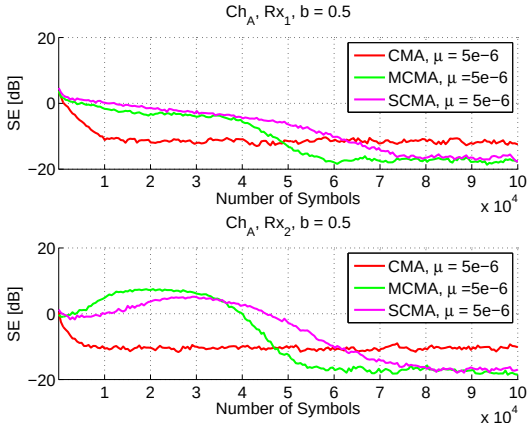

(b) Channel A, $b = 0.5, V_{\mathrm{MS}} = 0\ \lambda/\mathrm{s}$

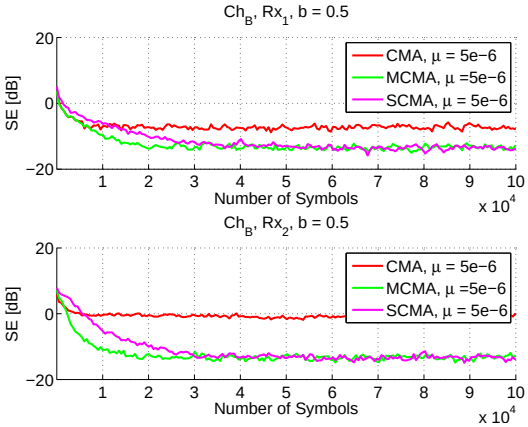

(c) Channel B : $b = 0.5, V_{\mathrm{MS}} = 0\ \lambda/\mathrm{s}$

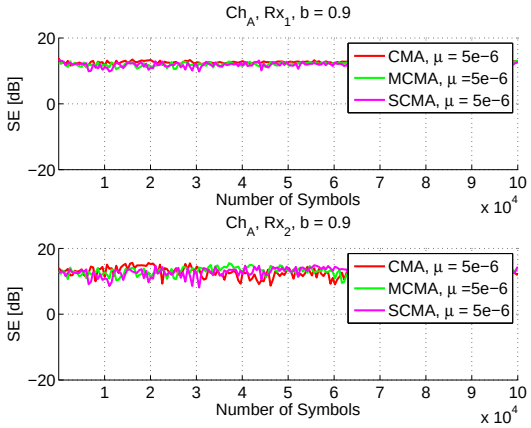

(d) Channel A : $b = 0.9, V_{\mathrm{MS}} = 0\ \lambda/\mathrm{s}$

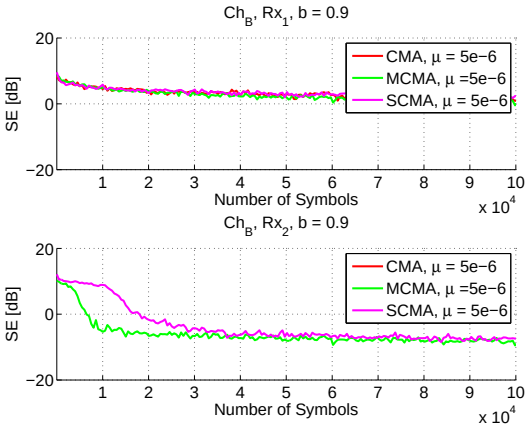

(e) Channel B : $b = 0.9, V_{\mathrm{MS}} = 0\ \lambda/\mathrm{s}$

Figure 6.8: Convergence of blind algorithms for the static channel

WRLS

The DD-WRLS algorithm is applied for a 2x2 SS-SP LoS MIMO system for different mast swing velocities. Three weighting factors were used to get a comparison of the performance.

Figures 6.9(a) and 6.9(b) plot the evolution of the SE for channel A and B respectively for both receivers. The velocity of the mast is about $V_{MS} = 182$ λ/s which means that the constellation is rotated seven times during the entire simulation. That produces about seven peaks which vary a little bit in shape due to the varying tilt of the masts. These peaks are introduced when for example a notch moves into or out of the bandwidth of the channel forcing an abrupt change in the equalizers.
There are three weights $\lambda = 0.98$, $\lambda = 0.99$ and $\lambda = 0.995$ chosen, and they are seen to give different results. The lower the weight the faster the algorithm will adapt (smaller exponential window), thus it can become too susceptible to erroneous decisions. This is seen to happen for the lower weights which loose track when there are decision errors (high MSE).
Choosing the weighting factor too large will make the algorithm too slow and at high velocities it will lose track as can be seen in Figures 6.10(a) and 6.10(b) where $\lambda = 0.999$ performs notably worse. None of the weights are able to keep track of the channel when the mast velocity reaches $V_{MS} = 286$ λ/s for channel B.

LMS

The LMS algorithm is much more sensitive to the velocity of the mast since its convergence speed is much slower. Figures 6.11(a) and 6.11(b) show the SE for channel A at velocities $V_{MS} = 4$ λ/s and $V_{MS} = 8$ λ/s respectively. A training sequence is transmitted every 10^6 symbols. A new channel estimate for every training sequence is obtained using the LS algorithm. The step-size of $\mu_{\text{LMS}} = 6 \cdot 10^{-4}$ is seen to be unstable since it diverges completely even after receiving a training sequence[2]. The step-size of $\mu_{\text{LMS}} = 5 \cdot 10^{-5}$ is too slow even for this moderate mast swing velocity of $V_{MS} = 4$ λ/s. At a velocity of $V_{MS} = 8$ λ/s all the step-sizes diverges for Rx_2. As can be seen the adaptation speed is greatly inferior to the WRLS algorithm. The step-size of $\mu_{\text{LMS}} = 0.0006$ is seen to be unstable while the lowest step-sizes are too slow even for a moderate mast swing.

Higher Order Modulation

A larger constellation requires a more precise channel estimate and thus more stringent requirements on the DD-algorithm that is compensating for mast swing. Thus a reduced tolerance to mast swing is expected for 256QAM compared to 16QAM. Figures 6.12(a) and 6.12(b) show the evolution of the SE for the WRLS algorithm. It fails to track somewhere between $V_{MS} = 46$ and $V_{MS} = 91$ λ/s which are much lower velocities than for 16QAM.

SISO Systems

The SISO channel is much easier to track since the channel conditions can not become as complex as in the MIMO case. Figure 6.13(a) shows how the LMS adapts to mast swing for five different step-sizes. The two largest of them are seen to be unstable and the two smallest do not have sufficient adaptation speed. Only one step-size of $\mu_{\text{LMS}} = 10^{-3}$ is able to track at the mast swing velocity of $V_{MS} = 46$ λ/s. The evolution of the SE at $V_{MS} = 2.3$ kλ/s is plotted for three different weights of the WRLS algorithm in Figure 6.13(b). The weight $\lambda = 0.98$ is able to track at this velocity.

[2] Only every 1:1000 symbol is plotted.

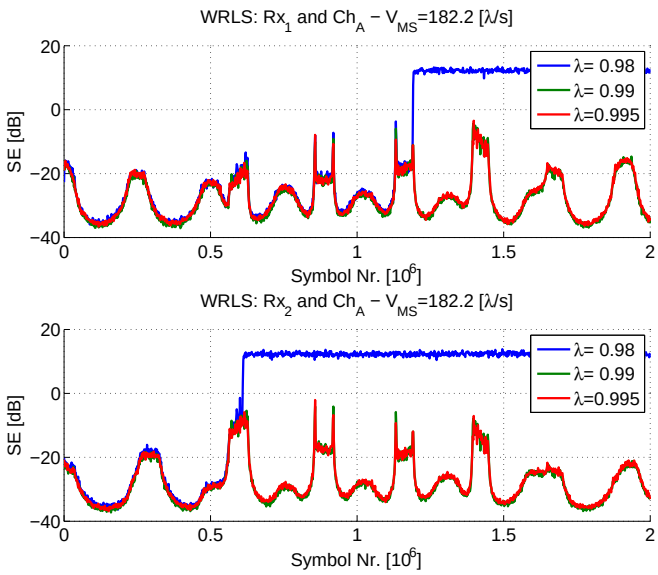

(a) Channel A

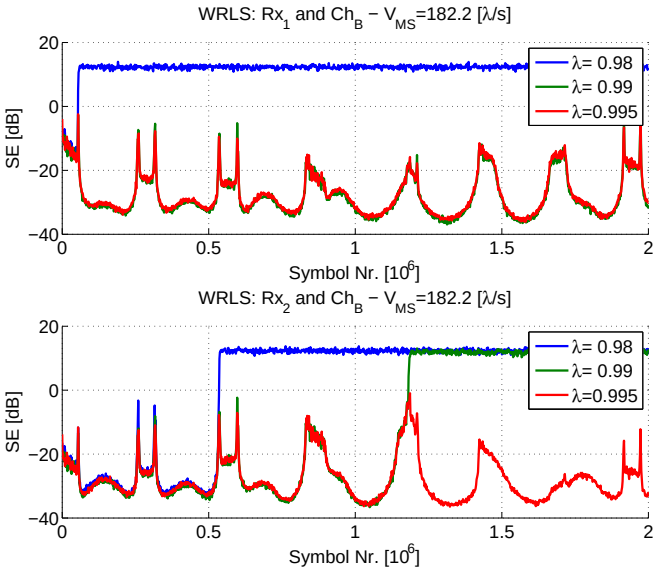

(b) Channel B

Figure 6.9: Evolution of the squared error (SE) for three different weights in the WRLS algorithm in DD-mode in the presence of Mast Swing. $V_{MS} = 182$ [λ/s].

It is clear that mast swing is a much easier to compensate for in SISO systems compared to MIMO.

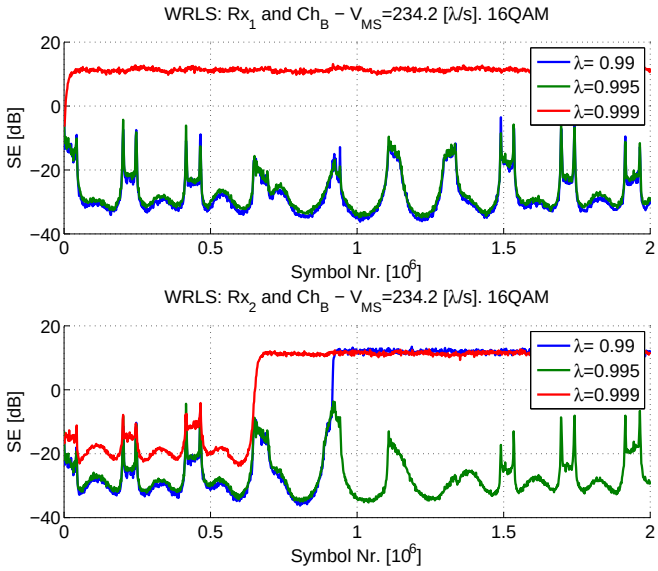

(a) $V_{MS} = 234\ \lambda/\mathrm{s}$

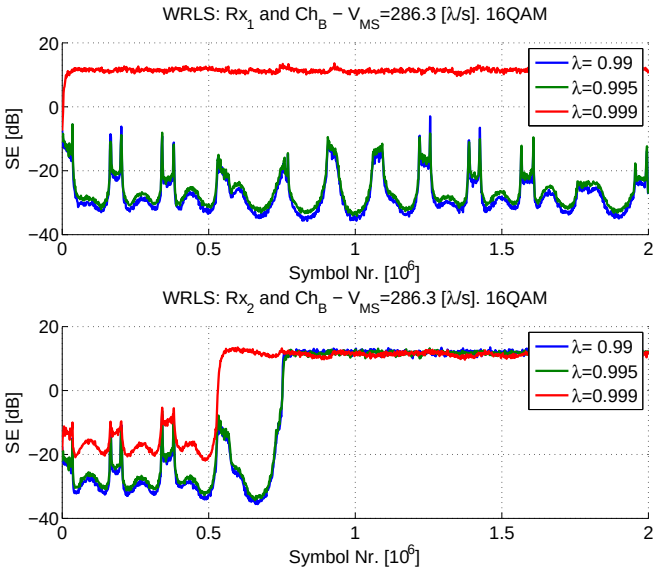

(b) $V_{MS} = 286\ \lambda/\mathrm{s}$

Figure 6.10: Channel B: Evolution of the squared error (SE) for three different weights for the WRLS algorithm in DD-mode in the presence of Mast Swing.

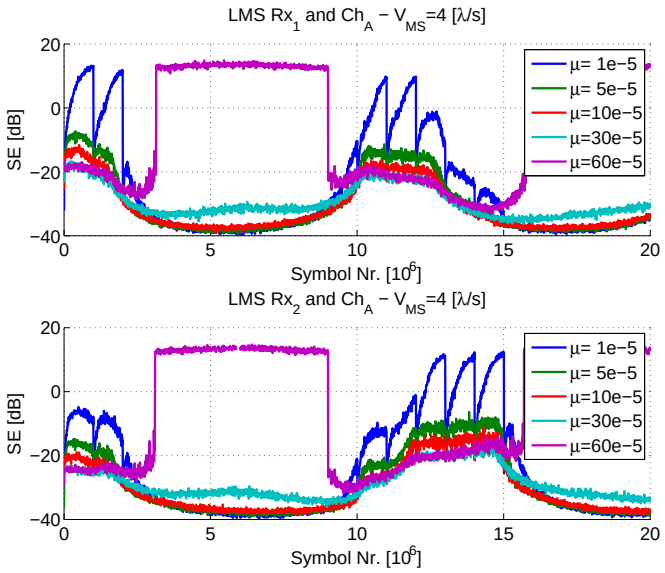

(a) Channel A

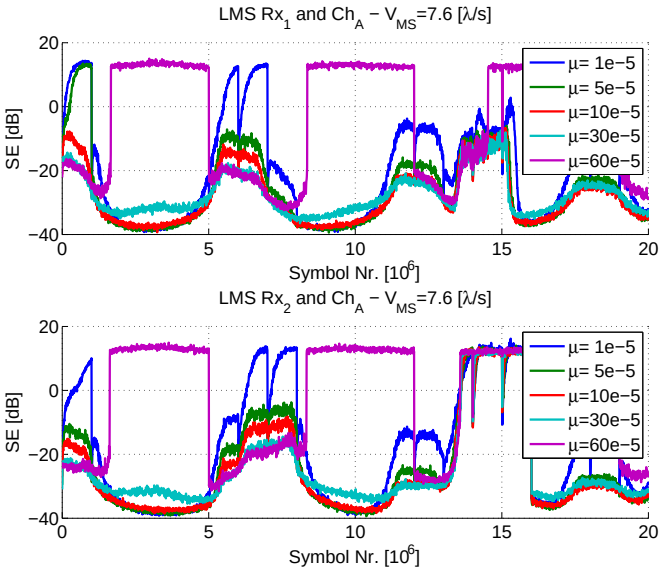

(b) Channel B

Figure 6.11: Channel A: LMS with a training sequence after every 10^{-6} Tx symbols.

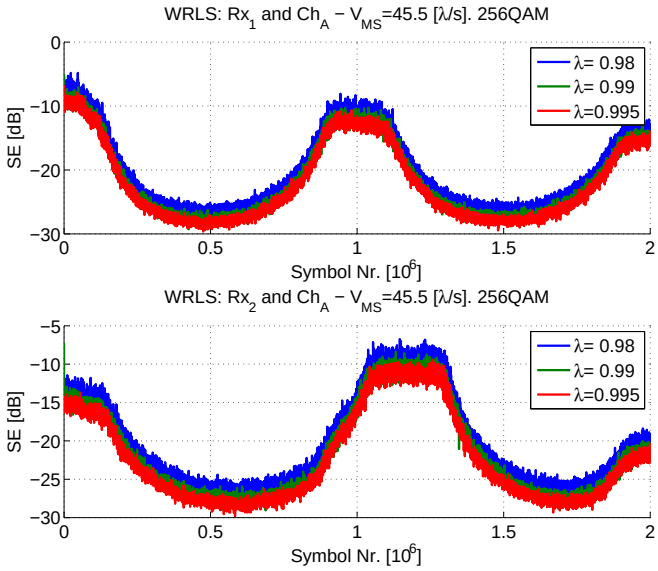

(a) 256QAM: $V_{MS} = 46$ λ/s

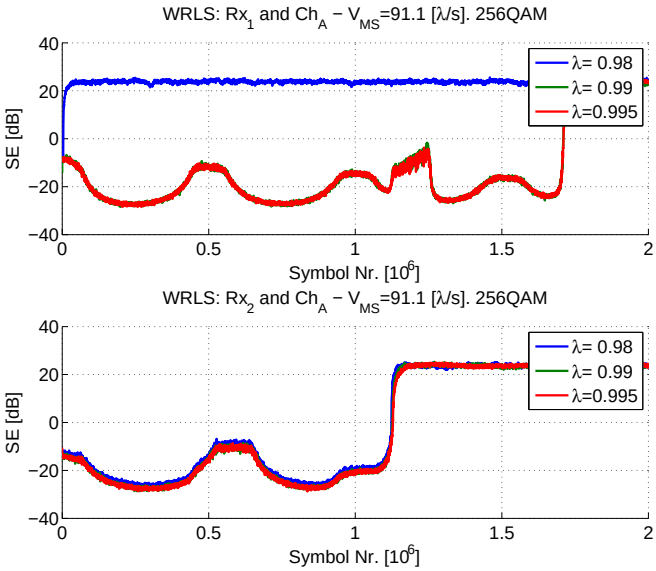

(b) 256QAM: $V_{MS} = 91$ λ/s

Figure 6.12: Channel A: Evolution of the squared error (SE) for three different weights for the WRLS algorithm in DD-mode in the presence of Mast Swing.

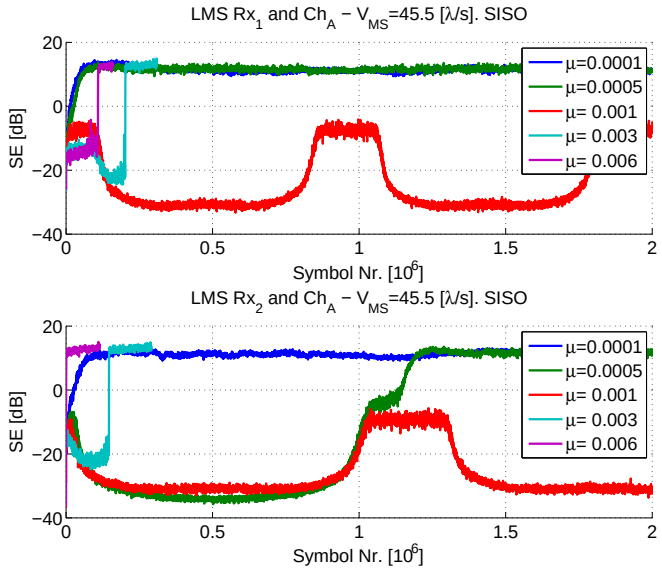

(a) SISO, LMS: $V_{MS} = 46\ \lambda/\mathrm{s}$

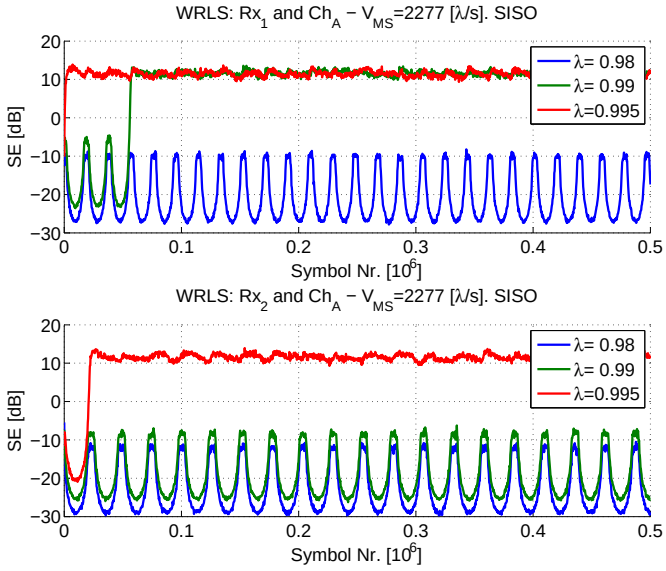

(b) SISO, WRLS: $V_{MS} = 2.3\ \mathrm{k}\lambda/\mathrm{s}$

Figure 6.13: Evolution of the squared error (SE) for a SISO representation of channel A.

6.5.2 Blind Algorithms

Flat channel

For a flat channel, mast swing behaves as a phase rotator that constantly rotates the phase of received signals, this results in a constant carrier frequency offset between the transmitters and receivers. Figure 6.14(a) illustrates the signal constellation of the equalized signals. The plots to the left illustrate the constellation of signals along with the soft decisions of the STE without suffering any mast swing. The plots to the right illustrate the impact of carrier frequency offset that is caused by mast swing.

The rotation shown in Figure 6.14(a) is caused by a carrier frequency offset and it is usually compensated for by using a carrier frequency recovery loop[31]. However, in Figure 6.14(b) and Figure 6.14(c) the algorithms MCMA and SCMA are able to accomplish blind equalization and carrier phase recovery simultaneously without the use of a carrier frequency recovery loop[3].

The convergence of three blind algorithms is compared in Figure 6.5.2. In order to compare the convergence of CMA with other blind algorithms, phase recovery is used for CMA, all three algorithms use the same step-size. It can be seen that all algorithms have converged after 20,000 symbols and that the residual MSE floor is stable even when the mast swing velocity equals to $V_{\mathrm{MS}} = 131\ \lambda/\mathrm{s}$. The conclusion is that the convergence of blind algorithms is not affected by mast swing if there is a flat channel.

Frequency Selective Channel

Mast swing varies the MIMO channel so that the notch placements moves inside and outside the bandwidth of the signals. After convergence, blind algorithms can track the channel for a slow varying frequency selective channel but with a relatively high residual MSE floor. One solution is that the system uses blind algorithms to initialize the channel estimation and then it switches into DD (Decision Directed) mode to track the faster channel changes and improve the residual MSE simultaneously. Figure 6.16 shows the convergence of different blind algorithms with a mast swing velocity of $V_{\mathrm{MS}} = 131\ \lambda/\mathrm{s}$ and the ground reflection factor $b = 0.9$.
As seen from Figure 6.16, all algorithms converge and the residual MSE floor is relatively stable for certain ranges (*e.g.* 100,000 to 300,000 symbols). The blind algorithms are able to track the channel to some extent but often with a relatively high MSE. The blind algorithms never diverge or lose track since they do not rely on previous decisions. They can thus override bad channel conditions and then converge again when the channel conditions become better. Compared to LMS or WRLS, blind algorithm have a very high MSE which can result in decision errors. Thus it is desirable to switch to DD (Decision Directed) mode to improve the channel tracking and MSE as shown in Figure 6.5.1 for example.

Figures 6.17(a) and 6.17(b) shows square error curves when the step-size is set to $\mu = 1 \cdot 10^{-5}$ for channels A and B respectively. CMA and SCMA can become unstable and fail. MCMA

[3] If no other carrier frequency offset is introduced.

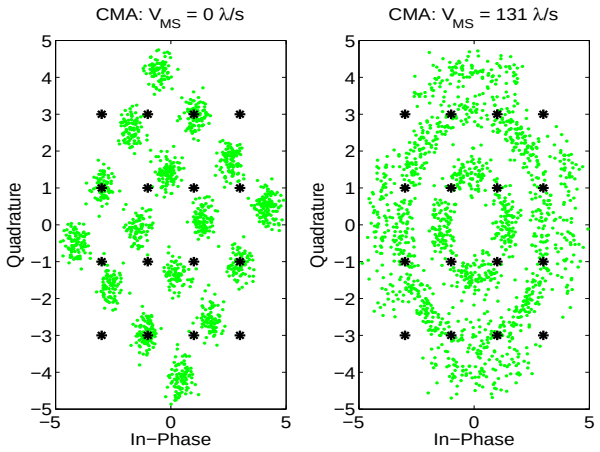

(a) Equalized signals using CMA

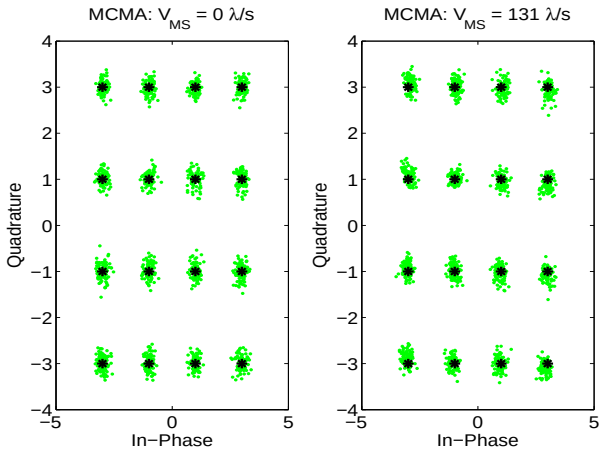

(b) Equalized signals using MCMA

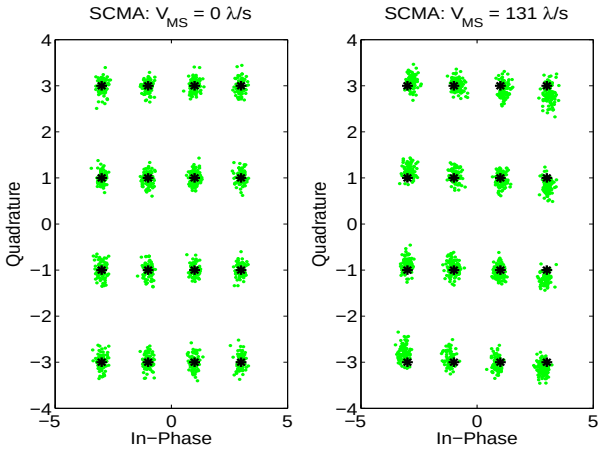

(c) Equalized signals using SCMA

Figure 6.14: The compensation of carrier frequency offset using different blind algorithms

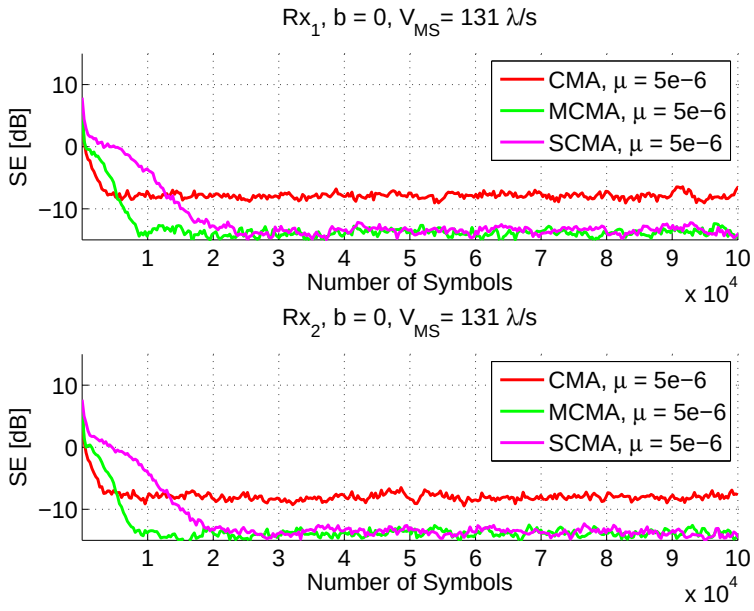

Figure 6.15: Convergence for a time varying flat channel

is though still able to converge for this step-size. This goes to show that the algorithms are very sensitive to the step-size.

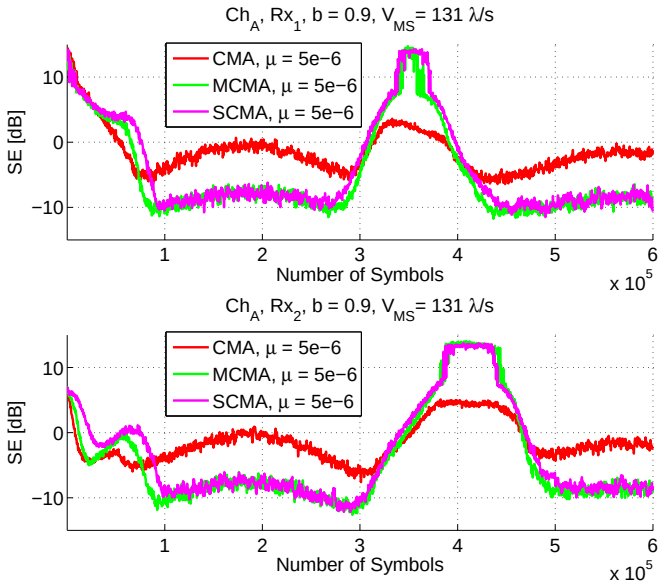

(a) Channel A: $b = 0.9$, $V_{\mathrm{MS}} = 131\ \lambda/\mathrm{s}$

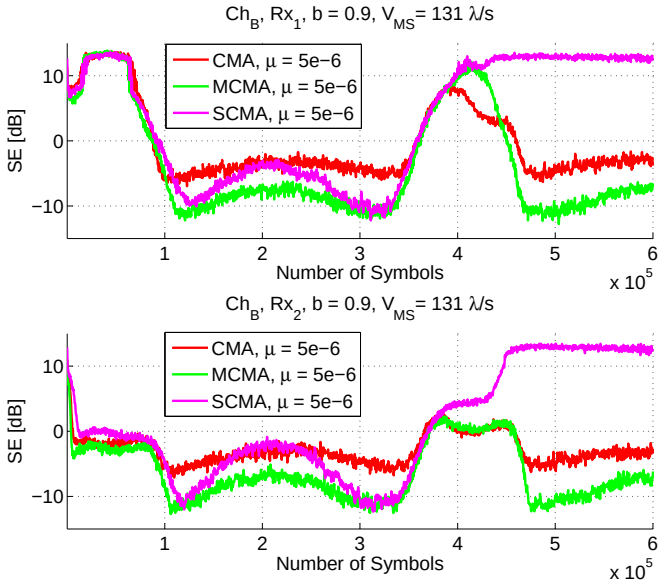

(b) Channel B: $b = 0.9$, $V_{\mathrm{MS}} = 131\ \lambda/\mathrm{s}$

Figure 6.16: Square error curve for a time varying frequency selective channel.

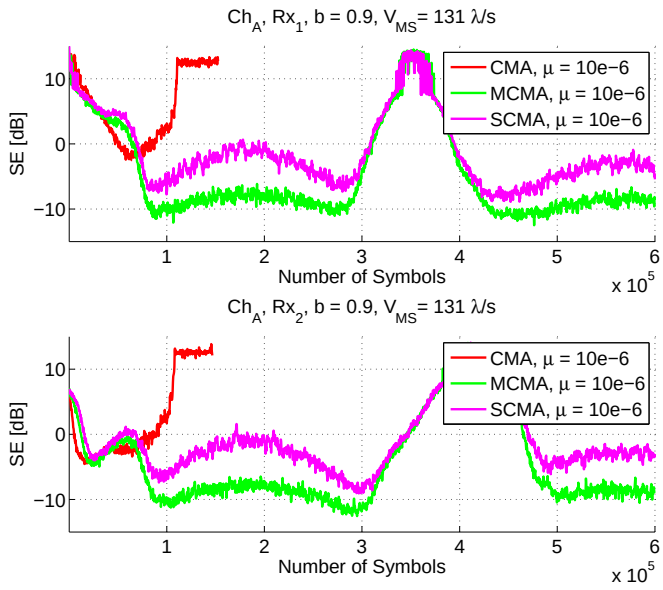

(a) Channel A:$b = 0.9$ $V_{\mathrm{MS}} = 131$ λ/s

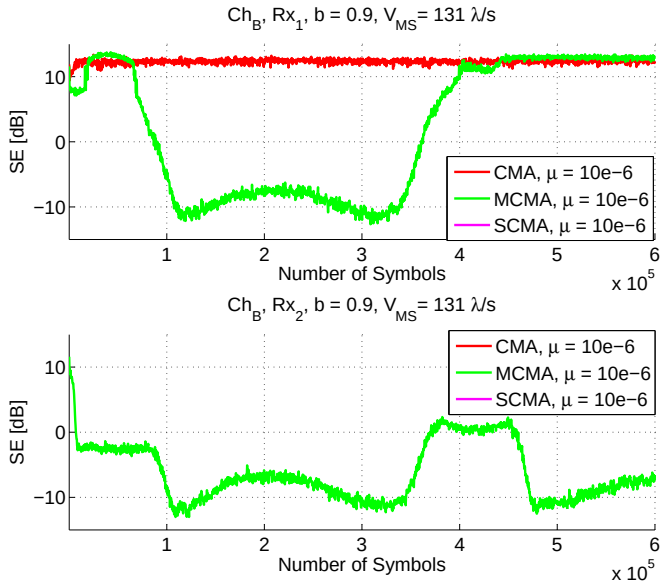

(b) Channel B: $b = 0.9$ $V_{\mathrm{MS}} = 131$ λ/s

Figure 6.17: Square error curves for a time varying frequency selective channel with a larger step-size.

6.6 Phase Noise

The amount of phase noise power that a communication system can tolerate is highly dependent on the actual implementation of the PLL (or phase tracker). The power spectrum of the phase noise is also important to consider as well as its correlation between Rx branches in a MIMO system. This complicates simulations that aim to give a general result. Comparing the performance for different channel conditions using a fixed implementation can though be enlightening.

The phase noise is simulated as $1/f^2$ noise and it has a power of -66 dB[rad^2]/Hz power at 100 kHz from carrier (see Figure 5.11).

6.6.1 Decision Directed

Figures 6.18(a) and 6.18(b) show the MSE for different powers of the phase noise for 2x2 SS-SP LoS MIMO and a corresponding SISO system respectively. The parameter W_{ph} is added to the spectrum shown in Figure 5.11[4]. The simulations for both the MIMO and SISO use the same implementation of STE and phase tracking and the phase noise is perfectly correlated between the receivers.
The phase tracker should compensate for the phase noise before the STE so little noise enhancement is observed for different b factors other than the usual white Gaussian noise enhancement. The step-size is seen to play only a minor role due to the fact that the channel is static.
As can be seen from Figure 6.6.2 the MIMO and SISO systems behave similar for fully correlated phase noise. For a differential phase noise the SISO system has the same tolerances but a MIMO system will perform worse for the setup illustrated in Figure 5.1. Applying differential phase tracking, that is a separate phase rotator in front of every equalizer, can compensate for this. Differential phase noise is applied to the received signal in Figures 6.19(a) and 6.19(b) with and without a phase tracking respectively. Since the phase tracking is not designed for differential phase noise the system is seen to be rather sensitive. For very low phase noise power the simple phase tracking performs marginally better than no phase tracking but is seen to saturate the error for higher noise powers. Now the channel will enhance the phase noise power since the phase tracker does not compensate in front of the inter-stream-cancelers and thus the performance is sensitive to the b factor.

6.6.2 Blind Algorithms

In Figures 6.20(a) and 6.20(b) the convergence and residual MSE for the blind algorithms can be seen at different phase noise power levels for fully correlated phase noise. Behind the STE is a phase rotator that rotates the symbols back using the information from the last 10 symbols, this is done to obtain a SE curve. At high phase noise powers the phase will actually vary quite a bit over 10 symbols raising the achievable residual MSE.
CMA is unaffected by the phase noise while MCMA and SCMA are somewhat affected by it[5]

[4] W_{ph} is added equally to all frequencies.

[5] MCMA and SCMA both use not only amplitude but some phase information as well and are thus not completely unaffected by phase noise.

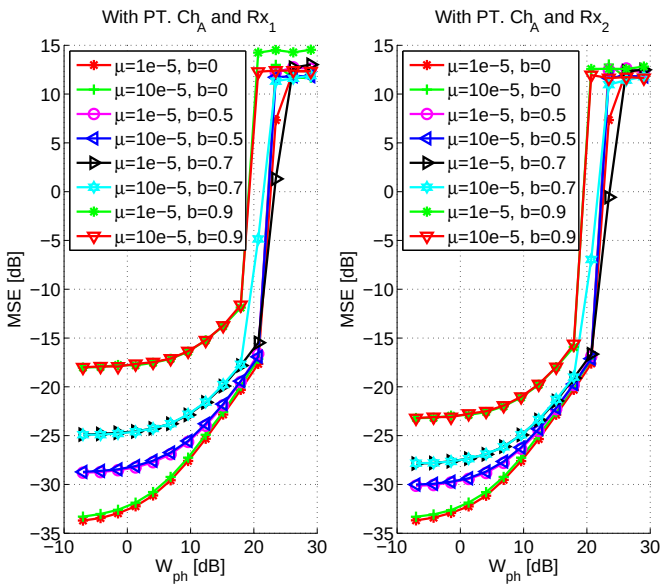

(a) 2x2 SS-SP LoS MIMO

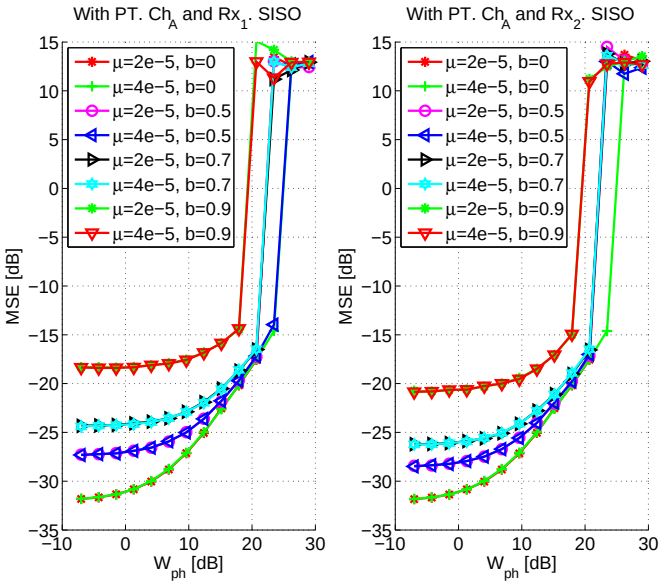

(b) SISO

Figure 6.18: Channel A: The MSE for different power of the phase noise spectrum for fully correlated phase noise.

which can be seen by looking at Figures 6.20(a) and 6.20(b). Here MCMA and SCMA have a higher residual MSE than CMA does.
Figures 6.21(a) and 6.21(b) show the response of the blind algorithms to differential phase noise. Since the phase of the inter-stream-interference is constantly changing the STE can not converge fast enough at high phase noise powers. The blind algorithms are able to converge

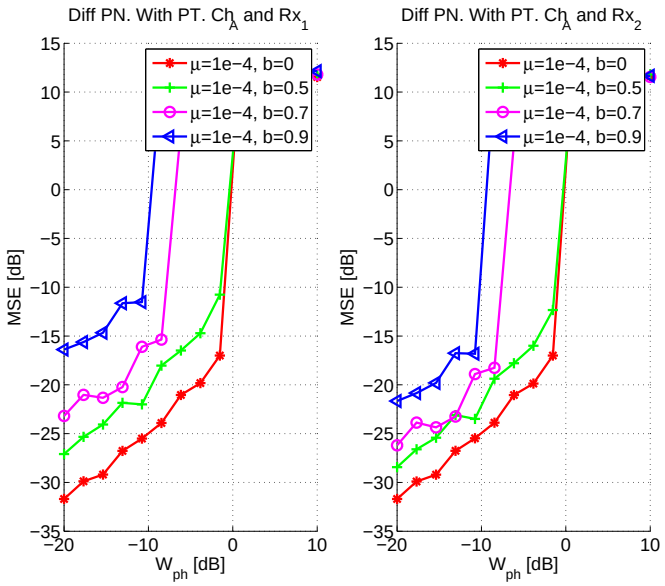

(a) Phase tracking

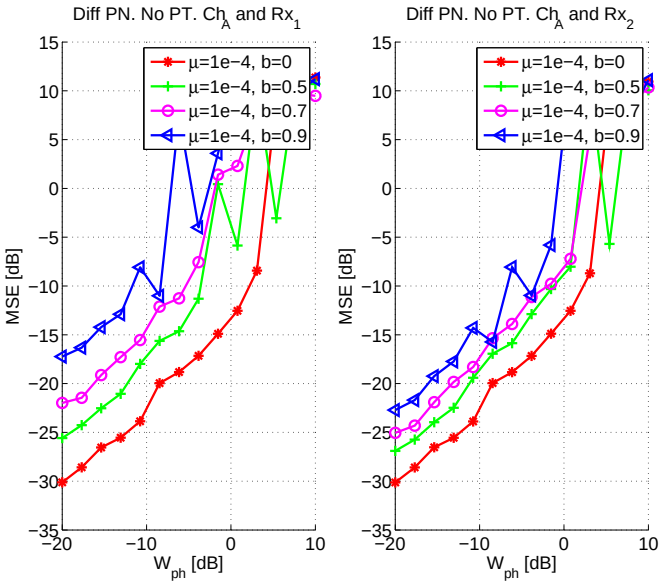

(b) No phase tracking

Figure 6.19: Channel A: The MSE for different power of the phase noise spectrum for differential phase noise.

for $W_{ph} = -5$ dB but fail for $W_{ph} = 0$ dB for this specified channel and step-size.

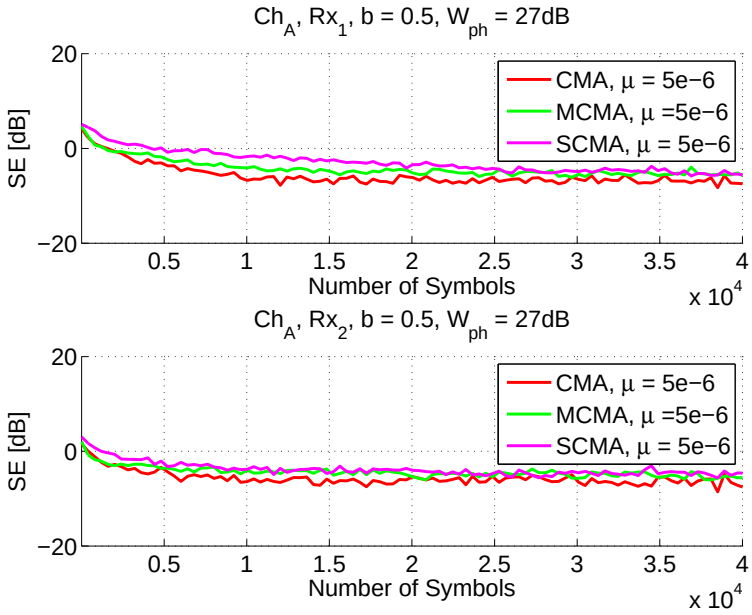

(a) Channel A: $W_{ph} = 27$ dB

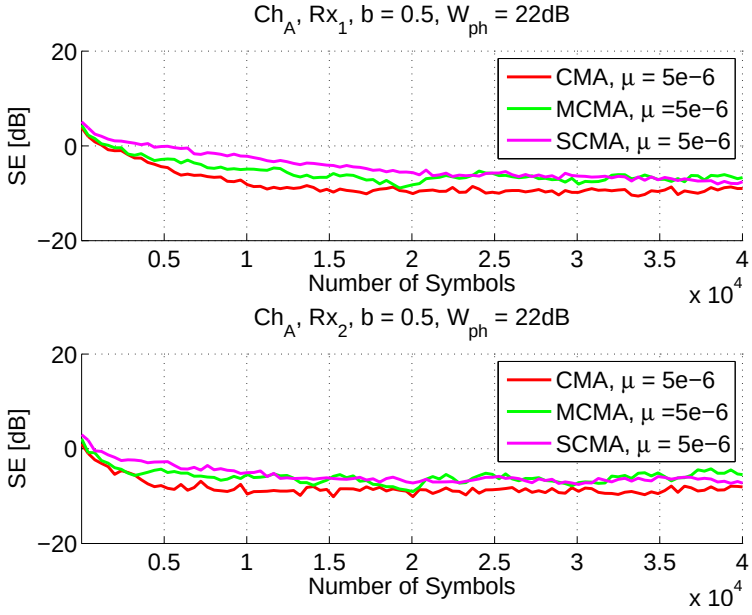

(b) Channel A: $W_{ph} = 22$ dB

Figure 6.20: Convergence of the blind algorithms in the presence of fully correlated phase noise.

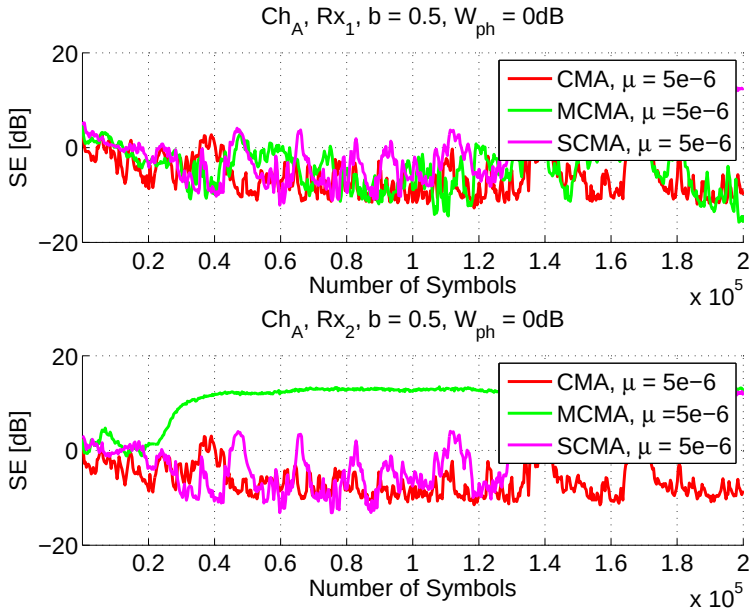

(a) Channel A: $W_{ph} = 0$ dB

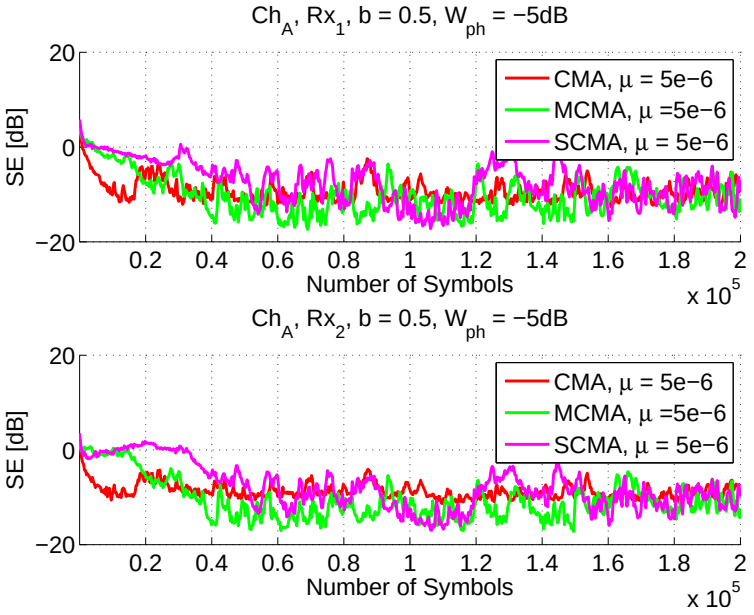

(b) Channel A: $W_{ph} = -5$ dB

Figure 6.21: Channel A: Evolution of the SE in the presence of differential phase noise for the blind algorithms.

Chapter 7

Conclusions and Discussions

The following conclusions have been drawn from the numerical analysis:

- Higher penalties can be seen for frequency selective LoS MIMO channels compared to SISO. The channels also place a higher demand on the equalizers, both their structure and their size. Equalizing a LoS MIMO channel is thus harder than its SISO counterpart.
- For a 2x2 SS-SP LoS MIMO system the penalty is below 1 dB if the separation between the antennas at the Rx and Tx are within 10% of the optimal.
- Comparing a 2x2 SS-SP LoS MIMO to a SISO system with a similar setup, tolerable mast swing velocity can be at least ten times lower for the MIMO system.
- For the equalizers WRLS outperforms LMS greatly for a time varying channel. The mast swing velocity that can be tolerated is about 100 fold greater for WRLS than it is for LMS.
- For the channels and system setup studied in this thesis the maximum mast swing velocity that can be tolerated lies around 5 m/s for WRLS.
- Blind algorithms may not convergence in the presence of strong ground reflection. However, since mast swing introduces a time varying channel it can assist the blind algorithms by moving them out of an unfavorable channel condition.
- In the absence of phase tracking, convergence is difficult to achieve in the presence of differential phase noise for the blind algorithms. Having decision directed phase tracking the blind algorithms need to be able to converge before phase tracking can be initiated.
- MCMA and SCMA are able to compensate for carrier frequency offset in the kHz range.
- CMA is more tolerant to phase noise than MCMA and SCMA who use some phase information.
- SCMA has lower computational complexity without loss in performances.
- Blind algorithms may converge to the same source signals. This issue can be avoid by adding a cross-correlation term into the error functions.

Implementing SS LoS MIMO will put higher requirements on the structure of the system than on a SISO system, especially on signal processing. Channel conditions have a higher degree of freedom which means that it can be harder to tolerate unfavorable channel conditions. For wireless microwave links that need to be almost always operational this translates to larger system margins with some associated cost.
Blind equalization is seen to be less reliable for MIMO than SISO and especially in the presence of differential phase noise and strong ground reflection. This might become a possible issue for future systems.

7.1 Further Studies

There is much room for further studies in this field. There are many components that are needed to build even a basic communication system. Their interaction as well as their implementation is challenging to handle. In order to be able to interpret and focus on specific phenomena in this thesis some simplifications were made to relax the requirement on the design. These simplifications should be dropped for future research.
By dropping the approximation of a synchronous system the requirements on the system are increased. Carrier frequency offset recovery, symbol timing estimation, phase adjustment and tracking between different parts of the system and frame synchronization would for example be needed. These are all candidates for further studies and simulations.
The simulations here have shown that in the presence of differential phase noise there can be convergence issues with blind equalization if there is no phase tracking available. This could represent an interesting research topic.
Blind algorithm may converge in order to recover the same source signals at many outputs. Researches for improving and assuring the output separation are needed.
Symbol timing estimates, fractionally spaced equalizers, non-linear equalizers and coded systems are a few obvious extensions to the work already done. Another thing that might be improved on is the channel modeling. With some real measurement data for LoS MIMO channels some statistical representation of the channel could be made which should allow for more typical results.

So to summarize the future work suggested is as follows.

- Handling differential phase noise
- Improving the convergence of the blind algorithms
- Fractionally spaced equalization and non-linear equalization
- Symbol timing estimates
- Using real channel measurements when available

Bibliography

[1] John B. Anderson. *"Digital Transmission Engineering"*. IEEE Press and Wiley-Interscience, 2nd edition, 2005.

[2] Henrik Asplund, Jan-Erik Berg, Fredrik Harrysson, Jonas Medbo, and Mathias Riback. "Propagation characteristics of polarized radio waves in cellular communications". Technical report, Ericsson Research, Stockholm Sweden, 2007.

[3] P. Balaban and V.P. Dewal. "Statistical Distribution of Parameters in a Variable Delay Two-Ray Propagation Model". Technical report, AT&T Bell Laboratories, Holmdel, NJ 07733, 1989.

[4] Bruce B. Barrow. "Diversity Combination of Fading Signals With Unequal Mean Strength". *IEEE Transactions On Communications*, 1963.

[5] Frode Bøhagen. *"Modeling, Characterization and Design of Line-of-Sight Wireless MIMO Channels"*. PhD thesis, University of Oslo, 2007.

[6] Frode Böhagen, Pål Orten, and Geir E. Öien. "Optimal Design of Uniform Planar Antenna Arrays for Strong Line-of-Sight MIMO Channel". In *Signal Processing Advances in Wireless Communications*, 2006.

[7] Mikael Coldrey. "Modeling and capacity of polarized MIMO channels". In *Proc. Vehicular Technology Conference, VTC 2008*, pages 440–444, Singapore, May 2008.

[8] Mikael Coldrey and Patrik Bohlin. "Training-Based MIMO Systems Part I: Performance Comparison". *IEEE Transaction on Signal Processing*, 55(11), Nov 2007.

[9] Mikael Coldrey and Patrik Bohlin. "Training-Based MIMO Systems: Part II Improvements Using Detected Symbol Information". *IEEE Transaction on Signal Processing*, 56:296–303, 2008.

[10] C. Cozzo and B. L. Hughes. "Joint channel estimation and data detection in space-time communication". *IEEE Trans. Communication*, 51:1266–1270, Aug 2003.

[11] C.R.Johnson. *"Unsuperivised Adaptive Filtering"*. Wiley, 1999.

[12] David. A. de Wolf and Albert J. Zwiesler. "Rayleigh-Mei Approximation for Line-of-Sight Propagation Through Rain at 5-90 GHz". *IEEE Transactions on Antennas And Propagation*, 44(3), 1996.

[13] D.N.Godard. "Self-Recovering Equalization and Carrier Tracking in Two-Dimensional Data Communication Systems". *IEEE Transactions on Communications*, COM-28:1867 – 1875, 1980.

[14] P. F. Driessen and G. Foschini. "On the capacity formula for multiple input-multiple output wireless channels: A geometric interpretation". *IEEE Trans. Commun*, 47(2):173–176, Feb 1999.

[15] Vinko Erceg, Hemanth Sampath, and Severine Catreux-Erceg. "Dual-Polarization Versus Single-Polarization MIMO Channel Measurement Results and Modeling". *IEEE Transaction on Wireless Communication*, 5(1), Jan 2006.

[16] G. J. Foschini. "Layered space-time architecture for wireless communication in fading environments when using multi-element antennas". *Bell Labs Technical Journal*, pages 41–59, 1996.

[17] Maurice G.Bellanger. *"Adaptive Digital Filters"*. Marcel Dekker,INC, 2nd edition, 2001.

[18] D. Gesbert, H. Bölcskei, D. A. Gore, and A. J. Paulraj. "Outdoor MIMO wireless channels: Models and performance prediction". *IEEE Trans. on Communications*, 50(12):1926–1934, Dec 2002.

[19] Godard. "Self-Recovering Equalization and Carrier Tracking in Two-Dimensional Data Communication Systems". *IEEE Transactions on Communications*, 28:1867 – 1875, 1980.

[20] Andrea Goldsmith. *"Wireless Communications"*. Cambridge University Press, 2005.

[21] John G.Proakis and Dimitris G. Manolakis. *"Digital Signal Processing"*. Prentice Hall, Upper Saddle River, New Jersey, 4th edition, 2007.

[22] Ali Hajimiri and Thomas H. Lee. "A General Theory of Phase Noise in Electrical Oscillators". *IEEE Journal of Solid-State Circuits*, 33(2), Feb 1998.

[23] David Hammarwall, Mats Bengtsson, and Björn Ottersten. "On Downlink Beamforming With Indefinite Shaping Constraint". *IEEE Transaction On Signal Processing*, 54(9), 2006.

[24] B. Hassibi and B. M. Hochwald. "How much training is needed in multiple-antenna wireless links?". *IEEE Trans. Inf. Theory*, 49(4):951–963, April 2003.

[25] T. Haustein and U. Krüger. "Smart geometrical antenna design exploiting the LOS component to enhance a MIMO system based on Rayleigh-fading in indoor scenarios". *Proc. PIMRC*, 2:1144–1148, Sep 2003.

[26] P. Hoeher and F. Tufvesson. "Channel estimation with superimposed pilot sequence". In *Global Telecommunications Conference*, volume 4, pages 2162–2166, 1999.

[27] A. A. Hutter, F. Platbrood, and J. Ayadi. "Analysis of MIMO capacity gains for indoor propagation channel with LOS component". *Proc. PIMRC*, 3:1337–1347, Sep 2002.

[28] J.Treichler and B.Agee. "A new approach to multipath correction of constant modulus signals". *IEEE Transactions on Acoustics,Speech,and Signal Processing*, 31:459 – 472, 1983.

[29] K.N.Oh and Y.O.Chin. "Modified constant modulus algorithm: blind equalization and carrier phase recovery algorithm". In *Proceedings of the IEEE International Conference on Communications*, volume 1, pages 498 – 502, 1995.

[30] William C.Y. Lee and Yu S. Yeh. "Polarization Diversity System for Mobile Radio". *IEEE Transactions on Communications*, 20(5), Oct 1972.

[31] Aissa Lkhlef and Daniel L. Guennec. "Blind Recovery of MIMO QAM Signals: A criterion with its convergence Analysis". In *Proceedings of the 14th European Signal Processing Conference*, 2006.

[32] Aissa Lkhlef and Daniel L. Guennec. "A Simplified Constant Modulus Algorithm for Blind Recovery of MIMO QAM and PSK Signals : A Criterion with Convergence Analysis". *Eurasip Journal on Wirless Communication and Networking*, 2007, 2007.

[33] M.D. Loundu, C.L. Despins, and J. Conan. "Estimating The Capacity of a Frequency-Selective Fading Mobile Radio Channel With Antenna Diversity". In *Vehicular Technology Conference*, volume 3, pages 1490–1493, 1994.

[34] M.D. Loundu, C.L. Despins, and J. Conan. "Estimating the Capacity of a Frequency-Selective Fading Mobile Radio Channel with Antenna Diversity". Technical report, École Polytechnique de Montréal, Montréal Québec, Canada, 1994.

[35] F. Mazzenga. "Channel estimation and equalization for M-QAM transmission with a hidden pilot sequence". *IEEE Trans Broadcast*, 46:170–176, Jun 2000.

[36] Michael L. McCloud, Louis L. Scharf, and Mahesh K. Varanasi. "Beamforming, Diversity, and Interference Rejection for Multiuser Communication Over Fading Channels With a Receive Antenna Array". *IEEE Transaction On Communication*, 51(1), 2003.

[37] A. Medles and D. T. M. Slock. "Semiblind channel estimation for MIMO spatial multiplexing systems". *Proc. VTC2001-Fall*, 2:1240–1270, Oct 2001.

[38] M.G.Larimore and J.treichler. "Convergence behavior of the constant modulus algorithm". In *Not found*, volume 1, pages 13 – 16. Proceedings of the IEEE International Conference on Acoustics, Speech, and Signal Processing, 1983.

[39] Larsson P. "Lattice array receiver and sender for spatially orthonormal MIMO communication". In *Vehicular Technology Conference*, volume 1, pages 192–196, 2005.

[40] Arogyaswami J. Paulraj, Dhananjay A. Gore, Rohit U. Nabar, and Helmut Bölcskei. "An Overview of MIMO Communications-A Key to Gigabit Wireless". *Proceeding of the IEEE*, 92(2), Feb 2006.

[41] P.Sansrimahachai, D.B.Ward, and A.G.Constantinides. "Blind source separation for BLAST". In *Digital Signal Processing*, volume 1, pages 139 – 142. Proceedings of the 14th International Conference on Digital Signal Processing, 2002.

[42] Kati Sulonen, Pasi Suvikunnas, Lasse Vuokko, Jarmo Kivinen, and Pertti Vainikainen. "Comparison of MIMO Antenna Configurations in Picocell and Microcell Environments". *IEEE Journal on Selected Areas in Communications*, 21(5), June 2003.

[43] Mikael Tapio. "Adaptive Equalizer Functions for QAM in Digital Microwave Radio Systems". Master's thesis, Linköpings University, 2000.

[44] E. Telatar. "Capacity of multi-antenna Gaussian channels". *European Transactions on Telecommunications*, June 1995.

[45] L. Tong, B. M. Sadler, and M. Dong. "Pilot-assisted wireless transmissions". *IEEE Signal Process*, 21(6):12–25, Nov 2004.

[46] J.R Treichler and M.G Larimore. "New Processing Techniques Based on the Constant Modulus Algorithm". *IEEE Transactions on Acoustics,Speech,and Signal Processing*, ASSP-33:420 – 431, 1985.

[47] Mats Viberg, G. Tong Zhou, and Tomas McKelvey. "Superimposed Periodic Pilots for blind channel estimation". Technical report, Chalmers University of Technology and Georgian Institute of Technology, 2001.

[48] Mats Viberg, G. Tong Zhou, and Tomas McKelvey. "A First-Order Statistical Method for Channel Estimation". *IEEE Signal Processing Letters*, 10(3), March 2003.

[49] Mattias Wennström. *"On MIMO Systems and Adaptive Arrays for Wireless Communication. Analysis and Practical Issues"*. PhD thesis, Uppsala University, 2002.

[50] J. Winters. "On the capacity of radio communication systems with diversity in a Rayleigh fading environment". *IEEE J. Sel. Areas Commun*, pages 871–878, June 1987.

[51] Y.Sato. "A Method of Self-Recovering Equalization for Multilevel Amplitude-Modulation Systems". *IEEE Transactions on Communications*, COM-23:679 – 682, 1975.

[52] Yonghong Zeng and Tung Sang Ng. "Blind MIMO Channel Estimation Method Tolerating Order Overestimation". Technical report, The University of Hong Kong, Hong Kong, 2002.

[53] Rodger E. Ziemer and Roger L. Peterson. *"Introduction To Digital Communication"*. Prentice Hall, Upper Saddle River, New Jersey, 2nd edition, 2001.

Appendix A

Derivations

A.1 Singular Values For 2x2 LoS MIMO

The singular values for a MIMO system are obtained by calculating the eigenvalues of $\mathbf{W}$ where

$$\mathbf{W} = \left\{ \begin{array}{ll} \mathbf{H}\mathbf{H}^{\mathrm{H}} & \text{if} \quad N \leq M \\ \mathbf{H}^{\mathrm{H}}\mathbf{H} & \text{if} \quad N > M \end{array} \right\}$$

For a 2x2 LoS MIMO we have

$$\begin{aligned} \mathbf{H}_{\mathrm{LoS}} &= \begin{bmatrix} \exp(jkd_{11}) & \exp(jkd_{12}) \\ \exp(jkd_{21}) & \exp(jkd_{22}) \end{bmatrix} \Rightarrow \\ \mathbf{W} &= \mathbf{H}_{\mathrm{LoS}}\mathbf{H}_{\mathrm{LoS}}^{\mathrm{H}} = \begin{bmatrix} 2 & e^{jk(d_{11}-d_{21})} + e^{jk(d_{12}-d_{22})} \\ e^{jk(d_{21}-d_{11})} + e^{jk(d_{22}-d_{12})} & 2 \end{bmatrix} \end{aligned}$$

The eigenvalues are found by solving the following equation

$$\det\left(\mathbf{W} - c\mathbf{I}\right) = 0$$

This yields

$$(2-c)^2 - 2 - e^{jk(d_{11}+d_{22}-d_{12}-d_{21})} - e^{jk(d_{12}+d_{21}-d_{22}-d_{22})} = 0$$

which gives

$$c = 2 \pm \left[2 + 2\cos(kA)\right]^{1/2} \tag{A.1}$$

where $A = d_{11} + d_{22} - d_{12} - d_{21}$. The singular values are now the square roots of the ordered eigenvalues c. The condition for optimality for the 2x2 MIMO system is that $d_{11} - d_{12} = \frac{\pi}{2k}$, thus we have $A_{\mathrm{opt}} = \frac{\pi}{k}$. For η defined in (3.16) the eigenvalues in (A.1) become

$$c = 2 \pm \left[2 + 2\cos(\pi\eta^2)\right]^{1/2}$$

Thus the singular values can be expressed as

$$\sigma_1 = \left[2 + \left[2 + 2\cos(\pi\eta^2)\right]^{1/2}\right]^{1/2}$$
$$\sigma_2 = \left[2 - \left[2 + 2\cos(\pi\eta^2)\right]^{1/2}\right]^{1/2} \tag{A.2}$$

And finally the condition number is

$$\kappa = \frac{\sigma_1}{\sigma_2}$$

A.2 Derivation of the normal equations

For simpleness, we only proof the least square based on the output of the first receiving antenna. It can be extended into any number of receiving antennas. We use y_1 to express the output of the equalizer at the first receiving antenna and we are assuming there are N samples of the received signal.

$$y_1(k) = \sum_{j=1}^{M \cdot L} r_{k,j} w_j \tag{A.3}$$

For all $k = 1, 2, \ldots, N$. M, L is the number of Rx antennas and equalizer filter length respectively. $r_{k,j}, w_j$ is the k, jth element in $\mathbf{R}$ matrix and jth element in column vector $\mathbf{W}_1$.

$$e_{\mathbf{W}_1}(k) = s_1(k) - \sum_{j=1}^{M \cdot L} r_{k,j} w_j, (k = 1, 2, \ldots, N). \tag{A.4}$$

So to minimize the function under LS algorithm.

$$\varepsilon = \sum_{k=1}^{N} e^2_{\mathbf{W}_1}(k). \tag{A.5}$$

where N is the number of samples from the first receiving antenna output before the equalization operation. ε is minimized when its gradient with respect to each element of vector $\mathbf{W}_1$ is equal to zero.

$$\frac{\partial \varepsilon}{\partial \mathbf{W}_1} = 2 \sum_{k=1}^{N} e_{\mathbf{W}_1}(k) \frac{\partial e_{\mathbf{W}_1}(k)}{\partial \mathbf{W}_1} = 0. \tag{A.6}$$

since

$$e_{\mathbf{W}_1}(k) = s_1(k) - \sum_{j=1}^{M \cdot L} r_{k,j} w_j \quad (k = 1, 2, \ldots, N).$$

the derivative is

$$\frac{\partial e_{\mathbf{W}_1}(k)}{\partial \mathbf{W}_1} = - \sum_{j=1}^{M \cdot L} r_{k,j}.$$

Substitution of the expression for the residuals and derivatives into the gradient equations obtains:

$$\frac{\partial \varepsilon}{\partial \mathbf{W}_1} = -2 \sum_{k=1}^{N} \sum_{j=1}^{M \cdot L} r_{k,j} (s_1(k) - \sum_{i=1}^{M \cdot L} r_{k,i} w_i) = 0. \tag{A.7}$$

After re-arrangement, the normal equation is re-written as:

$$\sum_{j=1}^{N} \sum_{i=1}^{M \cdot L} \sum_{k=1}^{N} r_{k,j} \cdot r_{k,i} \cdot w_i = \sum_{j=1}^{M \cdot L} \sum_{k=1}^{N} r_{k,j} \cdot s_1(k).$$

The normal equation is written in matrix notation as:

$$(\boldsymbol{R}^T \boldsymbol{R}) \boldsymbol{W}_1 = \boldsymbol{R}^T \boldsymbol{S}_1 \tag{A.8}$$

Thus (4.16) is proved.

Appendix B

Singular Value Decomposition

For every $N \times M$ matrix $\mathbf{H}$ one can write

$$\mathbf{H} = \mathbf{U}\mathbf{\Sigma}\mathbf{V}^{\mathrm{H}} \tag{B.1}$$

where $\mathbf{U}$ and $\mathbf{V}$ are $M \times M$ and $N \times N$ unitary matrices respectively. $\mathbf{\Sigma}$ is a $M \times N$ diagonal matrix of singular values σ_k of $\mathbf{H}$. These singular values have the property that $\sigma_k = \sqrt{\lambda_k}$ where λ_k is the ith largest eigenvalue of $\mathbf{H}\mathbf{H}^{\mathrm{H}}$. If the transmission system is designed in such a way that it has transmitter precoding an receiver shaping that is if the sequence to be transmitted is multiplied with $\mathbf{U}^{\mathrm{H}}$ and the received sequence with $\mathbf{V}$ the following result is obtained [20, ch. 10] (see figure 3.2 for reference)

$$\begin{aligned} \mathbf{r} &= (\mathbf{s}\mathbf{H} + \mathbf{n})\mathbf{V} \\ &= (\mathbf{s}\mathbf{U}\mathbf{\Sigma}\mathbf{V}^{\mathrm{H}} + \mathbf{n})\mathbf{V} \\ &= (\mathbf{x}\mathbf{U}^{\mathrm{H}}\mathbf{U}\mathbf{\Sigma}\mathbf{V}^{\mathrm{H}} + \mathbf{n})\mathbf{V} \\ &= \mathbf{x}\mathbf{U}^{\mathrm{H}}\mathbf{U}\mathbf{\Sigma}\mathbf{V}^{\mathrm{H}}\mathbf{V} + \mathbf{n}\mathbf{V} \\ &= \mathbf{x}\mathbf{\Sigma} + \tilde{\mathbf{n}} \end{aligned} \tag{B.2}$$

where $\tilde{\mathbf{n}} = \mathbf{n}\mathbf{V}$ has the same distribution as $\mathbf{n}$ since $\mathbf{V}$ is a unitary matrix ($\mathbf{V}^{\mathrm{H}}\mathbf{V} = \mathbf{I}_M$). The derivation above shows that with the proper precoding and receiver shaping a MIMO channel can be parallelized into R_H SISO channels which do not interfere with each other and are only connected through the total power constraint.

B.1 Example: 2x2 MIMO

Using SVD the SNRs for a 2x2 MIMO are given by (seen from (B.2))

$$\mathrm{SNR}_1 = \frac{\sigma_1^2}{\sigma_n^2} \quad \mathrm{SNR}_2 = \frac{\sigma_2^2}{\sigma_n^2} \tag{B.3}$$

where σ_n^2 is the noise power. Equalizing using direct matrix inversion will though give a different result as is shown here

$$\begin{aligned}
\mathbf{r} &= \mathbf{sH} + \mathbf{n} && \text{(B.4)}\\
\mathbf{y} &= \mathbf{rH}^{-1} = \mathbf{sHH}^{-1} + \mathbf{nH}^{-1} && \text{(B.5)}\\
&= \mathbf{s} + \mathbf{nV}\boldsymbol{\Sigma}^{-1}\mathbf{U}^{\mathrm{H}} && \text{(B.6)}\\
&= \mathbf{s} + \tilde{\mathbf{n}}\boldsymbol{\Sigma}^{-1}\mathbf{U}^{\mathrm{H}} && \text{(B.7)}
\end{aligned}$$

Now the SNRs can be written as

$$\begin{aligned}
\mathrm{SNR}_1 &= \frac{1}{\sigma_n^2|U_{11}|^2/\sigma_1^2 + \sigma_n^2|U_{21}|^2/\sigma_2^2} = \frac{\sigma_1^2}{\sigma_n^2}\frac{\sigma_2^2}{\sigma_2^2|U_{11}|^2 + \sigma_1^2|U_{21}|^2}\\
\mathrm{SNR}_2 &= \frac{\sigma_2^2}{\sigma_n^2}\frac{\sigma_1^2}{\sigma_2^2|U_{11}|^2 + \sigma_1^2|U_{21}|^2}
\end{aligned}$$

The SVD and direct matrix inversion approaches are thus not comparable.